Hydrodynamics, turbulence and instabilities

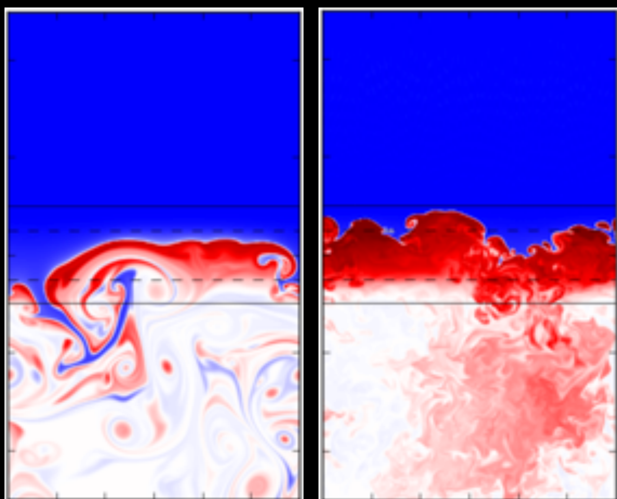

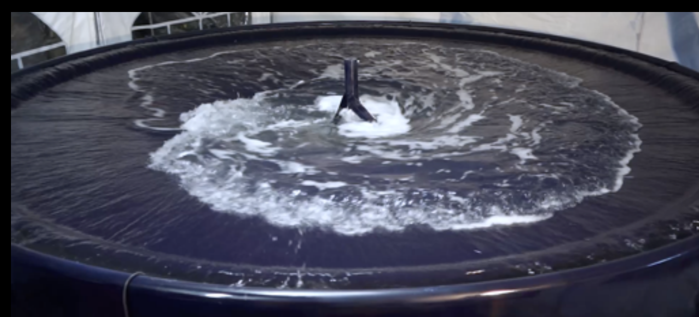

Thierry Foglizzo, CEA Saclay

Outline

Impact of hydrodynamics the explosion physics

2D vs 3D

The basics of hydrodynamical instabilities

Neutrino driven convection

The Standing Accretion shock instability

Rotational effects: spiral SASI, low T/W, MRI

core-collapse of a $27M_{sol}$ star in 3D
at the explosion threshold

Hanke+13, Melson+15

PRACE project 150 million hours
16.000 processors, 4.5 months/model

time evolution:
500ms
diameter: 300km

Why should we care about multiD instabilities

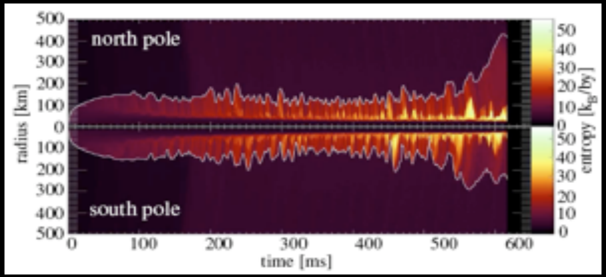

- successful explosion driven by neutrino energy
  (Marek & Janka 09, Suwa+10, Müller+12, Bruenn+13, Melson+15)

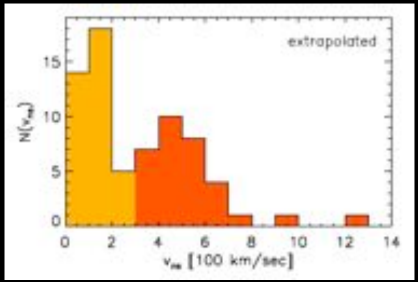

- pulsar kick
  (Scheck+04, 06, Nordhaus+10, +11, Wongwathanarat+10, +13)

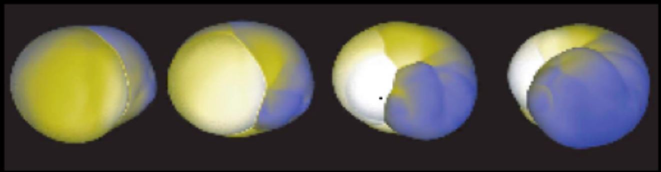

- pulsar spin
  (Blondin & Mezzacappa 07, Yamasaki & Foglizzo 08, Iwakami+09, Kazeroni+16)

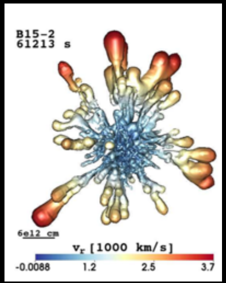

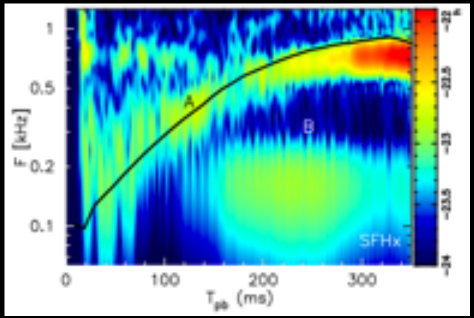

- H/He mixing and Ni clumps in SN1987A
  (Kifonidis+06, Hammer+09, Utrobin+15)

- gravitational waves
  (Ott+06, Kotake+07, Marek+09, Murphy+09, Kotake+11, Müller+13, Kuroda+16)

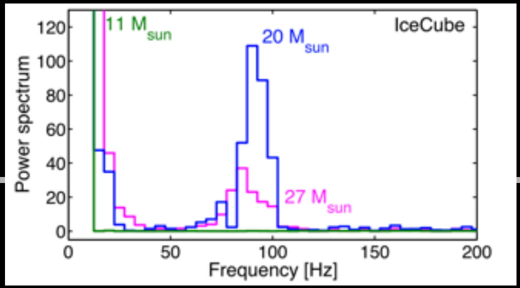

- neutrino signature
  (Marek+09, Müller+12, Lund+10, 12, Tamborra+13, Müller & Janka 14)

The positive effect of instabilities on the explosion threshold

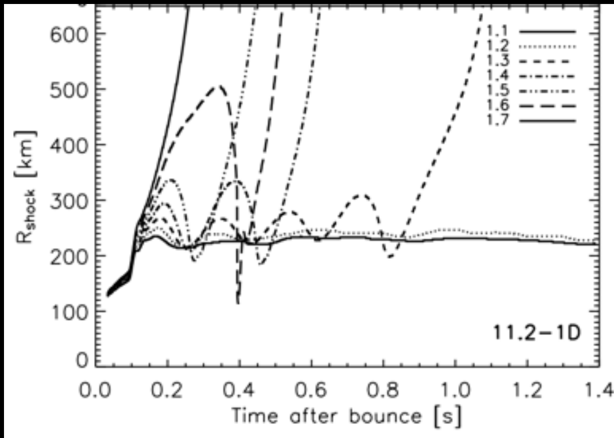

Since Burrows & Goshy 93, the explosion threshold is parametrized in the L_ν, dM/dt plane

The onset of explosion requires a high enough neutrino luminosity, or a low enough mass accretion rate.

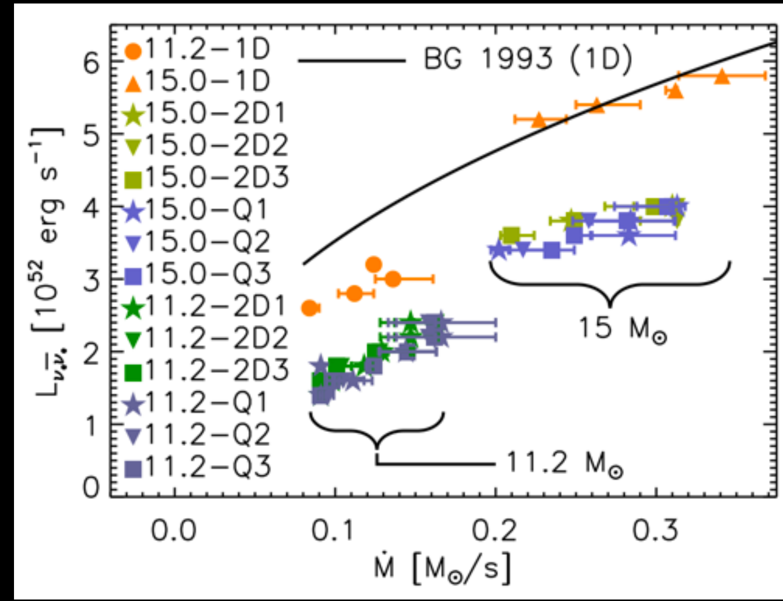

Murphy & Burrows 08

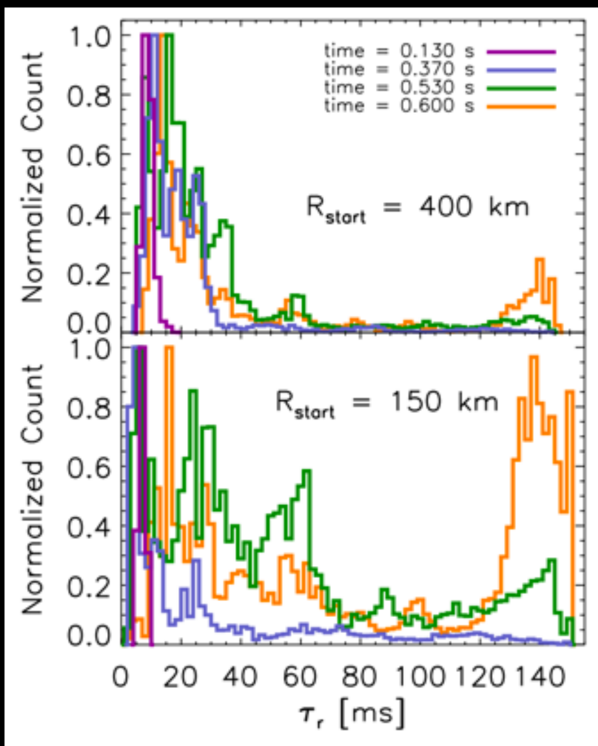

Murphy & Burrows 08 demonstrated that the SASI instability allows for explosions with a lower neutrino luminositiy threshold (-30%) than in 1D

Convective cells trap the gas and expose it to the neutrino flux for a longer time than with radial trajectories.

The contribution of turbulent pressure, either from the preshock material (Couch & Ott 15, Müller+16) or from the SASI instability (Cardal & Budiarja 16) decreases the amount of neutrino heating needed to trigger the explosion

MultiD allows for a continuous injection of accretion energy while the explosion proceeds

Progress of ab initio simulations: understandable diversity

-axisymmetric explosions from first principles
8.1, 9.6 ,11.2, 15, 27M$_{sol}$ (MPA)
12, 15, 20, 25 M$_{sol}$ (ORNL)
(Müller+12a,b,+13, Bruenn+13,+16)

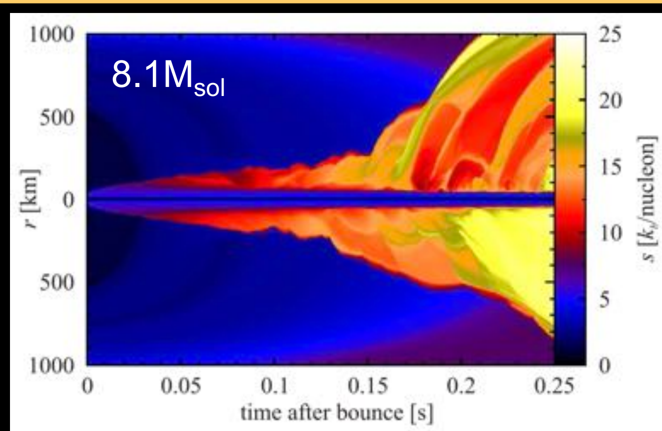

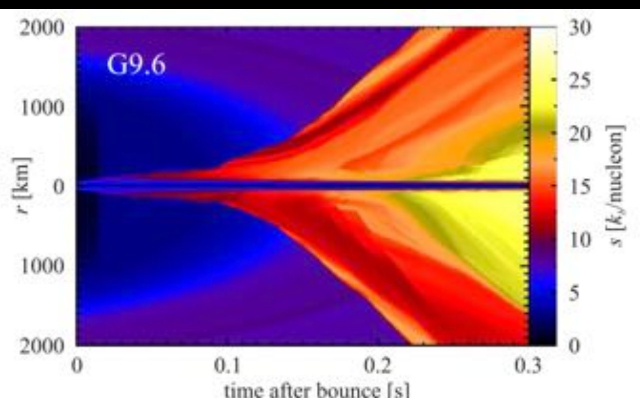

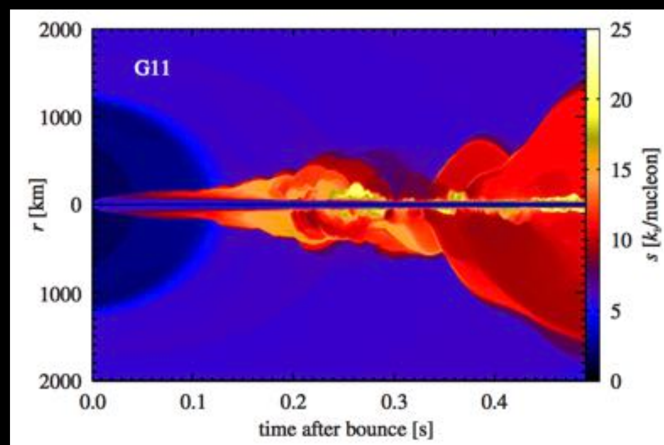

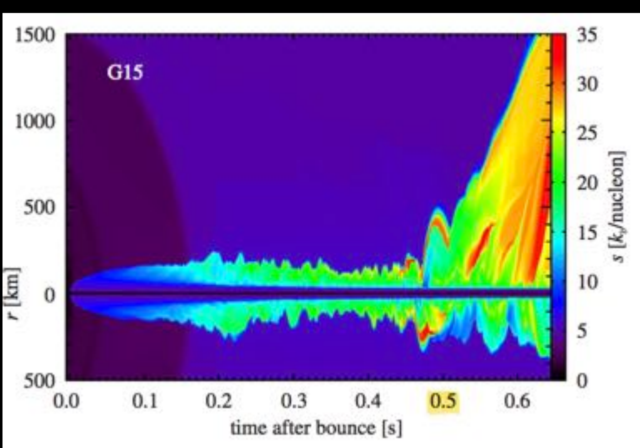

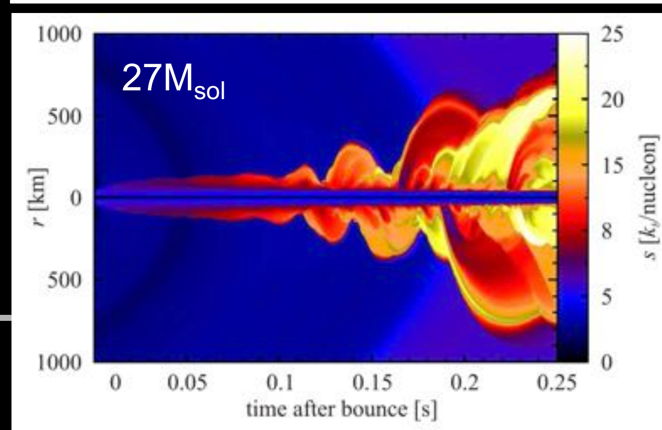

-depending on the progenitor, the dynamical evolution can be dominated by neutrino driven buoyancy (11.2M$_{sol}$) or by SASI (27M$_{sol}$) or by both (15M$_{sol}$)

-competition between advection and buoyancy
(Foglizzo+06, Fernandez+13)

$$\chi \equiv \int_{\mathrm{sh}}^{\mathrm{gain}} \omega_{\mathrm{BV}} \frac{\mathrm{d}r}{v_r} < 3$$

Two paths to explosion (Müller+12)

strength of ν-driven buoyancy:
parameter $\chi \sim \tau_{adv}/\tau_{buoy}$

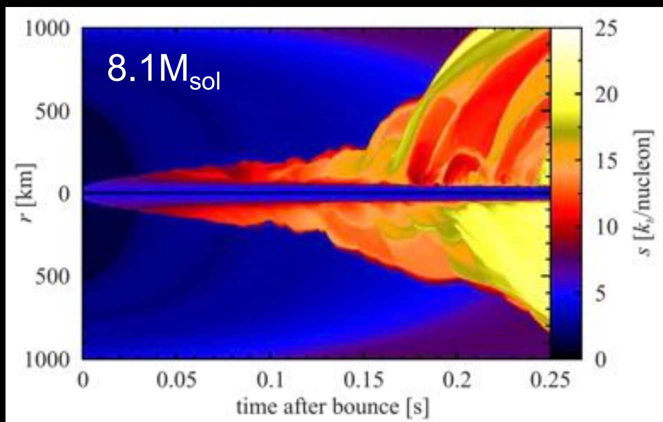

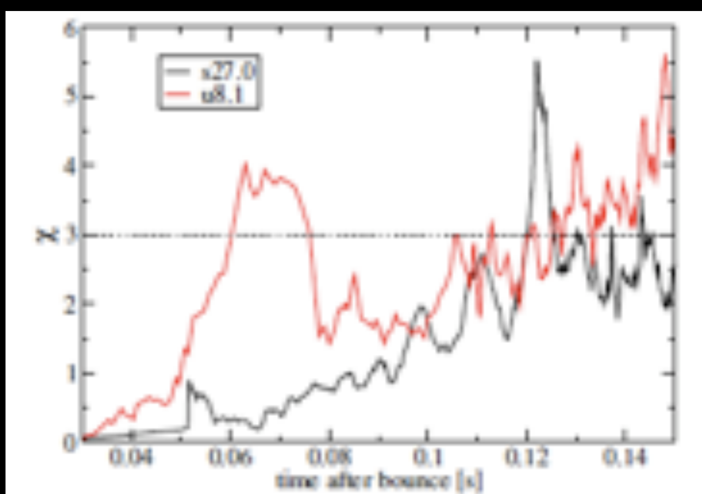

strength of SASI: amplification parameter Q

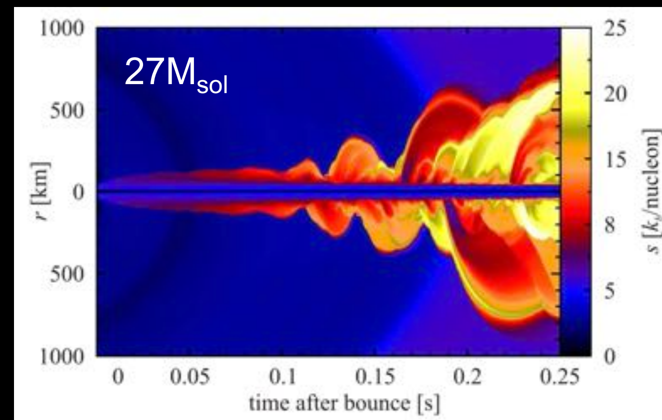

$$\omega_{\mathrm{i}}^{\mathrm{SASI}} = \frac{\log Q}{\tau_{\mathrm{Q}}}$$

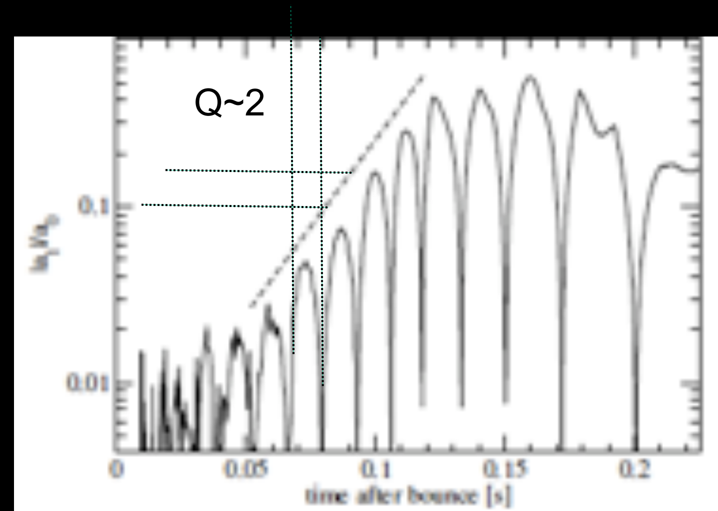

$27M_{sol}$ in 2D

Gravitational waves signatures from non axisymmetric features

(Ott+06, Kotake+07, Marek+09, Ott 08, Murphy+09, Kotake+11, 13, E.Müller+12, B.Müller+13, Hayama+15, Kuroda+14, +16)

Low T/W spiral modes of fast spinning cores produce strong gravitational waves (e.g. Hayama+15)

For a non rotating progenitor, the stochastic wobbling of the SASI spiral mode axis weakens the GW signature in 3D compared to 2D.

Nevertheless, the SASi induced GW signal is sensitive to the compactness of the core, the equation of state (Müller+13, Kuroda+16), and the rotation rate (Kotake+11, Kuroda+14).

Model	$\Omega_{\rm ini}$ (rad s^{-1})	$\rho_{{\rm max},b}$ (10^{14} g cm^{-3})	$\beta_{\rm b}$
R0	0	3.54	2.3×10^{-5}
R1	$\pi/6$	3.52	1.5×10^{-3}
R2	$\pi/2$	3.41	1.3×10^{-2}
R3	π	3.28	4.9×10^{-2}

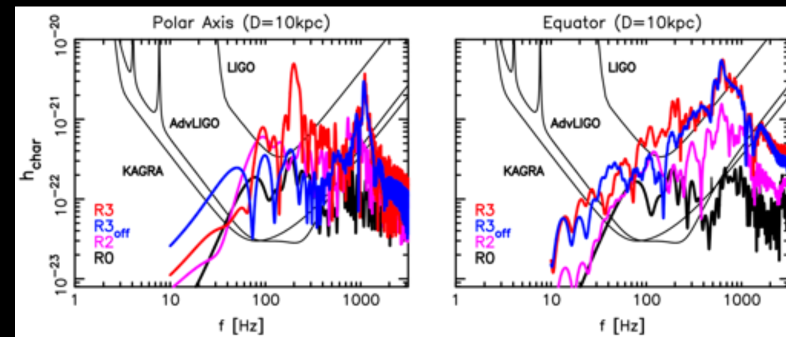

Kuroda+16

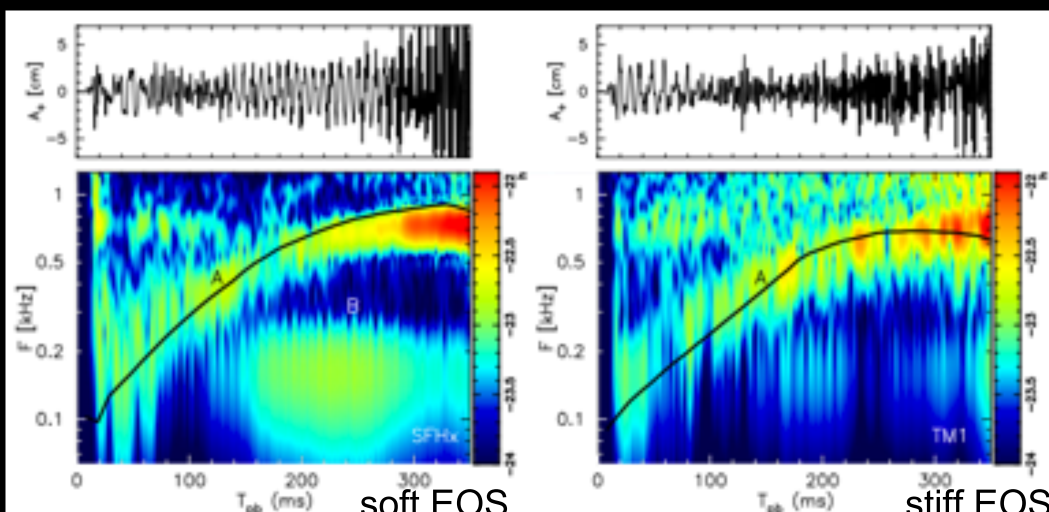

detection by LIGO, KAGRA for a non rotating galactic supernova at 10kpc:

g-mode activity with S/N=10
SASI activity with S/N~50

A: NS g-mode oscillations (600-700Hz)
B: SASI activity (100-200Hz)

Neutrino signature of 3D instabilities

(Marek+09, Müller+12, Lund+10, +12, Tamborra+13, +14, Müller & Janka 14)

$$\bar{\nu}_e + p \rightarrow n + e^+$$

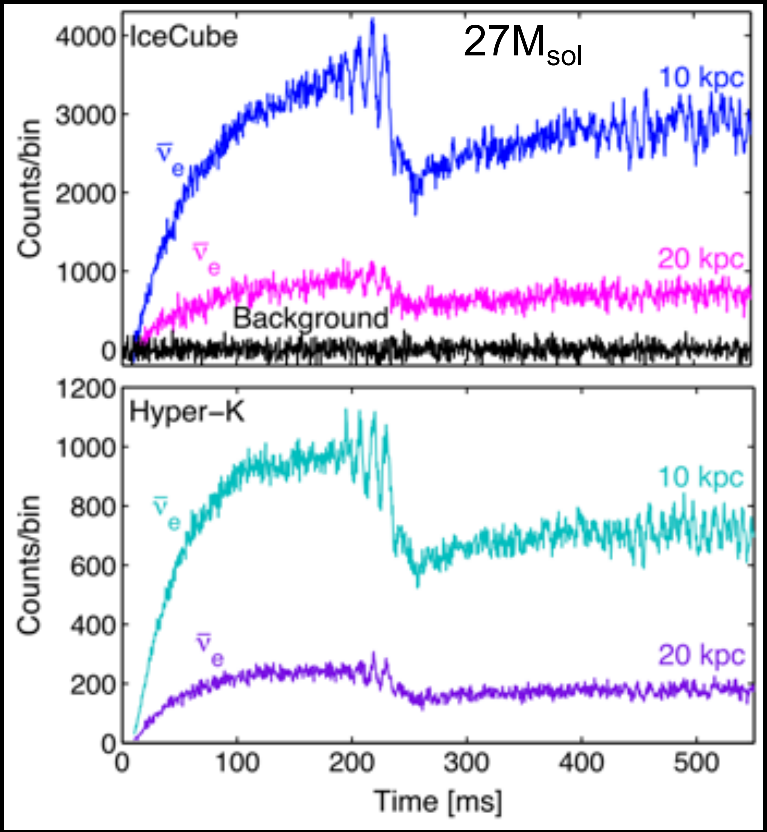

Tamborra+13

For a galactic supernova at 10kpc:

IceCube will detect 10^6 events above the background
Super-K (32kton): 10^4 events
Hyper-K (740kton): $3\text{x}10^5$ events background free

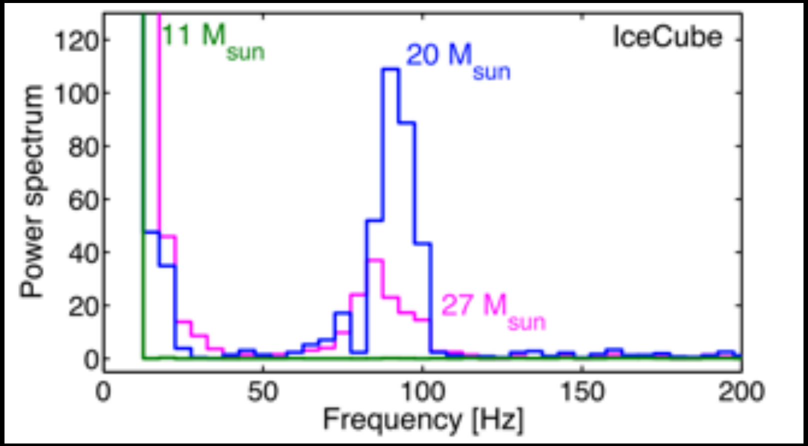

→direct signature of the SASI oscillation frequency

Outline

Impact of hydrodynamics the explosion physics

2D vs 3D

The basics of hydrodynamical instabilities

Neutrino driven convection

The Standing Accretion shock instability

Rotational effects: spiral SASI, low T/W, MRI

Asymmetric explosion of a $15M_{sol}$ star aided by SASI

Marek & Janka 09

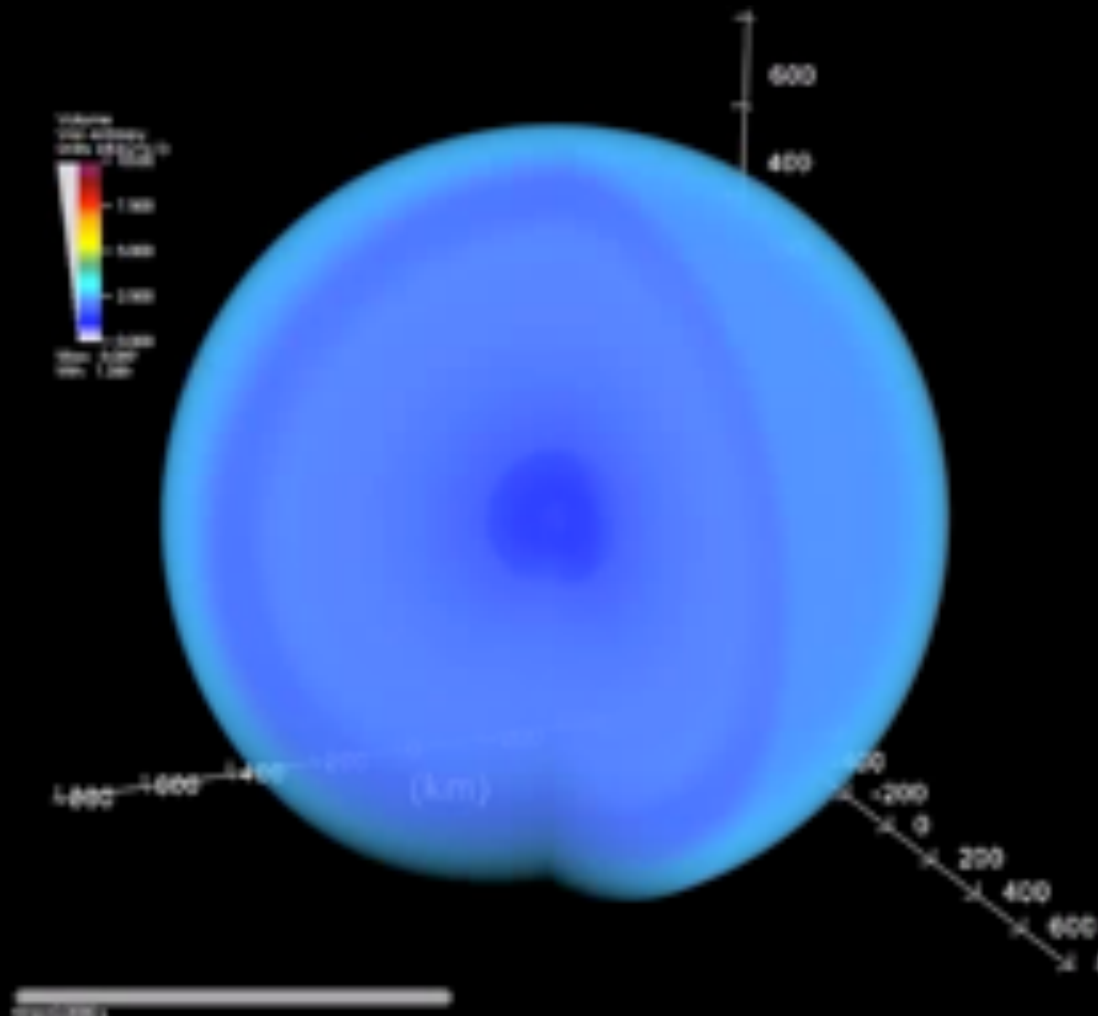

Homogeneous incompressible turbulence in 2D and 3D

Vallis+06

Wavenumber $k \sim 1/L$
viscosity $\nu \sim k^{-2}\tau^{-1}$
Kinetic Energy per unit mass $E=U^2/2 \sim k^{-2}\tau^{-2}$
Energy cascade rate $\varepsilon=dE/dt \sim k^{-2}\tau^{-3}$

Turnover timescale $\tau \sim k^{-2/3}\ \varepsilon^{-1/3}$
Energy spectrum in the inertial range $E_k \sim k^{-3}\tau^{-2} \sim k^{-5/3}\ \varepsilon^{2/3}$
Energy dissipation length $L_\nu \sim (\nu^3/\varepsilon)^{1/4}$
Vorticity $w \sim \tau^{-1} \sim k^{2/3}\ \varepsilon^{1/3}$ increases on small scales

In 2D the energy cascade to small scales is quenched
by the conservation of vorticity:
inverse cascade of energy to large scales

Vorticity $w \sim \tau^{-1}$
Enstrophy in 2D $w^2 \sim \tau^{-2}$
Enstrophy cascade rate $\eta \sim \tau^{-3}$

Turnover timescale set by vorticity conservation $\tau \sim \eta^{-1/3}$

Energy cascade rate $\varepsilon=dE/dt \sim k^{-2}\ \eta$
Energy spectrum in the inertial range
$$E_k \sim k^{-5/3}\ (\eta^{2/3}\ k^{-4/3}) \sim k^{-3}\ \eta^{2/3}$$
Enstrophy dissipation length $L_\nu \sim (\nu^3/\eta)^{1/6}$

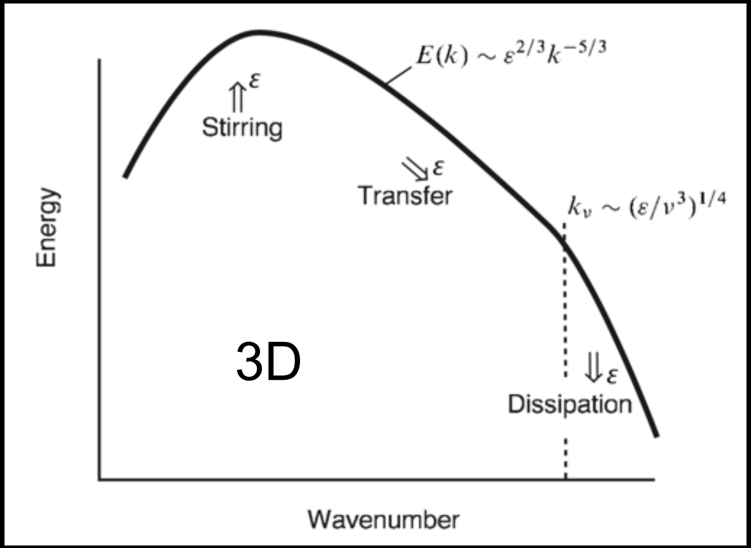

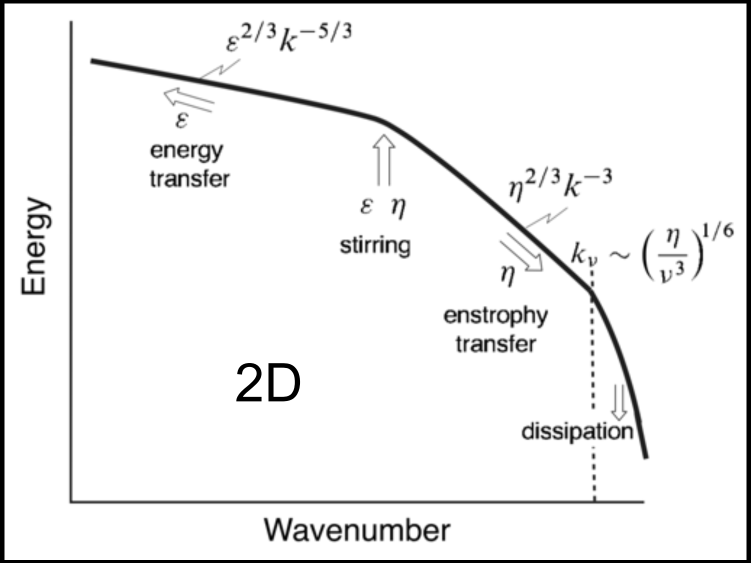

Convection vs advection in 2D/3D

Kazeroni +17

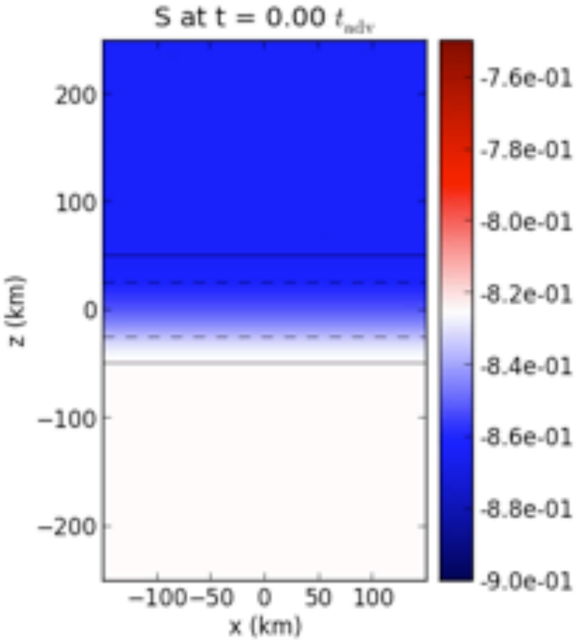

2D - y=0

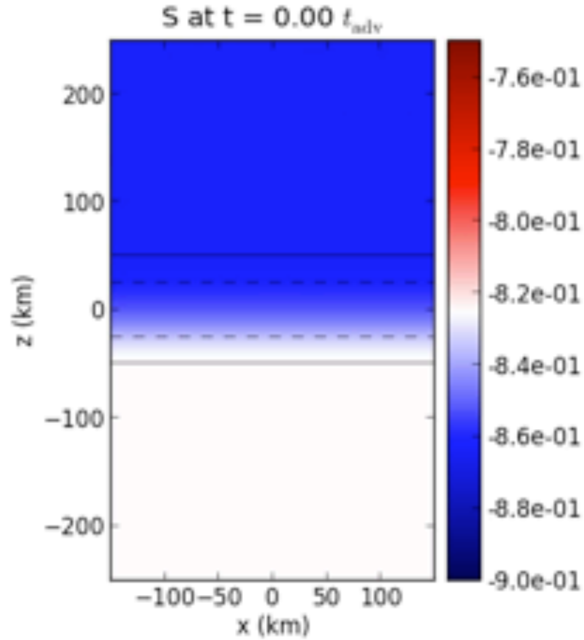

3D - y=0

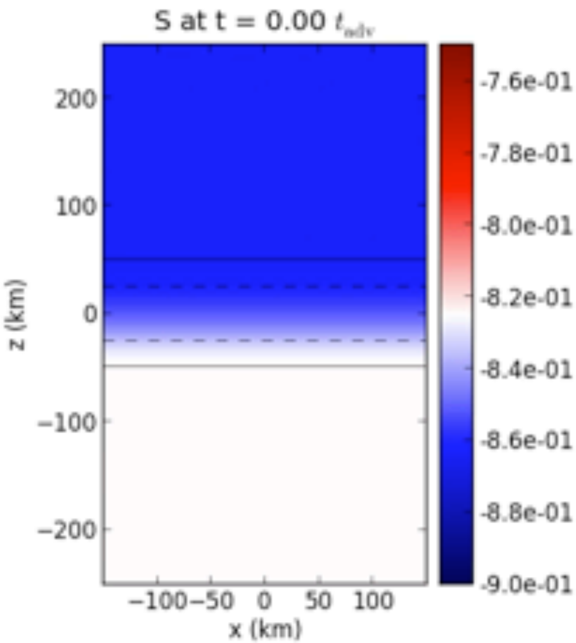

3D - y=-1.5

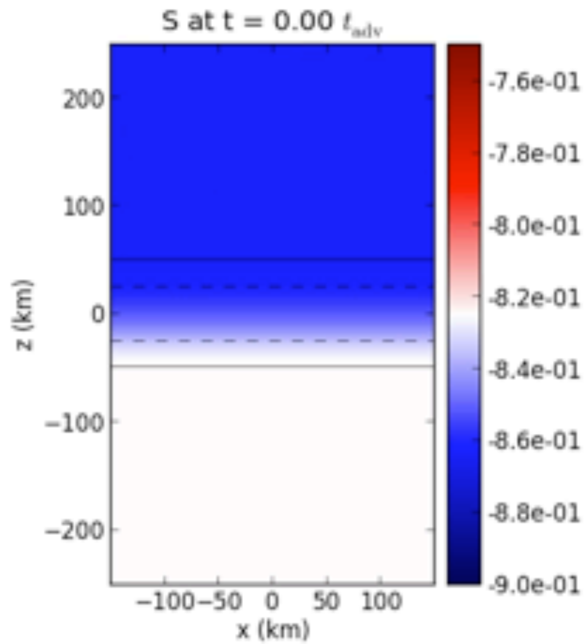

3D - y=1.5

The linear phase of the instability is identical in 2D and 3D

Small scale structures are more numerous in 3D than in 2D

Large scale motions are more vigorous in 2D than in 3D

The end of a controversy: the existence of SASI in 3D

-despite Burrows+12a,b, Murphy+13, Dolence+13,

SASI can be dominant even in the most realistic 3D simulations: 27M_{sol} progenitor (Hanke+13)

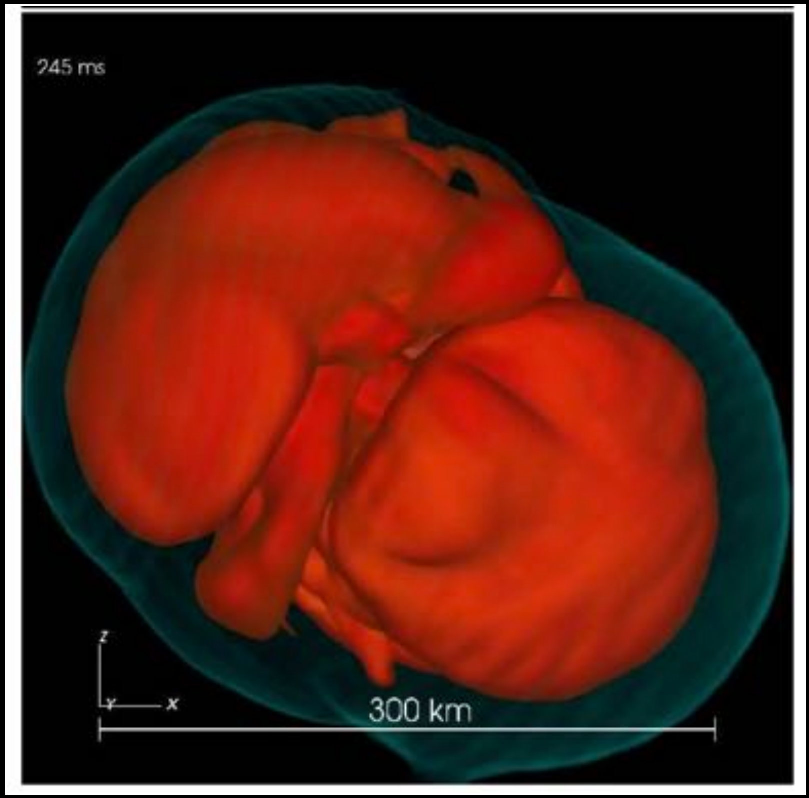

$27M_{sol}$ on the verge of explosion in 3D

-The first 3D ab initio simulation of $27M_{sol}$ did not explode after 380ms (Hanke+13)
... but a minor change in the nucleon strangeness was enough to produce an explosion (Melson+15)

Hanke+13

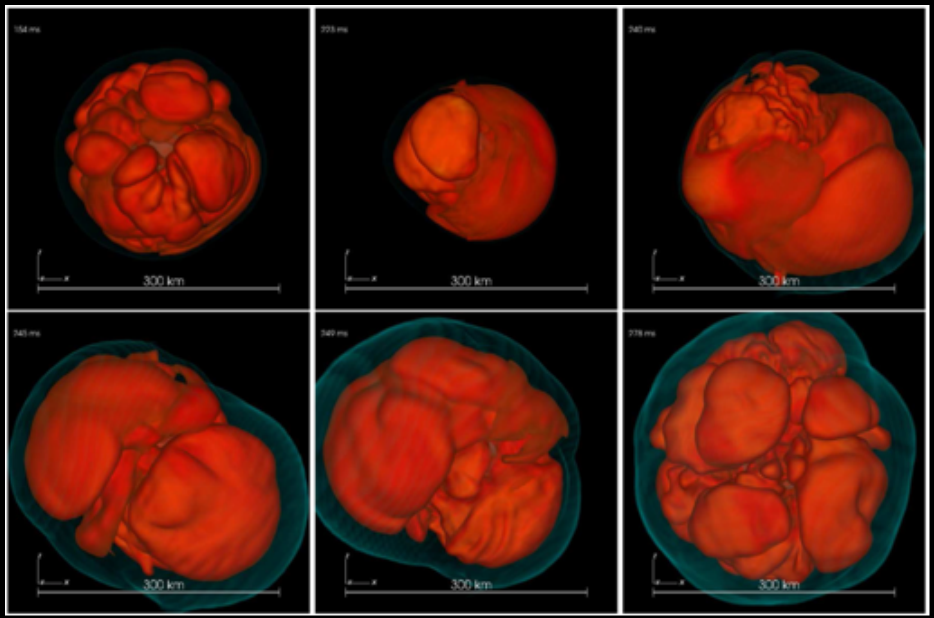

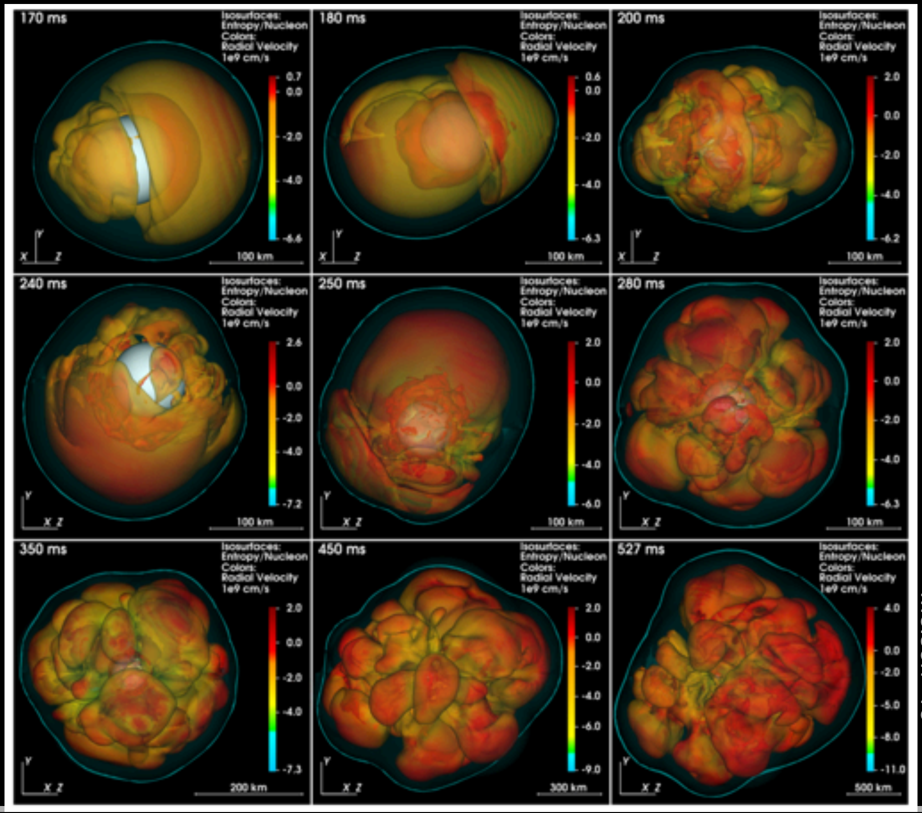

Melson+15

project PRACE 150 millions hours
16.000 processors, 4,5 months/model

Growing evidence that 3D explosions are more difficult than in 2D?

-Contrary to Nordhaus+10, Dolence+13, explosion is not obviously easier in 3D than in 2D
(Hanke+12, Couch & O'Connor 13)

-Inverse turbulent cascade in 2D favours the build up of larger scale motions than in 3D

-27M_{sol} did not explode in 3D (Hanke+13) but exploded in 2D (Müller+12)
-11.2M_{sol} exploded less energetically in 3D than in 2D (Takiwaki+14)
-15M_{sol} exploded later in 3D than in 2D (Lentz+15)

Lentz+15

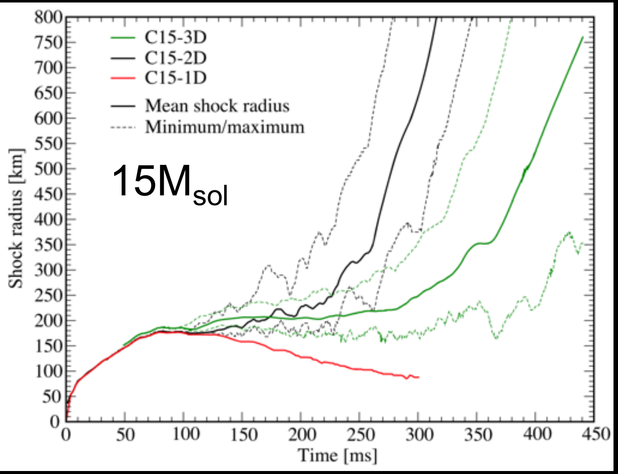

Takiwaki+14

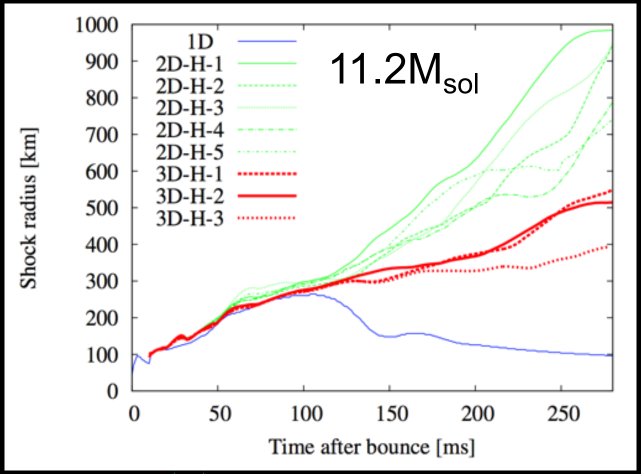

but...

-convection in 3D may better resist advection than in 2D (Kazeroni+17)

-3D SASI (27M_{sol}, Hanke+13) should be strengthened even by modest rotation (Yamasaki & Foglizzo 08)

Outline

Impact of hydrodynamics the explosion physics

2D vs 3D

The basics of hydrodynamical instabilities

Neutrino driven convection

The Standing Accretion shock instability

Rotational effects: spiral SASI, low T/W, MRI

How to characterize an instability

A linear instability is characterized by an exponential increase of small perturbation, with a rate independent of its amplitude in the linear regime.

The simplest example is the rigid pendulum:

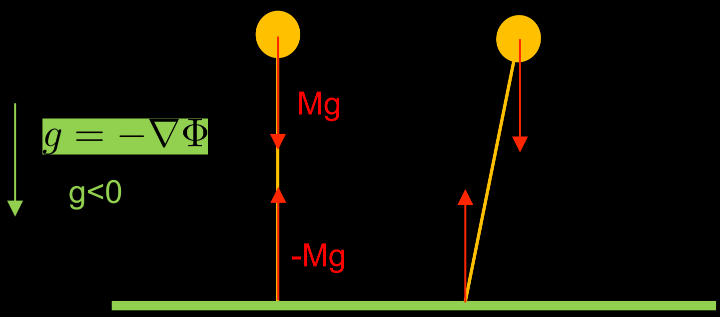

angular momentum and torques $$M z_G^2 \frac{\mathrm{d}^2\theta}{\mathrm{d}t^2} = M g z_G \sin\theta$$

linearized equation $$\frac{\mathrm{d}^2\theta}{\mathrm{d}t^2} - \frac{g}{z_G}\theta = 0$$ $$\omega^2 = \frac{g}{z_G}$$

$z_G<0$: stable oscillation

$z_G>0$: instability

initial perturbation $\delta\theta_0$, $(\mathrm{d}\delta\theta/\mathrm{d}t)_0$

solution
$$\begin{aligned}\delta\theta(t) &= A \exp\left(\frac{t}{\tau}\right) + B \exp\left(-\frac{t}{\tau}\right), \\ &= \delta\theta_0 \cosh\left(\frac{t}{\tau}\right) + \tau \left(\frac{\mathrm{d}\delta\theta}{\mathrm{d}t}\right)_0 \sinh\left(\frac{t}{\tau}\right).\end{aligned}$$

growth rate $$\omega_i \equiv \frac{1}{\tau} \equiv \left(\frac{-g}{z_G}\right)^{\frac{1}{2}}$$ (note: ω_i is independent of the mass)

Similarly, fluid instabilities develop on a stationary flow when the restoring forces result in an exponential amplification of the initial perturbation: e.g. a flapping flag, convective clouds...

Perturbative analysis

Example: perturbation of a uniform ideal gas with uniform velocity v_0 along the x direction

$$\frac{\partial \rho}{\partial t} + \nabla \cdot (\rho v) = 0,$$
$$\frac{\partial v}{\partial t} + (v \cdot \nabla) v + \frac{\nabla P}{\rho} = 0,$$
$$\frac{\partial S}{\partial t} + v \cdot \nabla S = 0.$$

$$\rho \equiv \rho_0 + \delta\rho,$$
$$v \equiv v_0 + \delta v,$$
$$P \equiv P_0 + \delta P,$$
$$S \equiv S_0 + \delta S.$$

Linearizing = keeping the first order terms

Since the unperturbed flow is stationary, a Fourier transform in time simplifies the time derivatives into multiplications by -iω →the solution is thus a combination of exponential functions exp(-iωt)

If the stationary flow is uniform, a Fourier transform in space simplifies the differential system into an algebraic system: $\exp(ik_x x+ik_y y)$

The relation between the eigenfrqequency ω and the wavenumber k of the perturbation is the dispersion relation.

$$\frac{\partial \delta\rho}{\partial t} + \nabla \cdot (\rho_0 \delta v + v_0 \delta\rho) = 0,$$
$$\frac{\partial \delta v}{\partial t} + (v_0 \cdot \nabla) \delta v + \frac{\nabla \delta P}{\rho_0} = 0,$$
$$\frac{\partial \delta S}{\partial t} + v_0 \cdot \nabla \delta S = 0.$$

→

$$(\omega - k_x v_0)\frac{\delta\rho}{\rho_0} = k \cdot \delta v,$$
$$(\omega - k_x v_0)\delta v = \frac{k}{\rho_0}\delta P,$$
$$(\omega - k_x v_0)\delta S = 0.$$

The three types of perturbations in a gas

$$(\omega - k_x v_0)\frac{\delta\rho}{\rho_0} = k\cdot\delta v,$$
$$(\omega - k_x v_0)\delta v = \frac{k}{\rho_0}\delta P,$$
$$(\omega - k_x v_0)\delta S = 0.$$

if $\delta S \neq 0$ then $\omega = k_x v_0$ and $\delta P = 0$: entropy perturbations are incompressible

If δS=0, then $\delta P = c_0^2 \delta\rho$ and $(\omega - k_x v_0)^2 \delta v = c_0^2 (k\cdot\delta v) k.$

If $\omega \neq k_x v_0$ the velocity perturbation δv is parallel to the wave vector k: acoustic perturbations are irrotational (kxδv=0). Their dispersion relation is $(\omega - k_x v_0)^2 = k^2 c_0^2$

Conversely, if δS=0 and $\omega = k_x v_0$ the perturbation is incompressible and corresponds to a vorticity perturbation advected with the flow.

In summary, three types of perturbations exist in a ideal uniform gas:

- -entropy perturbations
- -vorticity perturbations

} incompressible and advected with the flow, $\omega = k_x v_0$

- -acoustic waves — irrotational and adiabatic, $(\omega - k_x v_0)^2 = k^2 c_0^2$

Warning: non-uniform regions of the flow are regions of linear coupling between these 3 types of "waves"

Some examples of fluid instabilities

Gravitational potential:

Rayleigh-Taylor instability: feeds on potential energy, by carrying down dense matter exchanged with lighter matter

Sheared flow:

Kelvin-Helmholtz instability: feeds on sheared velocities, tends to smoothen the velocity gradient

Rotating flow:

Corotation instability: feeds on differential rotation and exchange angular momentum through a spiral acoustic wave

Magnetorotational instability: feeds on sheared velocities in a MHD flow, exchanging angular momentum along the field lines connecting different radial positions

Shocked flow:

Ritchmeyer Meshkov instability: similar to RT with an impulsional acceleration due to the crossing of a density interface by a shock

Standing accretion shock instability: advective-acoustic interplay of the shock surface and a downstream region of gradients

Outline

Impact of hydrodynamics the explosion physics

2D vs 3D

The basics of hydrodynamical instabilities

Neutrino driven convection

The Standing Accretion shock instability

Rotational effects: spiral SASI, low T/W, MRI

Instability of a top heavy disc

Denoting by I~$MR^2/2$ the moment of inertia of a disc with radius R and mass M
a density distribution $\rho(z)$ with a transition from ρ_{down} to ρ_{up} over a lengthscale $H=\rho/(d\rho/dz)$
z_G is the height of the center of mass above the geometric center.
The linearized variation of the angular momentum is ruled by the equation

$$I\frac{\mathrm{d}^2\theta}{\mathrm{d}t^2} - Mgz_G\theta = 0 \qquad \omega^2 = \left(\frac{MR^2}{2I}\right)\frac{gz_G}{R^2}.$$

If R>>H,
$$z_G \equiv \frac{1}{M}\int_0^{\frac{\pi}{2}} 2\rho R^3 \sin\theta\cos^2\theta \mathrm{d}\theta, = \frac{4R}{3\pi}\left(\frac{\rho_{up}-\rho_{down}}{\rho_{up}+\rho_{down}}\right).$$
the growth rate (or oscillation frequency) is thus

$$\boxed{\omega^2 = -\frac{8g}{3\pi R}\left(\frac{MR^2}{2I}\right)\left(\frac{\rho_{down}-\rho_{up}}{\rho_{down}+\rho_{up}}\right)}$$

$$g = -\nabla\Phi$$

→As for a pendulum, the smaller the disc, the shorter the time scale.

If R<<H, the density distribution is linearly approximated $\rho = \rho_0\left(1+\frac{z}{H}\right)$

$$z_G \equiv \frac{1}{M}\int_0^{\frac{\pi}{2}} 2\rho_0\left(1+\frac{R}{H}\sin\theta\right)R^3\sin\theta\cos^2\theta \mathrm{d}\theta, = \frac{R^2}{4H}.$$

the growth rate is: $\boxed{\omega^2 = \frac{g}{2H}\left(\frac{MR^2}{2I}\right)}$

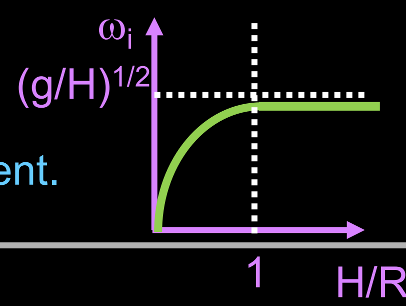

→As the radius of the disc decreases, the growth rate ω_i increases like ~$(g/R)^{1/2}$
and reaches a maximum ~$(g/H)^{1/2}$ as R approaches the scale H of the density gradient.

Instability of a top heavy superposition of incompressible fluids

Two incompressible fluids with uniform densities $\rho_{up} > \rho_{down}$

$$\frac{\partial \rho}{\partial t} + \nabla \cdot \rho v = 0,$$
$$\frac{\partial v}{\partial t} + (v \cdot \nabla) v + \frac{\nabla P}{\rho} + \nabla \Phi = 0.$$

$$g = -\nabla \Phi$$

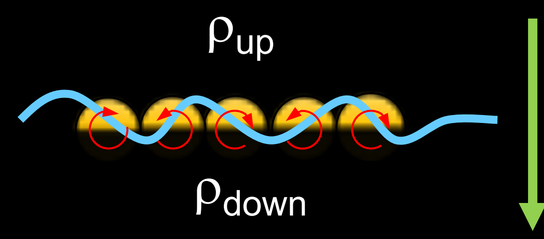

Linearizing, + Fourier transform in time and space: $\exp(-i\omega t + ik_x x + ik_z z)$

$$ik \cdot \delta v = 0,$$
$$-i\omega \delta v + ik \frac{\delta P}{\rho} = 0.$$
$$\rightarrow \quad k^2 \frac{\delta P}{\rho} = 0 \quad \rightarrow \quad k_x^2 + k_z^2 = 0 \quad \rightarrow \quad k_z = \pm i k_x$$

$$k_x \delta v_x + k_z \delta v_z = 0,$$
$$-i\omega \delta v_x + ik_x \frac{\delta P}{\rho} = 0,$$
$$-i\omega \delta v_z + ik_z \frac{\delta P}{\rho} = 0.$$

$$\delta v_z = -i\omega \; \delta\zeta \; \mathrm{e}^{-k_x|z|} \mathrm{e}^{ik_x x},$$
$$\delta v_x = \mp\omega \; \delta\zeta \; \mathrm{e}^{-k_x|z|} \mathrm{e}^{ik_x x},$$
$$\delta P = \pm \frac{\omega^2}{k_x} \rho \; \delta\zeta \; \mathrm{e}^{-k_x|z|} \mathrm{e}^{ik_x x}.$$

Boundary condition: continuity of the interface pressure $P(\zeta) + \delta P$ at $z = \zeta$

$$\delta P_{\mathrm{up}} + \rho_{\mathrm{up}} g \delta\xi = \delta P_{\mathrm{down}} + \rho_{\mathrm{down}} g \delta\xi$$

$$\omega^2 = -\underbrace{\left(\frac{\rho_{\mathrm{down}} - \rho_{\mathrm{up}}}{\rho_{\mathrm{down}} + \rho_{\mathrm{up}}} \right)}_{\text{Atwood number}} k_x g$$

The Rayleigh Taylor instability from solid to fluid mechanics

A solid mechanics analogue of the RT instability is a disc of radius R with a top heavy mass distribution from ρ to ρ+Δρ and a transition zone extended over a distance H from the rotation axis

if H/R<<1 $$\omega^2 \sim \frac{\Delta\rho}{\rho}\frac{g}{R}$$

if H/R>>1 $$\omega^2 \sim \frac{g}{2H}$$

The incompressible version of the RT instability is the instability of a dense fluid over a light fluid, noting k the horizontal wavelength and H the lengthscale of the density transition from ρ to ρ+Δρ

if kH<<1, $$\omega^2 \sim \frac{\Delta\rho}{\rho}kg$$

if kH>>1 $$\omega^2 \sim \frac{g}{H}$$

In a gas in pressure equilibrium in a gravitational field, the vertical displacement of a blob of gas leads to an adiabatic change of its density to adapt to the local pressure.
The density of the blob carried upward is lighter than the surrounding gas if the entropy decreases upward:

$$\rho \propto P^{\frac{1}{\gamma}} \exp\left(-\frac{\gamma-1}{\gamma}S\right)$$

if kH>>1 $$\omega_{\rm BV}^2 \sim \frac{g}{\rho}\left(\frac{\partial\rho}{\partial z}\right)_{P={\rm cte}} = -\frac{\gamma-1}{\gamma}g\nabla S$$

The Brunt Väisälä frequency ω_{BV} is the frequency of perturbations with a short horizontal wavelength compared to the stratification scale height.

The Rayleigh Taylor instability in core collapse supernovae

The oscillations driven by the buoyancy force are called internal gravity waves.

The vertical gradients of electron fraction participate in the same manner to the stability criterion.

The generalized Brunt Väisälä frequency is:

$$\omega_{\mathrm{BV}}^2 = -\frac{1}{\rho}\left[\left(\frac{\partial\rho}{\partial S}\right)_{Y_\mathrm{e},P}\frac{\mathrm{d}S}{\mathrm{d}r} + \left(\frac{\partial\rho}{\partial Y_\mathrm{e}}\right)_{S,P}\frac{\mathrm{d}Y_\mathrm{e}}{\mathrm{d}r}\right]\frac{\mathrm{d}\Phi}{\mathrm{d}r}.$$

The possibility to enhance the neutrino luminosity of the proto-neutron star through lepton-driven convective instability has been proposed by Epstein (1979)

3 locations where transverse motions can feed on potential energy:

-the negative entropy gradient left by the deceleration of the shock until it stalls at 150km: "prompt convection"

-the gradient of electronic pressure inside the proto-neutron star "thermolepton convection"

-"neutrino-driven convection" in the gain region

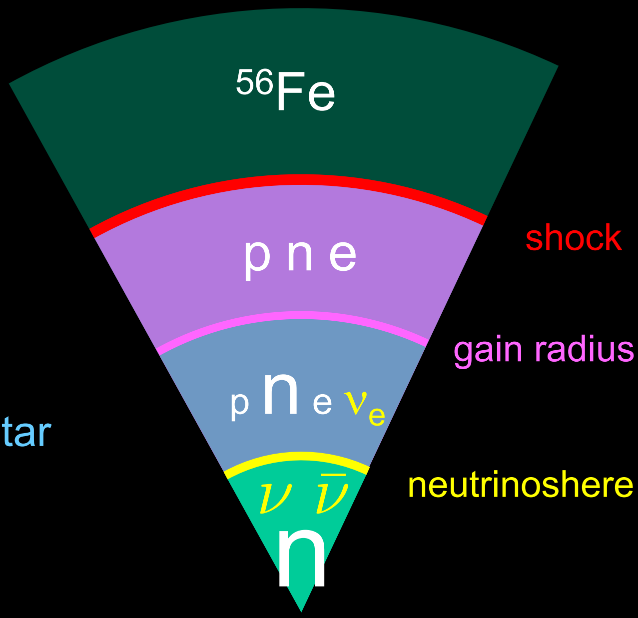

The Rayleigh Taylor instability in core collapse supernovae

Prompt convection is transient and does not affect the explosion threshold.

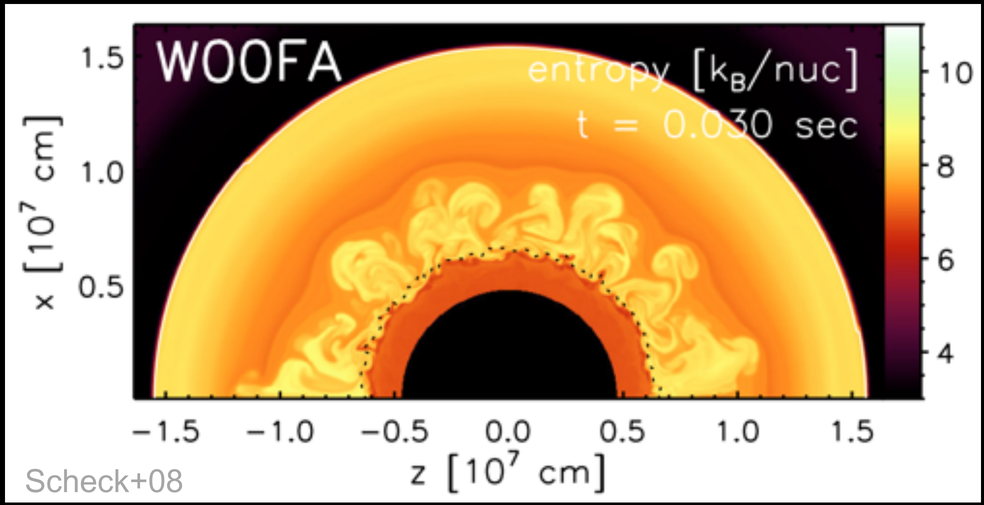

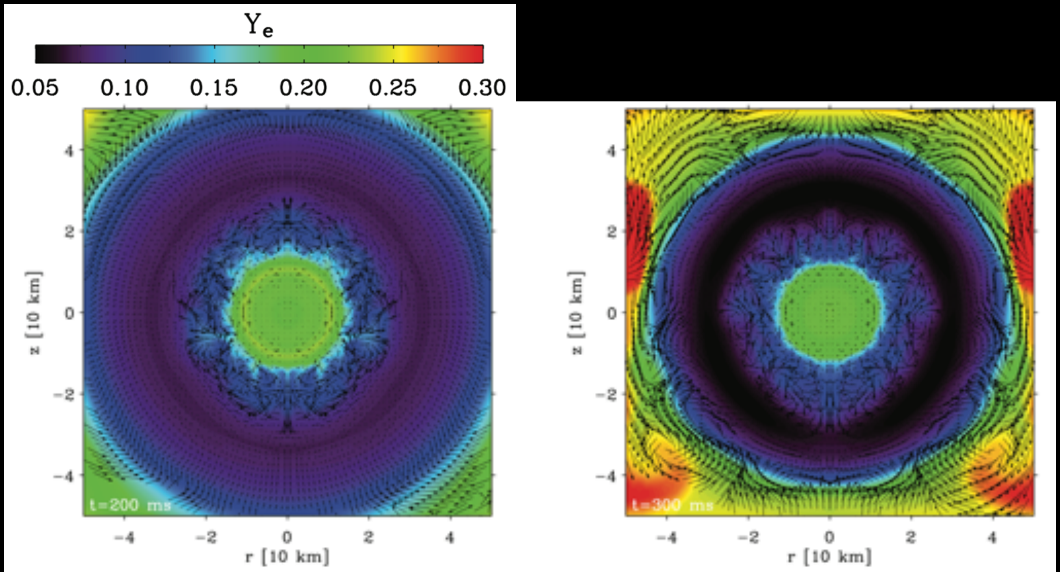

The proto-neutron star convection is embedded in a stably stratified region.
It has a moderate impact on the neutrino luminosity, at a 10-20% level (Dessart+06, Buras+06, Müller & Janka 14)

However, it may contribute to the amplification of magnetic fields (Thompson & Duncan 93).

Dessart+06

Neutrino-driven convection in the gain region

Foglizzo +06

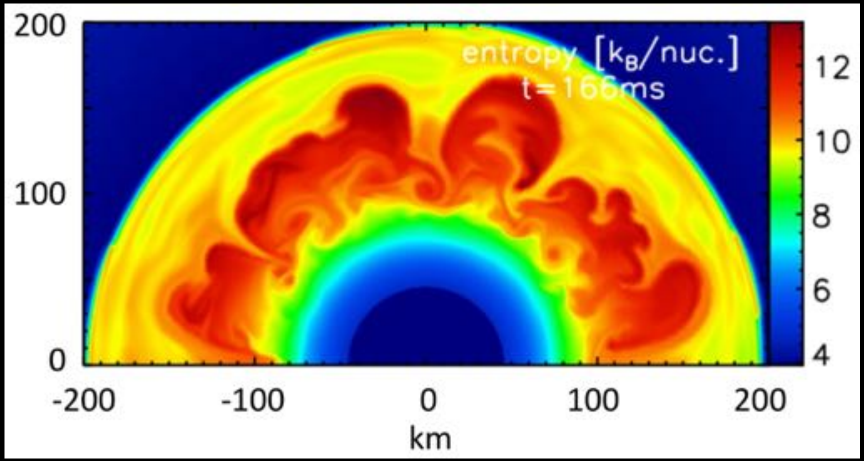

The negative entropy gradient is fed by the absorption in the gain region of neutrinos diffusing out of the neutrinosphere.

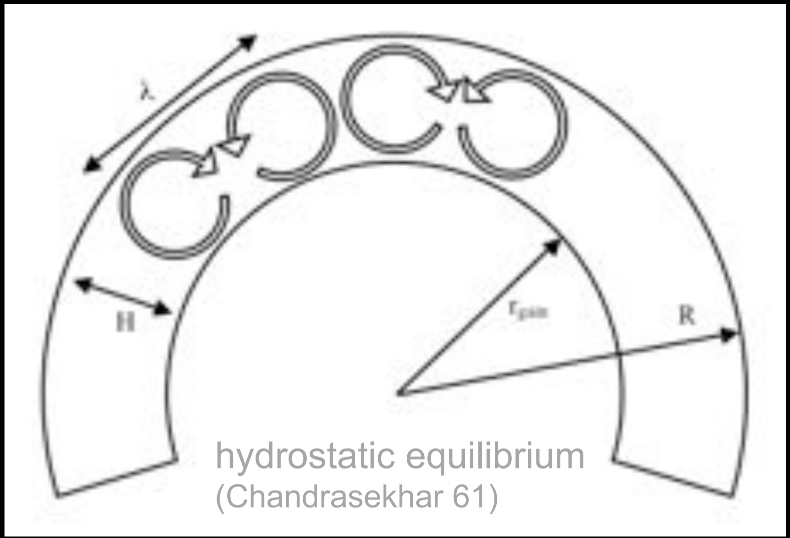

$$\omega_{\rm buoy} \equiv G^{1/2}\left|\frac{\nabla P}{\gamma P} - \frac{\nabla\rho}{\rho}\right|^{1/2} = \left(\frac{\gamma-1}{\gamma} G\nabla S\right)^{1/2}, \sim \left(\frac{G}{H}\right)^{1/2}.$$

The size of the largest unstable convective cells is comparable to the size of the gain region

$$l \sim \frac{\pi}{2}\frac{R + r_{\rm gain}}{H}$$

Neutrino-driven convection in the gain region

Foglizzo +06

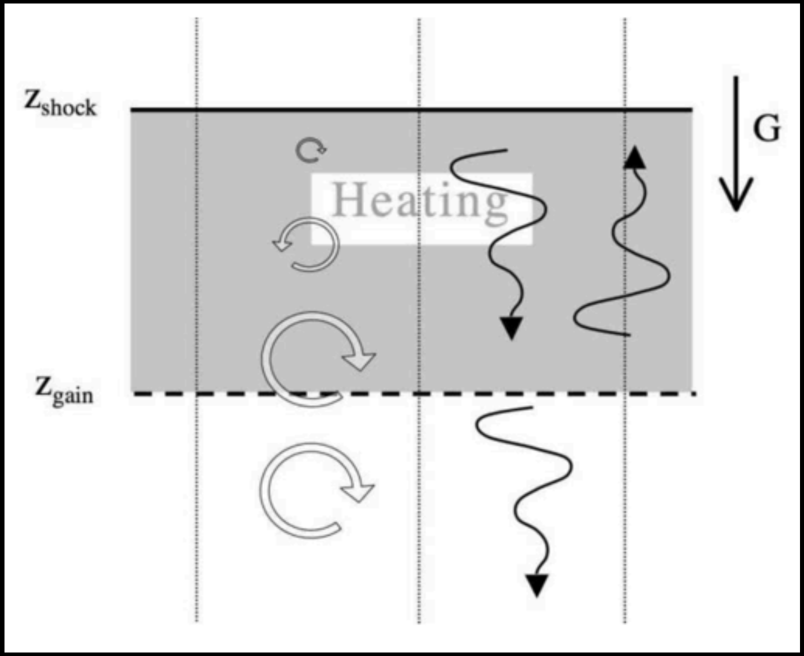

A planar toy model to study the RT instability below a stationary shock

Despite the negative entropy gradient, the flow is linearly stable if $\chi<\chi_{crit}$~3

$$\chi \equiv \int_{\rm gain}^{\rm shock} \omega_{\rm BV} \frac{{\rm d}r}{v_r} \sim \frac{\tau_{\rm adv}}{\tau_{\rm buoy}}$$

The local timescale of convection must be compared to the timescale of advection through the gain region

$$\frac{H\omega_{\rm buoy}}{v} \sim \left(\frac{\mathcal{G}M}{r_{\rm sh}v_2^2}\right)^{\frac{1}{2}} \left(\frac{H}{r_{\rm sh}}\right)^{\frac{1}{2}}$$

$$\sim 3.1 \left(\frac{v_1}{7v_2}\right) \left(\frac{H}{0.4r_{\rm sh}}\right)^{\frac{1}{2}}$$

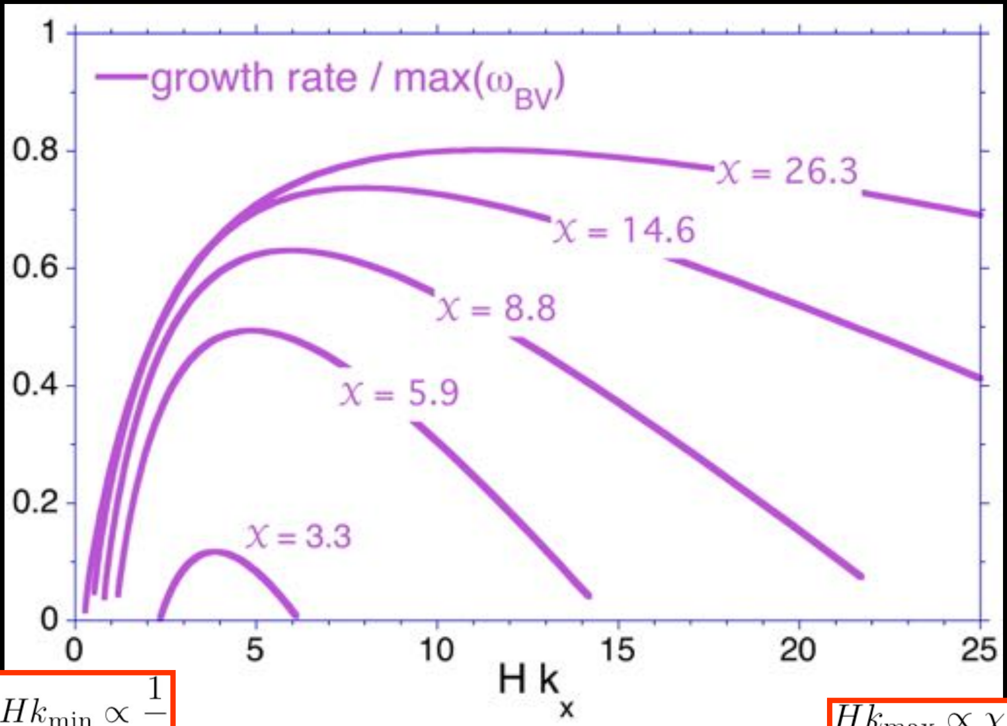

$Hk_{\rm min} \propto \frac{1}{\chi}$

$Hk_{\rm max} \propto \chi$

horizontal wavenumber

$$\chi \equiv \int_{\rm gain}^{\rm shock} \omega_{\rm BV} \frac{{\rm d}r}{v_r} \sim \frac{\tau_{\rm adv}}{\tau_{\rm buoy}}$$

Convection vs advection in 2D

Test case: a planar subsonic toy model without a shock

$\chi_{crit}=2$

Kazeroni +17

$\chi = 1.5$ $\frac{\delta\rho}{\rho} = 0.01\%$ $\chi = 5.0$

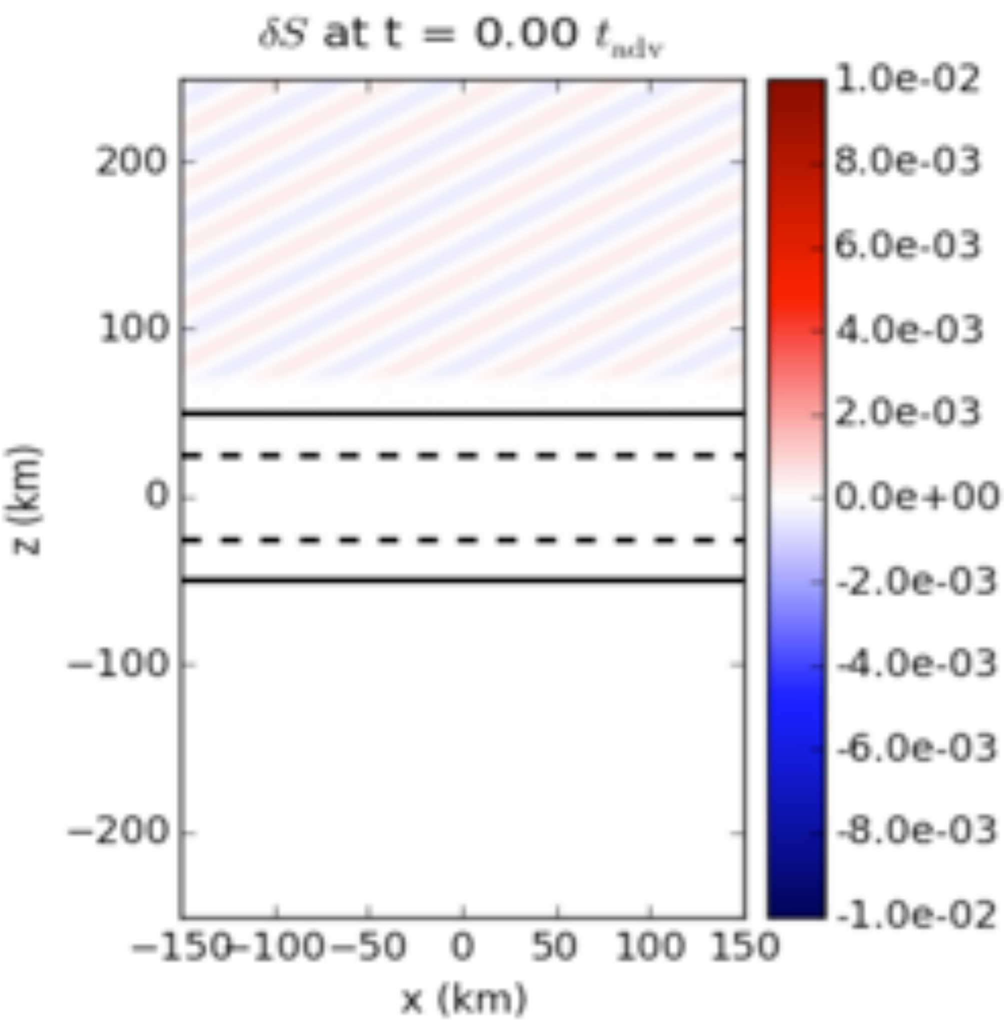

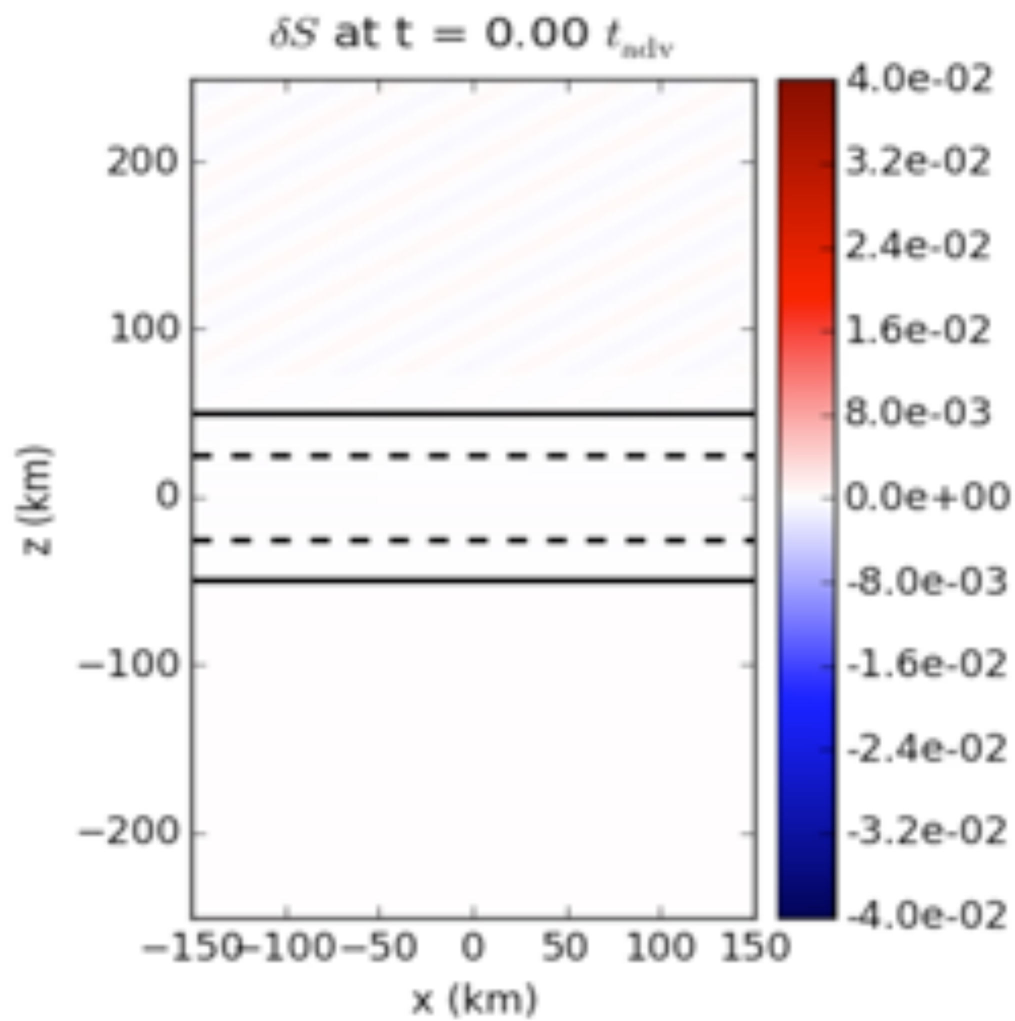

Convection vs advection in 2D/3D

Kazeroni +17

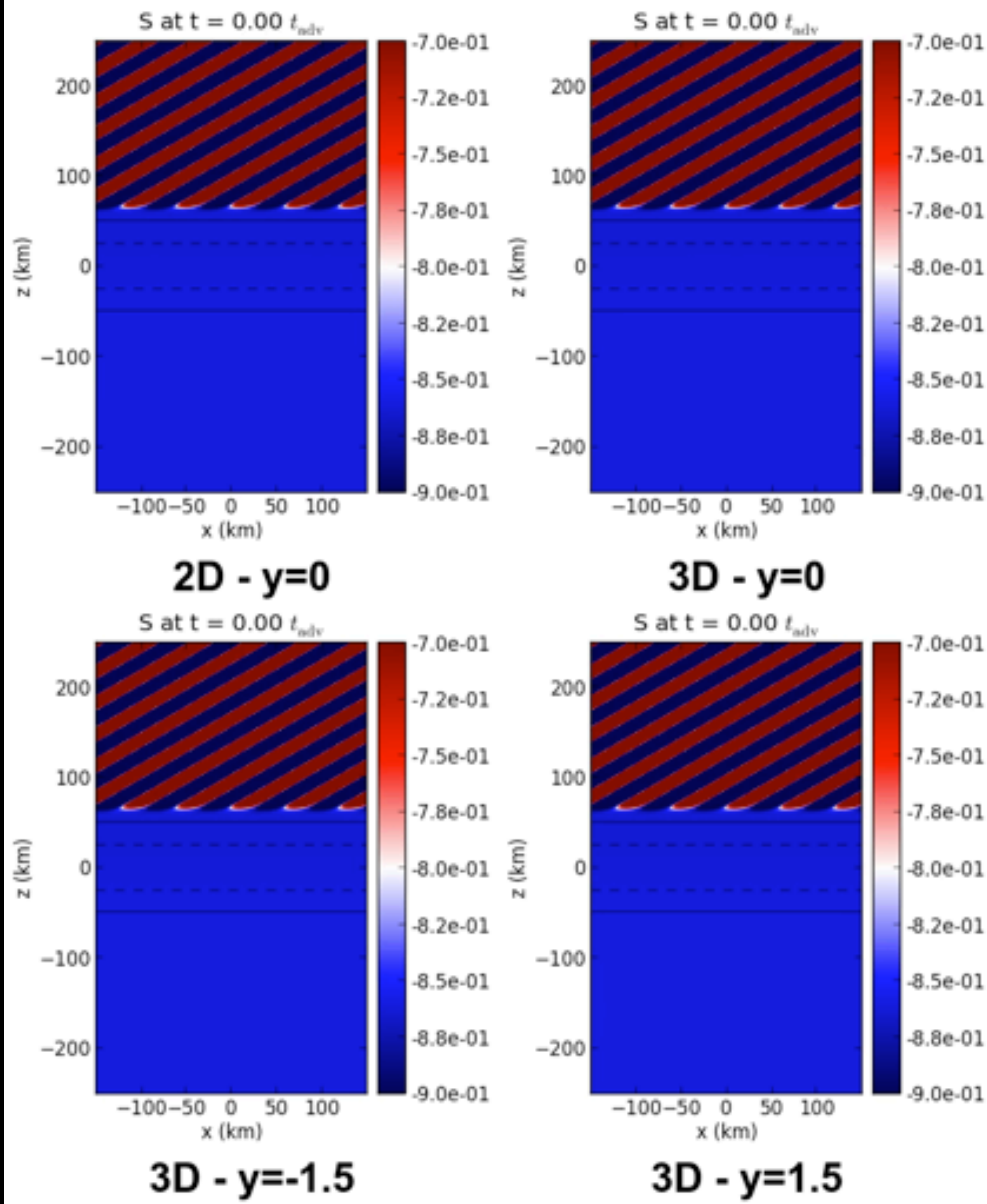

$$\chi \equiv \int_{\mathrm{gain}}^{\mathrm{shock}} \omega_{\mathrm{BV}} \frac{\mathrm{d}r}{v_r} \sim \frac{\tau_{\mathrm{adv}}}{\tau_{\mathrm{buoy}}}$$

$$\chi = 1.5 < \chi_{\mathrm{crit}} = 2$$

$$\frac{\delta\rho}{\rho} = 30\%$$

Density perturbations with a very large amplitude are buoyant but ultimately washed away if $\chi<\chi_{crit}$

Self sustained convective motions last longer if χ is close to the linear stability threshold χ_{crit}

Their evacuation is faster in 2D than in 3D

Convection vs advection in 2D/3D

Kazeroni +17

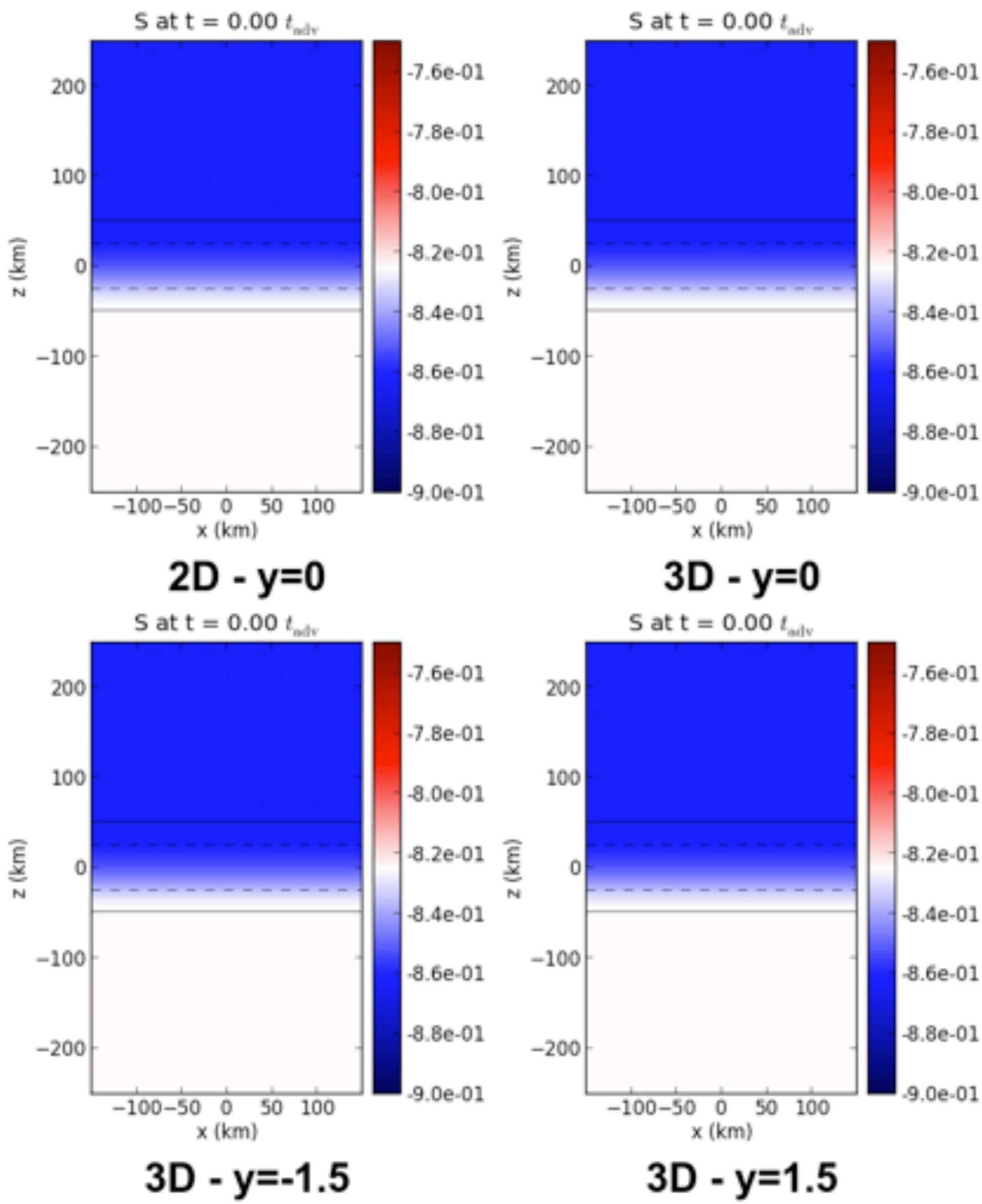

$$\chi \equiv \int_{\mathrm{gain}}^{\mathrm{shock}} \omega_{\mathrm{BV}} \frac{\mathrm{d}r}{v_r} \sim \frac{\tau_{\mathrm{adv}}}{\tau_{\mathrm{buoy}}}$$

$$\chi = 5 > \chi_{\mathrm{crit}} = 2$$

$$\frac{\delta\rho}{\rho} = 0.1\%$$

Density perturbations with a small amplitude are linearly unstable if $\chi > \chi_{crit}$

The linear phase of the instability is identical in 2D and 3D

Their non linear saturation is stronger in 3D than in 2D despite the stronger mixing in 3D

→favourable to 3D explosions

Outline

Impact of hydrodynamics the explosion physics

2D vs 3D

The basics of hydrodynamical instabilities

Neutrino driven convection

The Standing Accretion shock instability

Rotational effects: spiral SASI, low T/W, MRI

Instability of the stationary shock even without neutrino heating

The Standing Accretion Shock Instability has been found in simulations by Blondin+03 using a 2D axisymmetric stationary flow of a perfect gas $\gamma=1.25$ with a cooling function

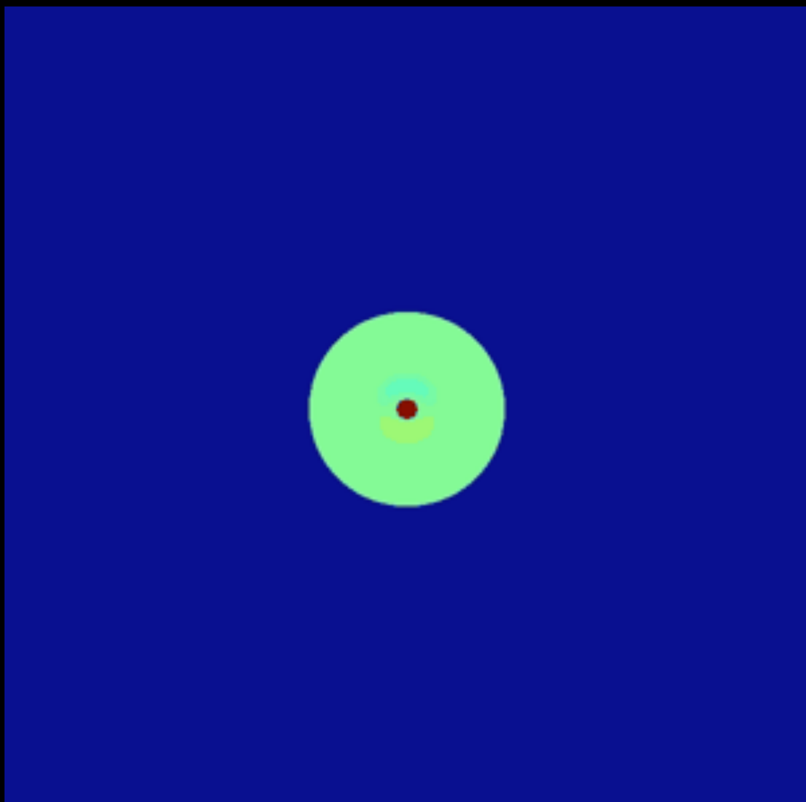

Blondin+03

The instability SASI in the linear regime is
-dominated by l=1,2 spherical harmonics
-exponential growth with oscillations with a period~30ms

By contrast, neutrino-driven convection is
-dominated by smaller angular scales l=5,6
-exponential growth without oscillations

The mechanism has been identified as the interplay of advected and pressure perturbations

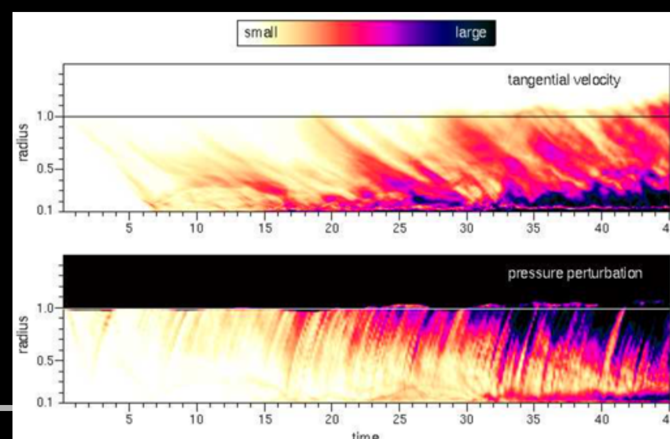

Blondin+03

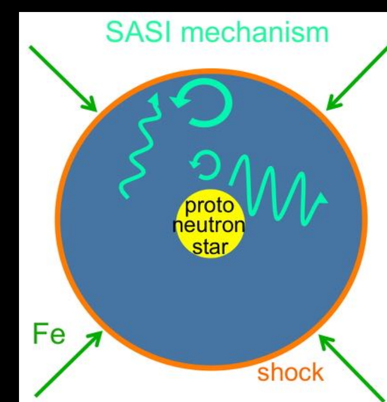

Advective-pressure cycle in simplified simulations of core-collapse

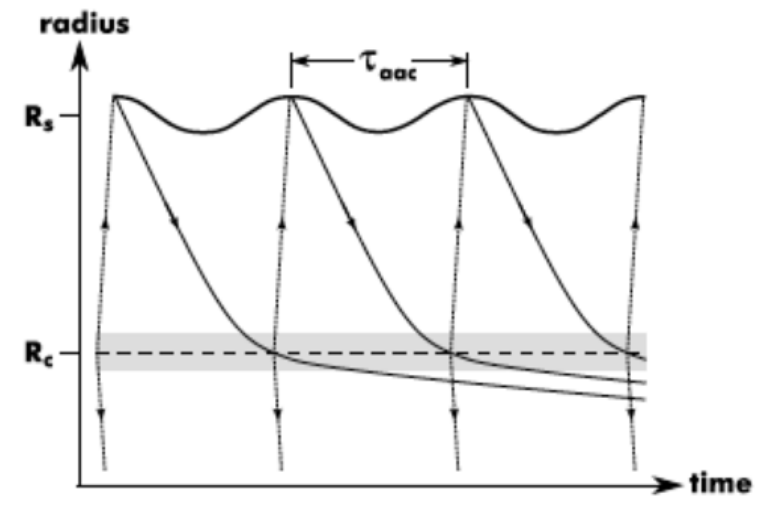

Scheck+08

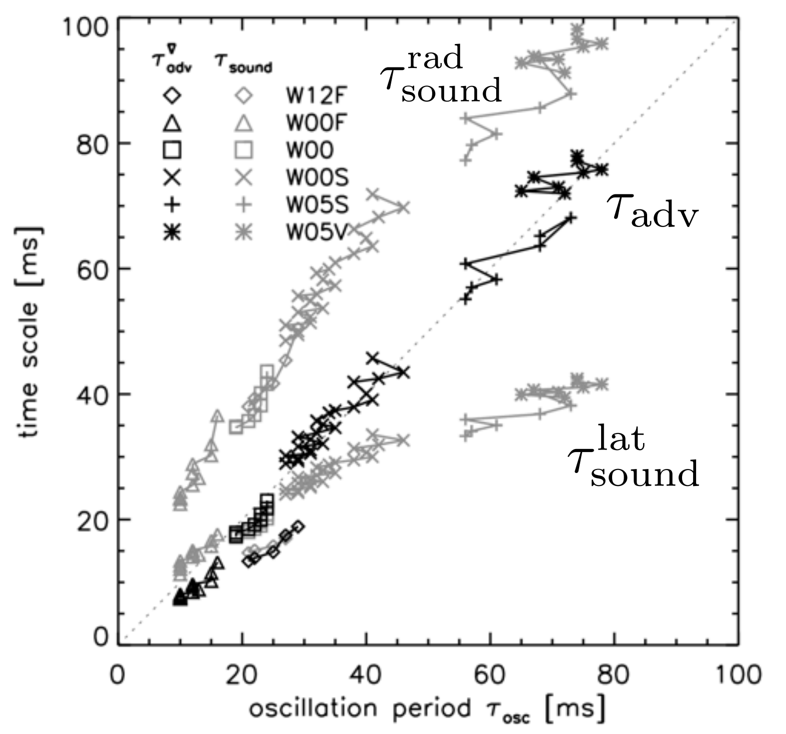

The feedback region of dominant advective-pressure coupling is identified as the radius of deceleration R_{∇} where the velocity gradients are strongest

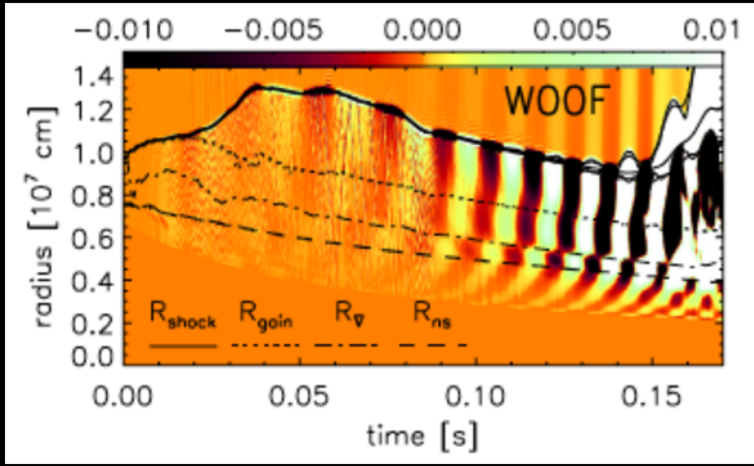

The timescale of the oscillation is better correlated with the advection timescale τ_{adv} than with the sound crossing times, either radial τ^{rad}_{sound} or azimuthal τ^{lat}_{sound}

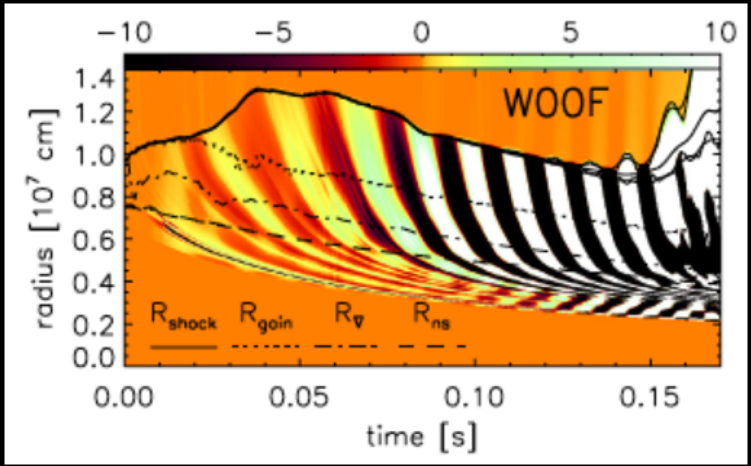

Scheck+08

$$\tau_{adv} \equiv \int_{\nabla}^{sh} \frac{dr}{v}$$

$$\tau^{rad}_{sound} \equiv 2\left(\int^{sh} \frac{dr}{c-v} + \int^{sh} \frac{dr}{c+v}\right)$$

$$\tau^{lat}_{sound} \equiv \frac{2\pi R_{sh}}{c_{sh}}$$

Should we trust the simulations of SASI ?

Validation of the simulations of SASI in the linear regime
(Blondin & Mezzacappa 06, Foglizzo+07, Fernandez & Thompson 09)

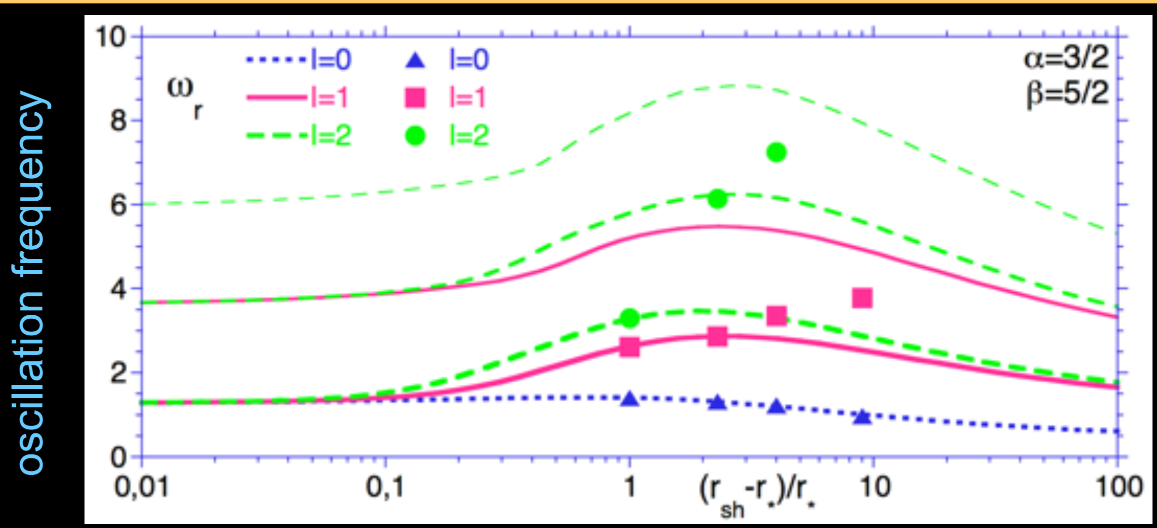

Foglizzo+07

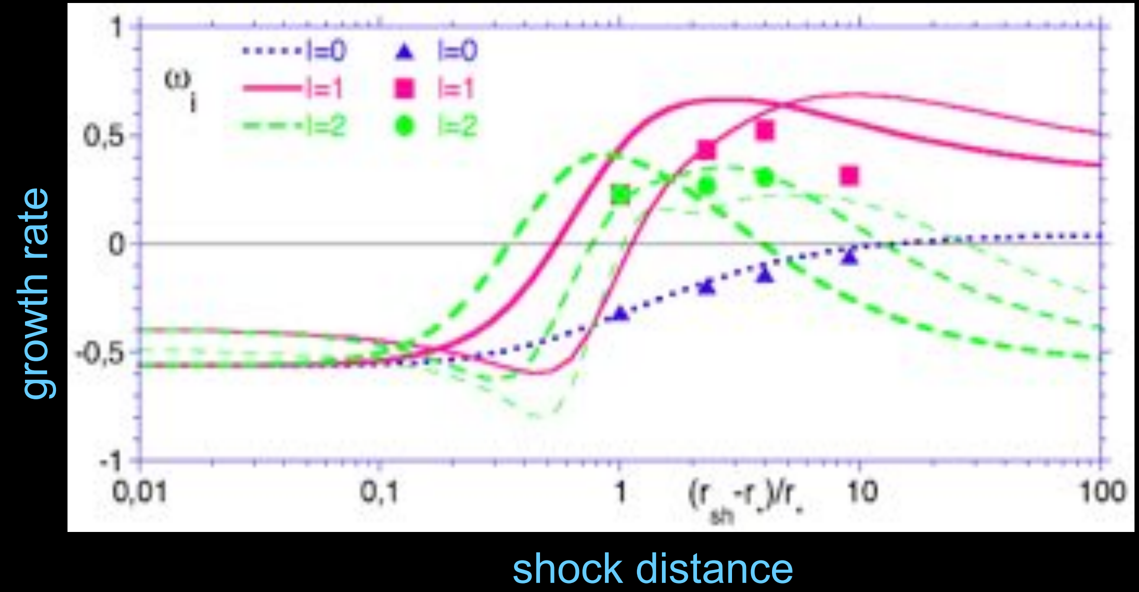

Comparing the eigenfrequencies to the perturbative approach is a good test of the minimum numerical resolution required for the linear stage.

The non linear stage can involve smaller scales and turbulence which can be difficult to capture numerically

Physical interpretation of the eigenspectrum using wave properties

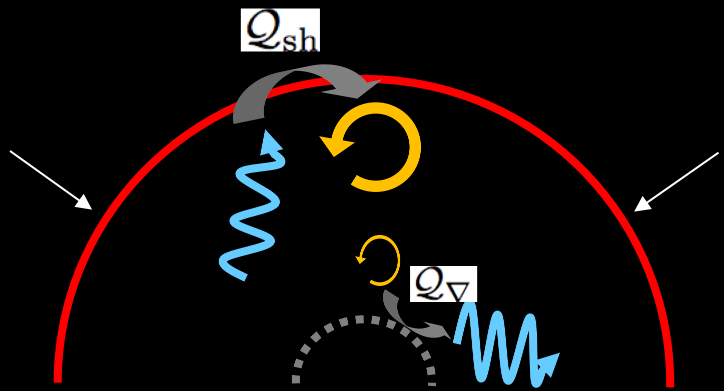

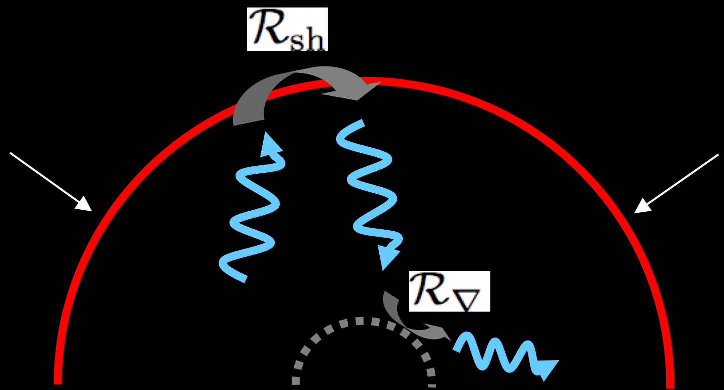

The calculation of the eigenspectrum solves a differential system with a discrete set of complex eigenfrequency.

It does not provide a physical explanantion

The calculation of wave properties and interactions relies on a differential system with a purely real frequency.

It requires additional approximations compared to the calculation of the eigenspectrum

-adiabatic approximation if possible, above the cooling layer and below the gain region

-WKB approximation except in coupling regions

-small growth rate compared to the oscillation frequency

These differences are best viewed in the analysis of the spherical model and plane parallel toy model (Foglizzo 09)

Advective-pressure cycle in a decelerated, cooled flow

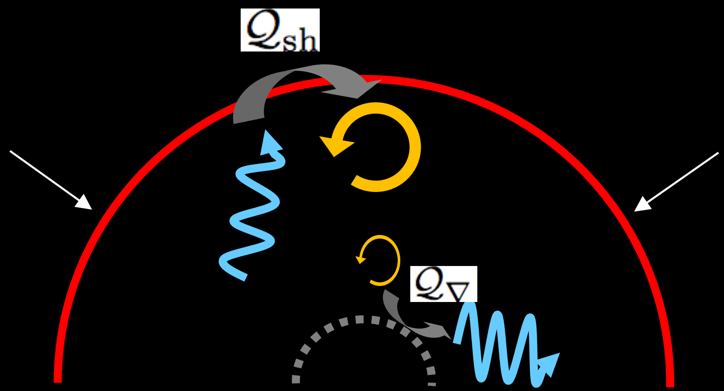

Unstable advective-acoustic cycle Q>1
Stable acoustic cycle R<1

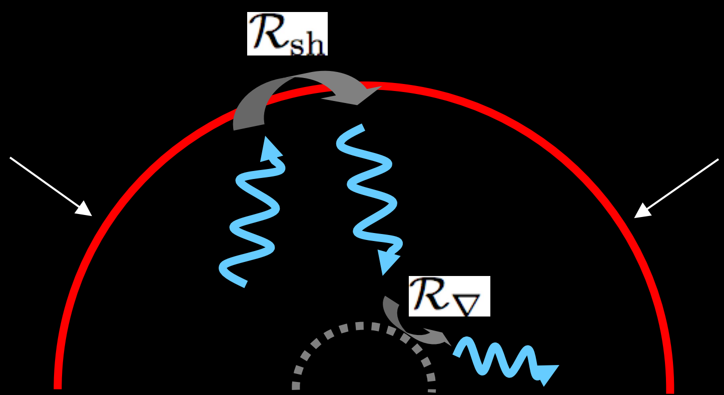

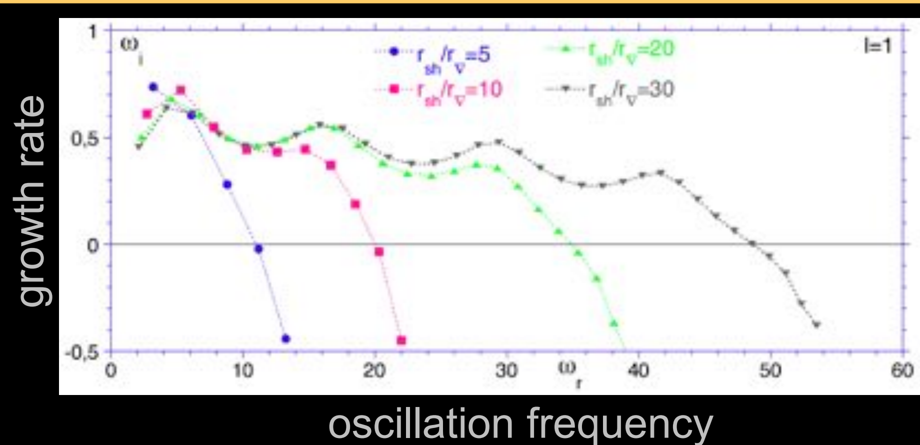

The oscillations $\omega_i(\omega_r)$ are the consequence of interferences between the advective-pressure and the purely acoustic cyles

The cycle efficiencies $Q(\omega)$, $R(\omega)$ can be deduced from the oscillations $\omega_i(\omega_r)$, or computed in the WKB limit which requires $r_{sh} >> r_{\nabla}$ (Foglizzo+07). The two cycles can also be discriminated using the frequency spacing of their harmonics (Guilet & Foglizzo 12)

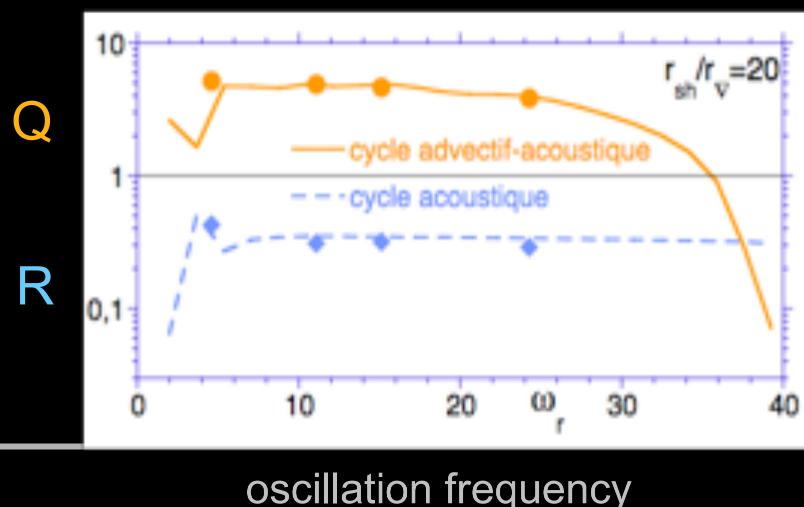

The instability mechanism for a small shock radius is extrapolated from the mechanism revealed by the WKB analysis for a larger radius

Interaction of advected and acoustic perturbations

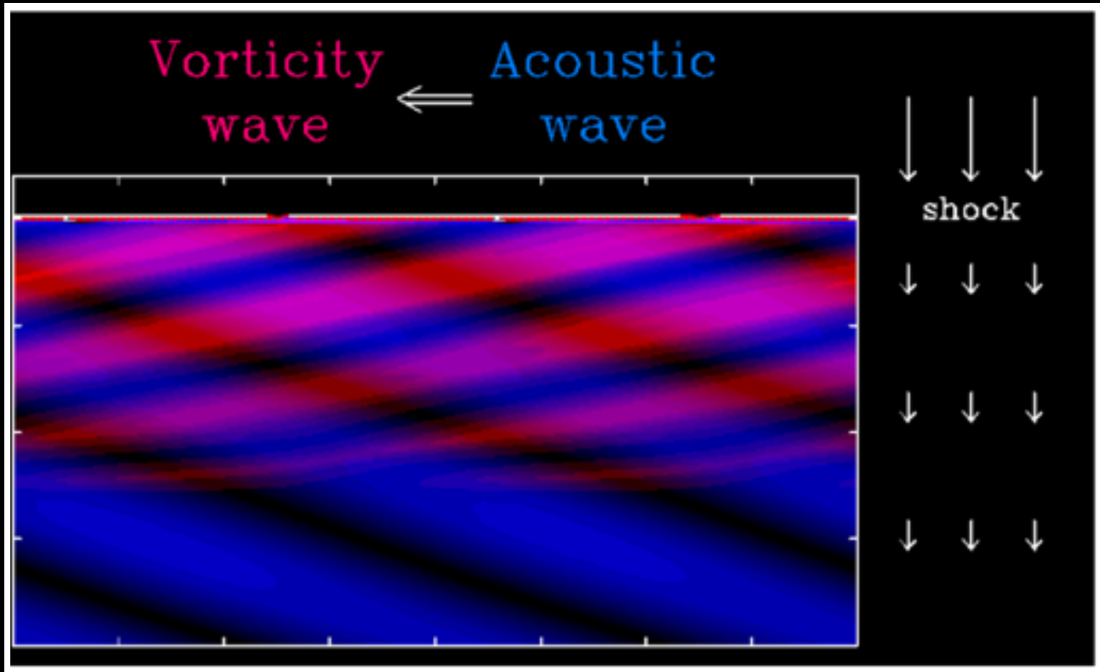

Sato+09

In a uniform stationary flow, advected and acoustic perturbations ignore each other.

If the stationary flow involves gradients, these perturbations are linearly coupled

The advected perturbations δS and δK are source terms in the acoustic equation

$$\frac{\partial^2}{\partial r^2}\frac{\delta p}{p}+a_1\frac{\partial}{\partial r}\frac{\delta p}{p}+a_0\frac{\delta p}{p}=b_0\delta S_{\rm R}+b_1\delta K_{\rm R}.$$

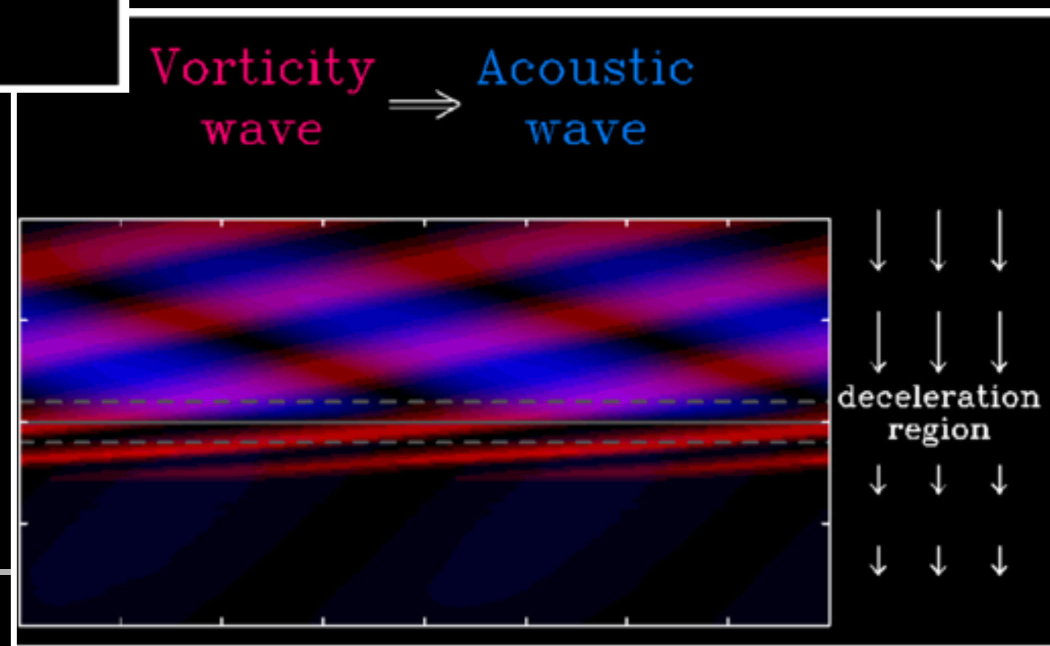

Interaction of advected and acoustic perturbations

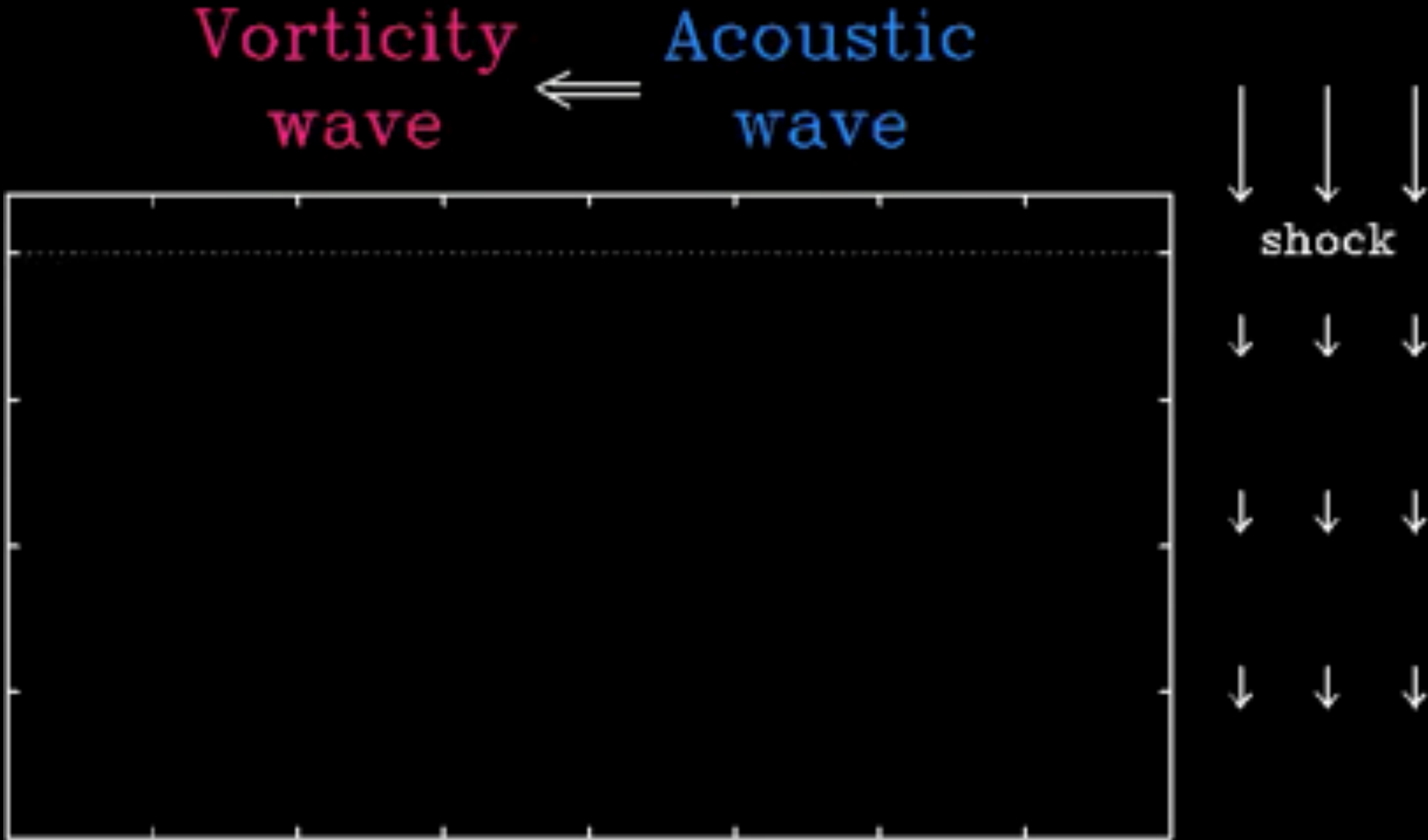

Interaction of advected and acoustic perturbations

Both entropic-acoustic and vortical-acoustic linear couplings can be understood intuitively

advection of entropy

↓

« entropic-acoustic » cycle

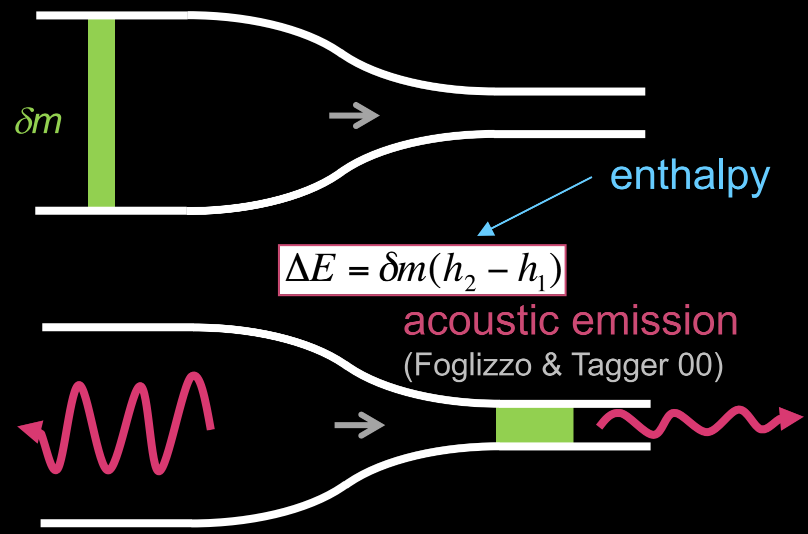

The expansion of a gas upon an adiabatic change of pressure depends on its entropy. Acoustic emission compensates for the change of advected energy: it is proportional to the enthalpy variation in the stationary flow.

advection of vorticity

↓

« vortical-acoustic » cycle

An advected vorticity perturbation cannot settle without breaking the pressure balance: it lifts up dense regions and push down lighter ones.

Shallow water analogue of the vortical-acoustic coupling

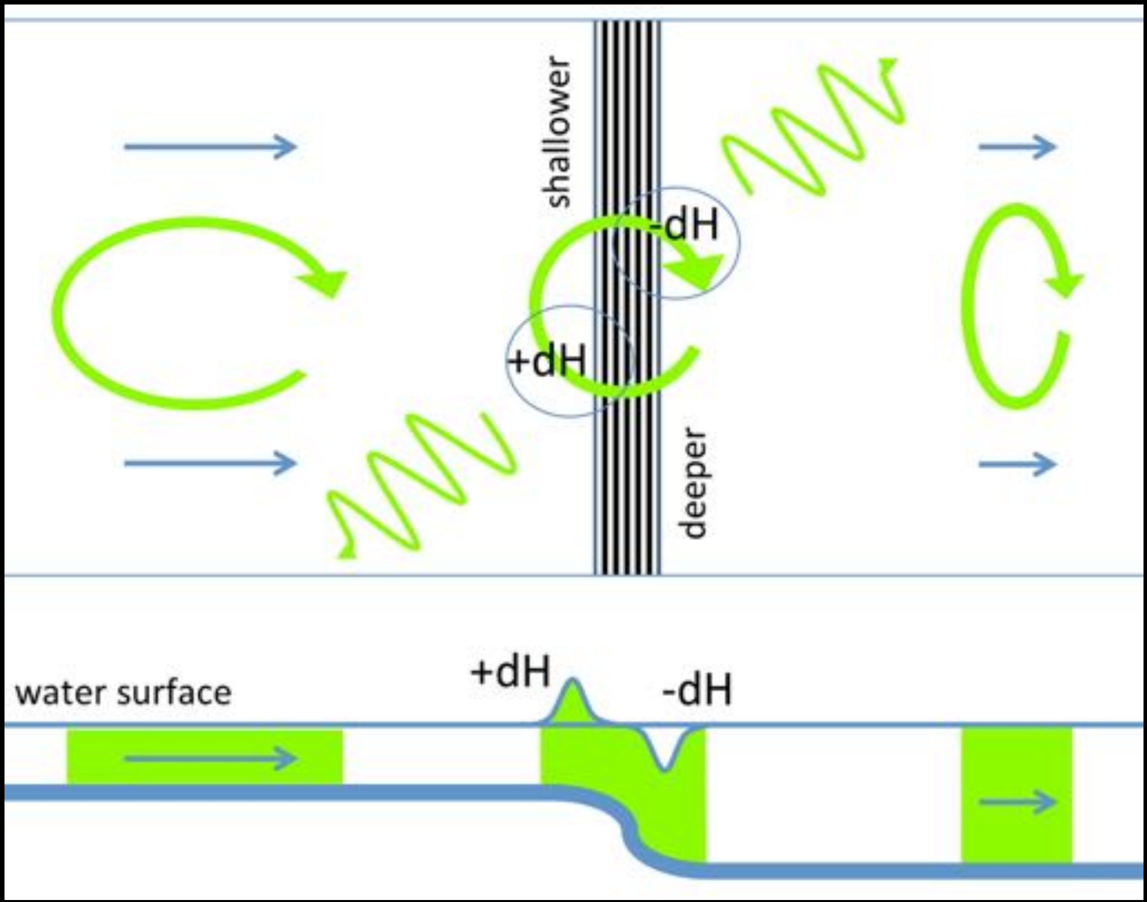

The vortical motion exchanges deep and shallow regions as the perturbation is advected over a change of depth

Aero-acoustic instabilities

- advected perturbations
- acoustic feedback

whistling kettle
Chanaud & Powell 65

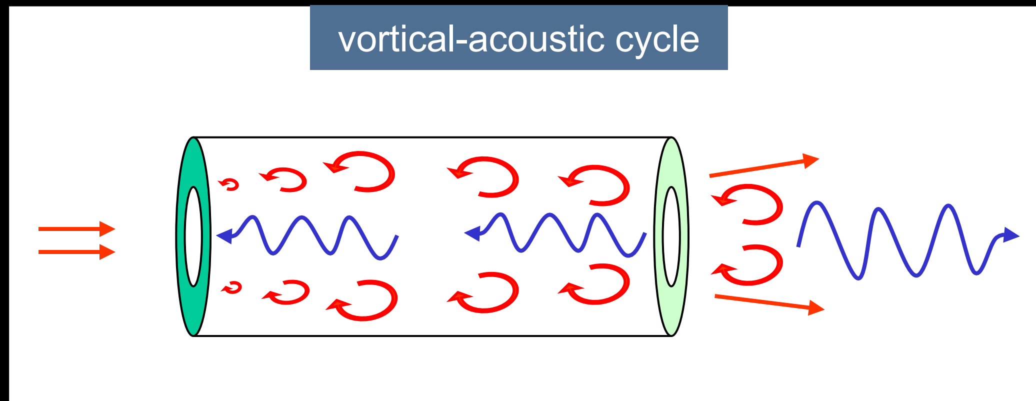

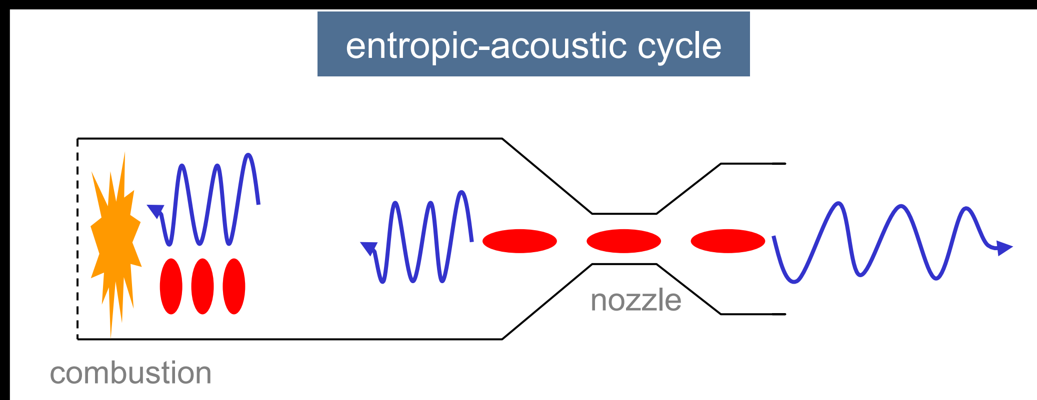

rumble instability of ramjets
Abouseif+84

vibrations
in Ariane 5
Mettenleiter+00

A planar toy model for the advective-acoustic coupling

The planar geometry and uniform flow between the shock and the compact deceleration region allows for a fully analytic calculation

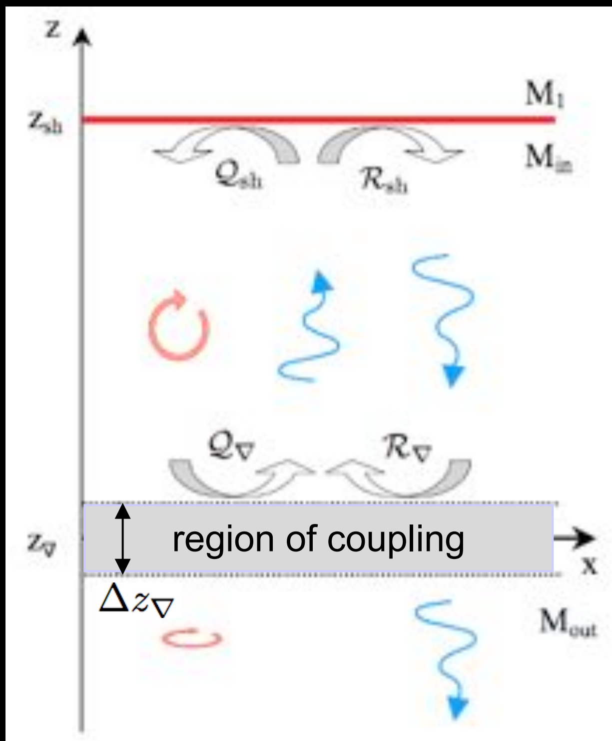

advective-acoustic cycle efficiency $\mathcal{Q} \equiv \mathcal{Q}_{sh}\mathcal{Q}_\nabla$

timescale $\tau_\mathcal{Q}$

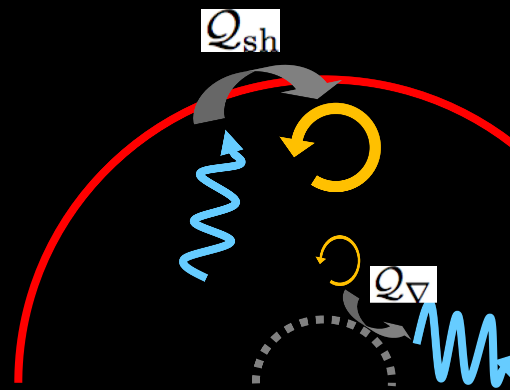

purely acoustic cycle efficiency $\mathcal{R} \equiv \mathcal{R}_{sh}\mathcal{R}_\nabla$

timescale $\tau_\mathcal{R}$

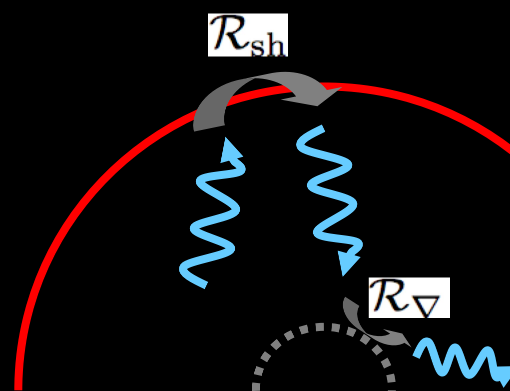

$$\mathcal{Q}e^{i\omega\tau_\mathcal{Q}} + \mathcal{R}e^{i\omega\tau_\mathcal{R}} = 1$$

Explicit analytical expressions for the coupling efficiencies for $\Delta z_\nabla \ll |z_{sh} - z_\nabla|$

A set of complex eigenfrequencies ω satisfy the phase equation relating the two cycles

$$\mathcal{Q}e^{i\omega\tau_\mathcal{Q}} + \mathcal{R}e^{i\omega\tau_\mathcal{R}} = 1$$

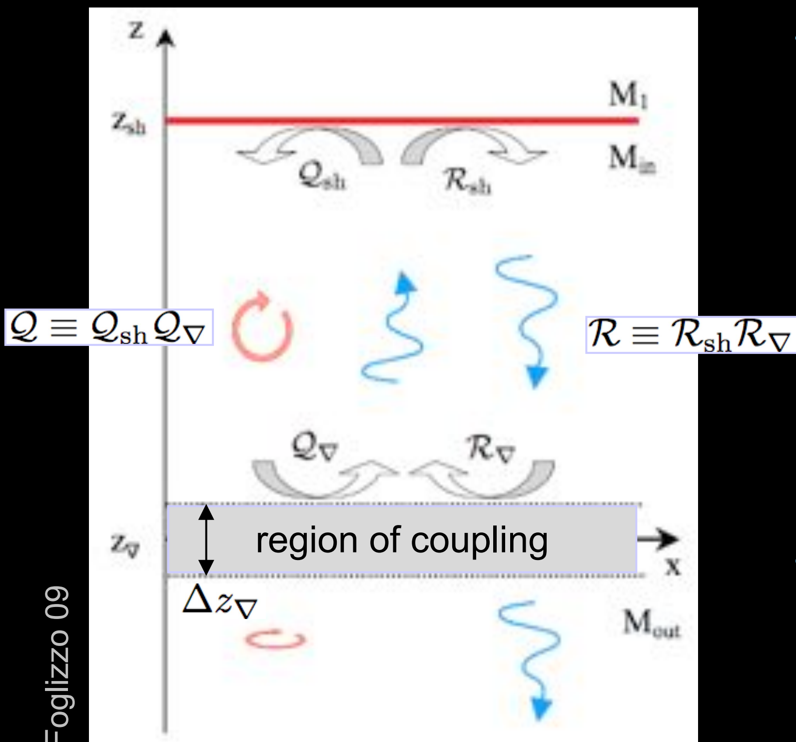

Foglizzo 09

$$\mu^2 \equiv 1 - \frac{k_x^2 c^2}{\omega^2}(1 - \mathcal{M}^2)$$

The coupling effciencies are defined from the ratio of energy densities δf^-, δf^+, δf_{adv} associated to acoustic and advected perturbations

R_{sh}, Q_{sh} are deduced from the conservation of mass, momentum and energy fluxes across a perturbed shock

$$\mathcal{R}_{\rm sh} \equiv \frac{\delta f_{\rm sh}^+}{\delta f_{\rm sh}^-} = \frac{1+\mu_{\rm sh}\mathcal{M}_{\rm sh}}{1-\mu_{\rm sh}\mathcal{M}_{\rm sh}}\frac{\delta p_{\rm sh}^+}{\delta p_{\rm sh}^-},$$

$$= -\frac{\mu_{\rm sh}^2 - 2\mathcal{M}_{\rm sh}\mu_{\rm sh} + \mathcal{M}_1^{-2}}{\mu_{\rm sh}^2 + 2\mathcal{M}_{\rm sh}\mu_{\rm sh} + \mathcal{M}_1^{-2}}\frac{1+\mu_{\rm sh}\mathcal{M}_{\rm sh}}{1-\mu_{\rm sh}\mathcal{M}_{\rm sh}}.$$

$$\mathcal{Q}_{\rm sh} \equiv \frac{\delta f_{\rm sh}^S}{\delta f_{\rm sh}^-} = \frac{1}{1-\mu_{\rm sh}\mathcal{M}_{\rm sh}}\frac{p_{\rm sh}\delta S_{\rm sh}}{\delta p_{\rm sh}^-},$$

$$= \frac{2}{\mathcal{M}_{\rm sh}}\frac{1-\mathcal{M}_{\rm sh}^2}{1+\gamma\mathcal{M}_{\rm sh}^2}\left(1 - \frac{\mathcal{M}_{\rm sh}^2}{\mathcal{M}_1^2}\right) \times \frac{\mu_{\rm sh}}{(1-\mu_{\rm sh}\mathcal{M}_{\rm sh})(\mu_{\rm sh}^2 + 2\mu_{\rm sh}\mathcal{M}_{\rm sh} + \mathcal{M}_1^{-2})},$$

R_∇, Q_∇ are deduced from the conservation of mass and energy fluxes across the compact deceleration region

$$\mathcal{R}_\nabla = \frac{\mu_{\rm in}\mathcal{M}_{\rm out}c_{\rm out}^2 - \mu_{\rm out}\mathcal{M}_{\rm in}c_{\rm in}^2}{\mu_{\rm in}\mathcal{M}_{\rm out}c_{\rm out}^2 + \mu_{\rm out}\mathcal{M}_{\rm in}c_{\rm in}^2}{\rm e}^{i\omega\tau_\mathcal{R}},$$

$$\mathcal{Q}_\nabla = \frac{\mathcal{M}_{\rm out} + \mu_{\rm out}}{1 + \mu_{\rm out}\mathcal{M}_{\rm out}}\frac{{\rm e}^{i\omega\tau_\mathcal{Q}}}{\mu_{\rm out}\frac{c_{\rm in}^2}{c_{\rm out}^2} + \mu_{\rm in}\frac{\mathcal{M}_{\rm out}}{\mathcal{M}_{\rm in}}} \times \left[1 - \frac{c_{\rm in}^2}{c_{\rm out}^2} + \frac{k_x^2 c_{\rm in}^2}{\omega^2}(\mathcal{M}_{\rm in}^2 - \mathcal{M}_{\rm out}^2)\right],$$

Efficiency of the advective-acoustic feedback from adiabatic gradients

As a vorticity perturbation δw is advected in a settling flow, the lifting up of dense regions is done at the expense of the kinetic energy of the perturbation. The energy of the acoustic feedback is thus limited by the kinetic energy of the vorticity perturbation.

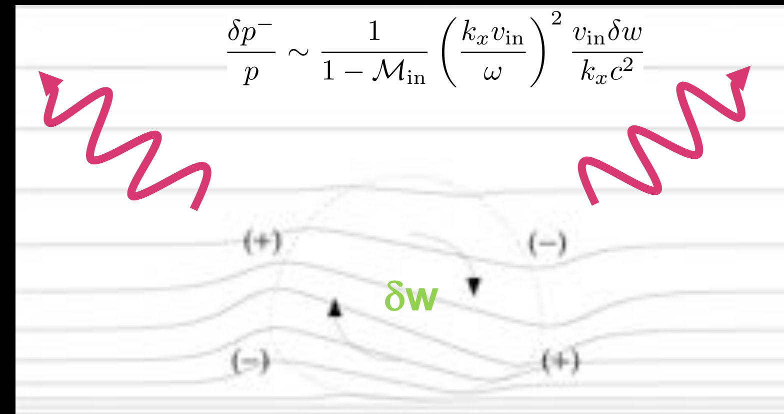

Foglizzo 09

$$Q_\nabla = \frac{\mathcal{M}_{\rm out} + \mu_{\rm out}}{1 + \mu_{\rm out}\mathcal{M}_{\rm out}} \frac{e^{i\omega\tau_Q}}{\mu_{\rm out}\frac{c_{\rm in}^2}{c_{\rm out}^2} + \mu_{\rm in}\frac{\mathcal{M}_{\rm out}}{\mathcal{M}_{\rm in}}} \times \left[1 - \frac{c_{\rm in}^2}{c_{\rm out}^2} + \frac{k_x^2 c_{\rm in}^2}{\omega^2}(\mathcal{M}_{\rm in}^2 - \mathcal{M}_{\rm out}^2)\right],$$

By contrast the acoustic feedback from the advection of an entropy perturbation can significantly exceed its internal energy: a small entropy perturbation δS can produce a huge acoustic feedback δp^- if the adiabatic increase of enthalpy $(c_{out}/c_{in})^2$ is large enough.

Efficiency of the advective-acoustic coupling

Foglizzo 09

$$
\begin{aligned}
\mathcal{Q}_{\rm sh} \equiv \frac{\delta f^S_{\rm sh}}{\delta f^-_{\rm sh}} &= \frac{1}{1-\mu_{\rm sh}\mathcal{M}_{\rm sh}}\frac{p_{\rm sh}\delta S_{\rm sh}}{\delta p^-_{\rm sh}},\\
&= \frac{2}{\mathcal{M}_{\rm sh}}\frac{1-\mathcal{M}^2_{\rm sh}}{1+\gamma\mathcal{M}^2_{\rm sh}}\left(1-\frac{\mathcal{M}^2_{\rm sh}}{\mathcal{M}^2_1}\right)\\
&\quad\times\frac{\mu_{\rm sh}}{(1-\mu_{\rm sh}\mathcal{M}_{\rm sh})(\mu^2_{\rm sh}+2\mu_{\rm sh}\mathcal{M}_{\rm sh}+\mathcal{M}_1^{-2})},
\end{aligned}
$$

The production of vorticity and entropy from an acoustic wave reaching the shock can be very large only for a strong shock in the isothermal limit

$$
\rightarrow\quad
\begin{aligned}
|\mathcal{Q}_{\rm sh}| &\sim \frac{1}{\mathcal{M}^2_{\rm sh}}\frac{1-\mathcal{M}^2_{\rm sh}}{1+\gamma\mathcal{M}^2_{\rm sh}}\\
&\sim \mathcal{M}^2_1 \ \text{ if } \ \gamma = 1
\end{aligned}
$$

A strong advective-acoustic cycle $Q = Q_{sh}\, Q_{\nabla} >>1$ could be fed:

-by a strong vortical-acoustic coupling at the shock $Q_{sh} \sim M_1^2 >>1$
if the shock were isothermal and strong,

-by a strong entropic-acoustic coupling in the feedback region $Q_{\nabla} \sim (\rho_{out}/\rho_{in})^{\gamma-1} >>1$
if the adiabatic compression were large.

The global efficiency is moderate $Q\sim1\text{-}3$ in the core-collapse accretion flow ($\gamma\sim4/3$, $M_1\sim5$, $r_{sh}/r_{\nabla}\sim2\text{-}4$).

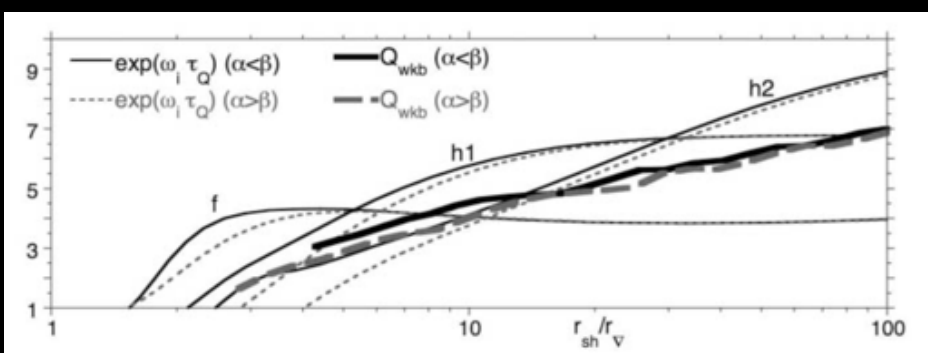

Foglizzo+07

Müller+12

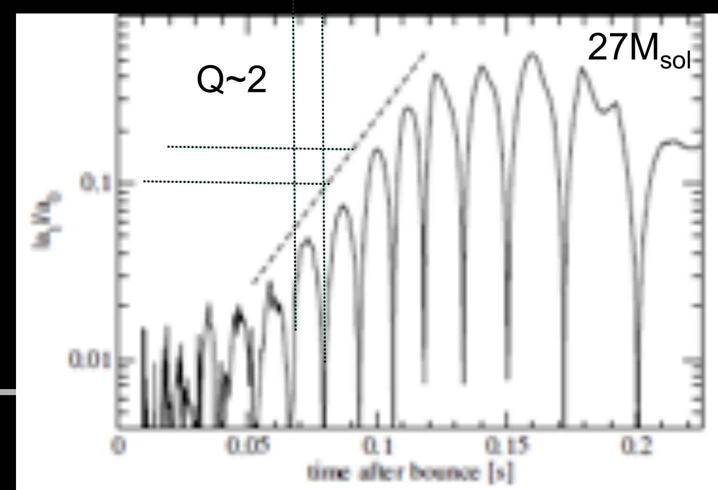

Interferences between the advective-acoustic cycle and the purely acoustic cycle

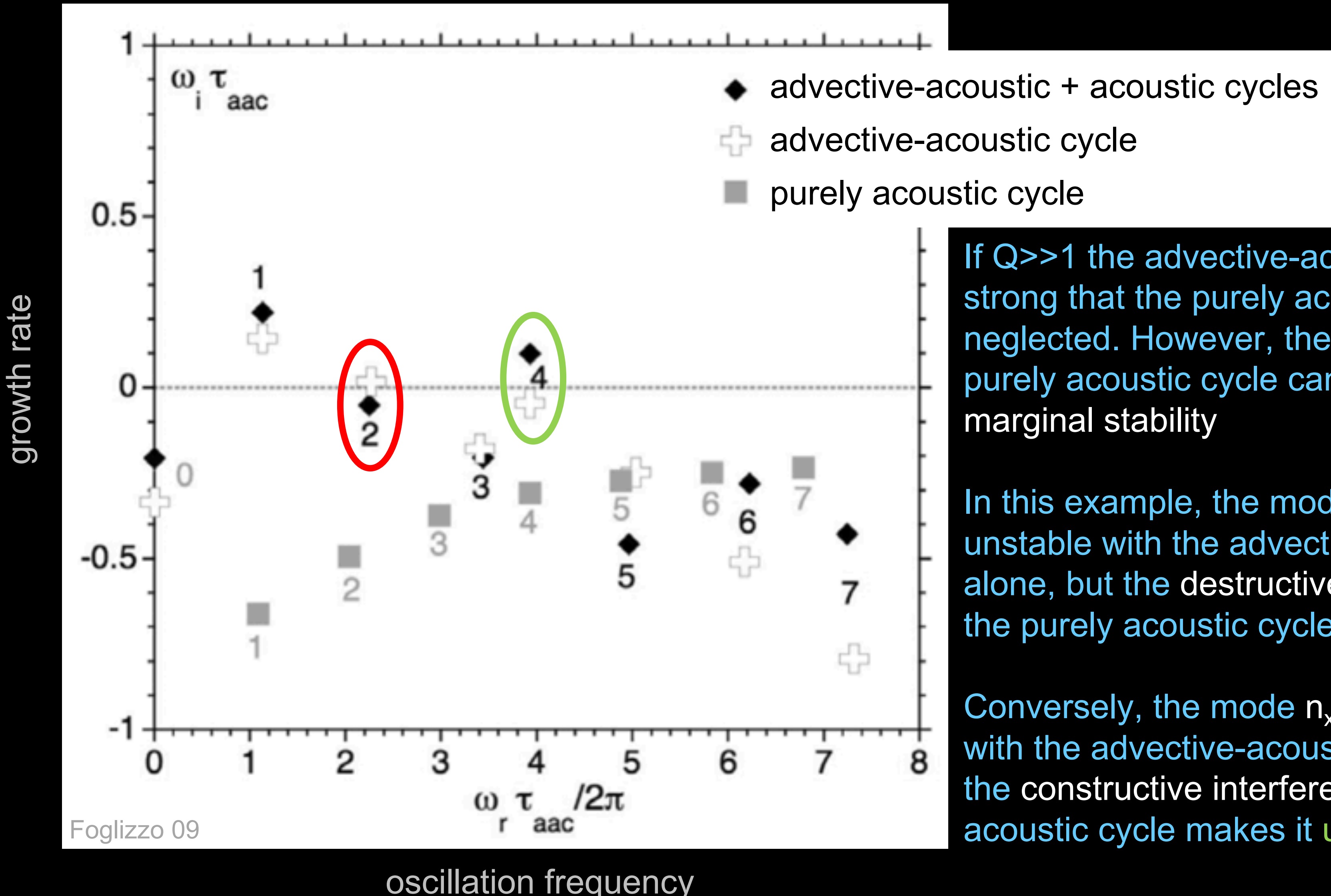

If Q>>1 the advective-acoustic cyle is so strong that the purely acoustic cycle can be neglected. However, the contribution of the purely acoustic cycle can be decisive near marginal stability

In this example, the mode $n_x=2$ would be unstable with the advective-acoustic cycle alone, but the destructive interference with the purely acoustic cycle makes it stable

Conversely, the mode $n_x=4$ would be stable with the advective-acoustic cycle alone, but the constructive interference with the purely acoustic cycle makes it unstable

see also Fernandez & Thompson 09

Understanding the efficiency of the acoustic feedback (Foglizzo 09)

$M_1=5$, $\gamma=4/3$, $T_{in}/T_{out}=0.75$

growth rate

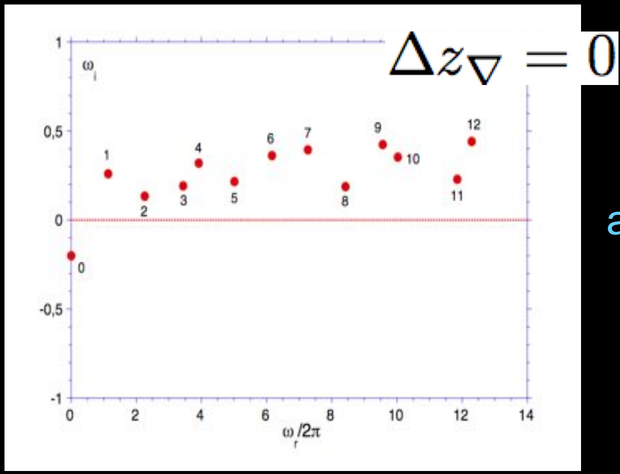

fully analytic

growth rate

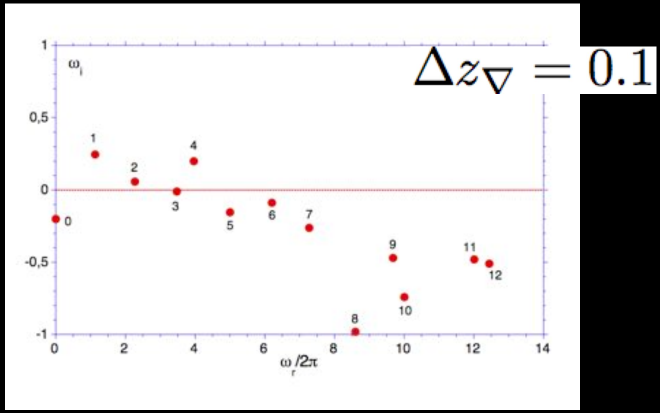

oscillation frequency

The finite lengthscale of the deceleration region introduces a frequency cut-off associated to the crossing time τ_∇

$$\omega_{\rm cut} \sim \frac{1}{\tau_\nabla}.$$

$$Q_\nabla = \int_{\rm bc}^{\rm sh} b_0 \frac{\delta p_0}{p} e^{\int_{\rm sh} \frac{i\omega}{v} {\rm d}z} \frac{\partial b_\nabla}{\partial z} {\rm d}z,$$

where

$$b_0 \equiv \frac{1}{2}\left(1+\frac{k_x^2 v_{\rm sh}^2}{\omega^2}\right)\left(1-\mathcal{R}_\nabla - \frac{1+\mathcal{R}_\nabla}{\mu_{\rm sh}\mathcal{M}_{\rm sh}}\right) \frac{1-\mathcal{M}^2}{1-\mathcal{M}_{\rm sh}^2}\frac{\mathcal{M}_{\rm sh}^2}{\mathcal{M}^2}\left(\frac{\delta p_0}{p}\right)_{\rm sh}^{-1} e^{-\int_{\rm sh} \frac{i\omega}{c}\frac{2\mathcal{M}}{1-\mathcal{M}^2}{\rm d}z},$$

$$b_\nabla \equiv \frac{i\omega}{c_{\rm sh}^2} \frac{i\omega - 2v\frac{\partial \log \mathcal{M}}{\partial z}}{k_x^2 \mathcal{M}^2 + \frac{\omega^2}{c^2} - v\mathcal{M}^2 \frac{\partial}{\partial z}\frac{i\omega}{v^2}}.$$

-high frequency perturbations are stabilized by phase mixing above the cut-off frequency

-high horizontal wavenumber perturbations correspond to higher frequencies. High order overtones produce an evanescent pressure feedback which does not affect the shock

→ SASI is a low frequency instability dominated by l=1,2

The saturation of SASI by parasitic instabilities

Guilet+10

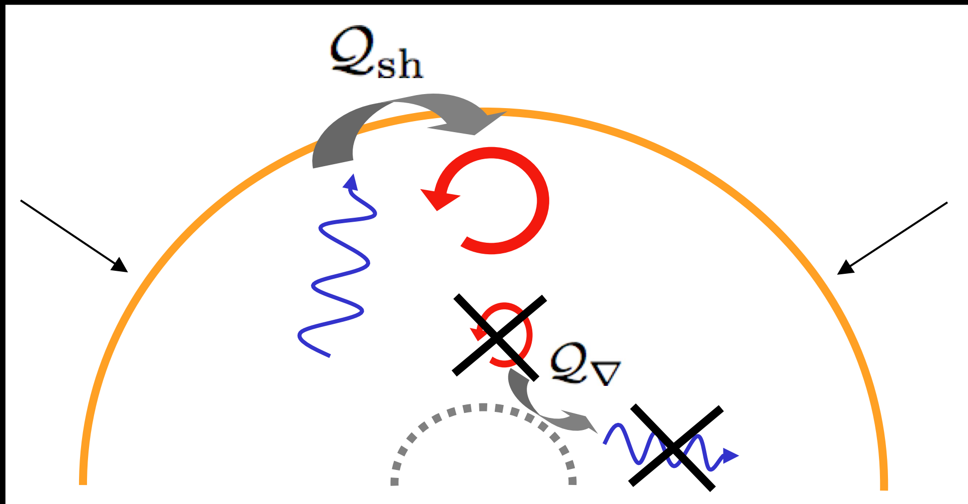

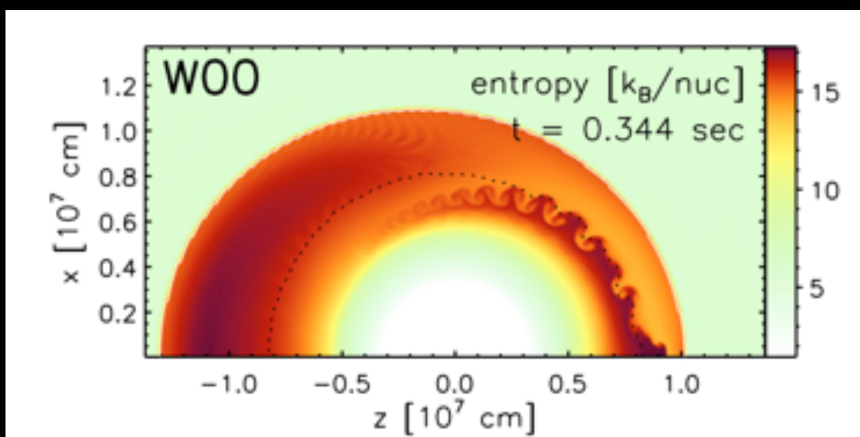

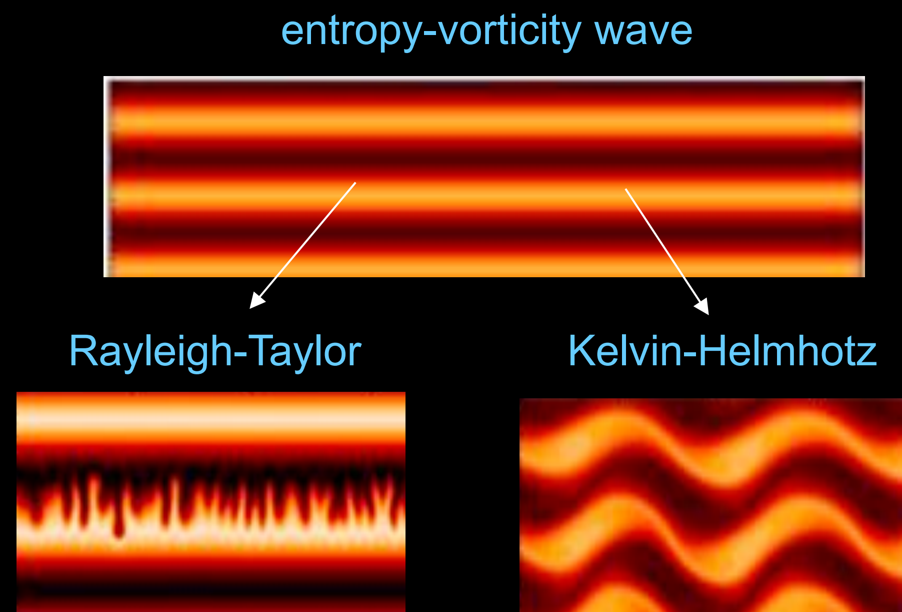

The entropy and vorticity waves produced by the shock oscillations are unstable to **parasitic instabilities** such as Rayleigh-Taylor and Kelvin-Helmholtz.

The advective-acoustic cycle is affected if

- the parasitic instabilities are able to propagate against the flow,
- their effective eulerian growth rate exceeds the SASI growth rate

Reminder about the Kelvin-Helmholtz instability

Two incompressible fluids with uniform velocities v_1 and v_2

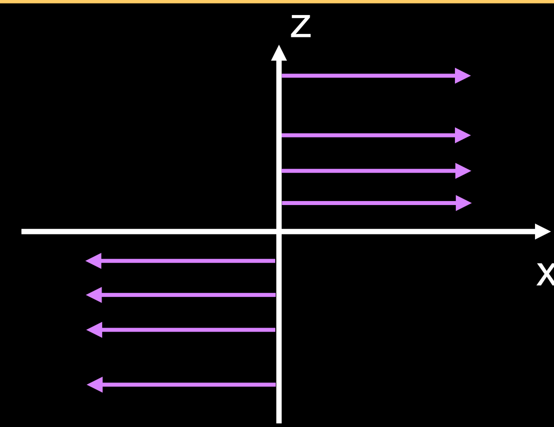

$$\frac{\partial \rho}{\partial t} + \nabla \cdot \rho v = 0,$$
$$\frac{\partial v}{\partial t} + (v \cdot \nabla) v + \frac{\nabla P}{\rho} = 0.$$

Linearizing, + Fourier transform in time and space: $\exp(-i\omega t + ik_x x + ik_z z)$

$$ik \cdot \delta v = 0,$$
$$-i(\omega - k_x v)\delta v + ik\frac{\delta P}{\rho} = 0.$$

$\rightarrow$ $$k^2 \frac{\delta P}{\rho} = 0$$ $\rightarrow$ $$k_x^2 + k_z^2 = 0$$ $\rightarrow$ $$k_z = \pm i k_x$$

$$k_x \delta v_x + k_z \delta v_z = 0,$$
$$(\omega - k_x v)\delta v_x = k_x \frac{\delta P}{\rho},$$
$$(\omega - k_x v)\delta v_z = k_z \frac{\delta P}{\rho}.$$

$\rightarrow$

$$\delta v_z = -i(\omega - k_x v)\ \delta\zeta\ \mathrm{e}^{-k_x|z|}\mathrm{e}^{ik_x x},$$
$$\delta v_x = \mp(\omega - k_x v)\ \delta\zeta\ \mathrm{e}^{-k_x|z|}\mathrm{e}^{ik_x x},$$
$$\delta P = \pm\frac{(\omega - k_x v)^2}{k_x}\rho\ \delta\zeta\ \mathrm{e}^{-k_x|z|}\mathrm{e}^{ik_x x}.$$

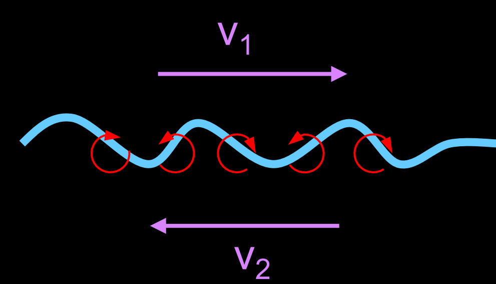

Boundary condition: continuity of the interface pressure δP at $z=\delta\zeta$

$$\delta P_1 = \delta P_2$$ $\rightarrow$ $$\omega = \frac{k_x}{2}\left(v_1 + v_2 + i|v_1 - v_2|\right)$$

for a step like velocity profile, the most unstable wavelengths are at the smallest scale

Reminder about the Kelvin-Helmholtz instability

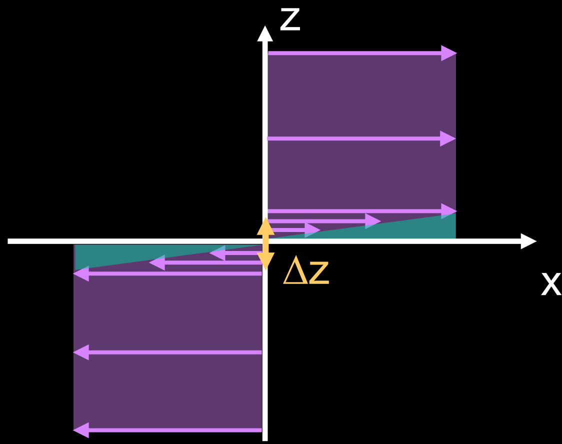

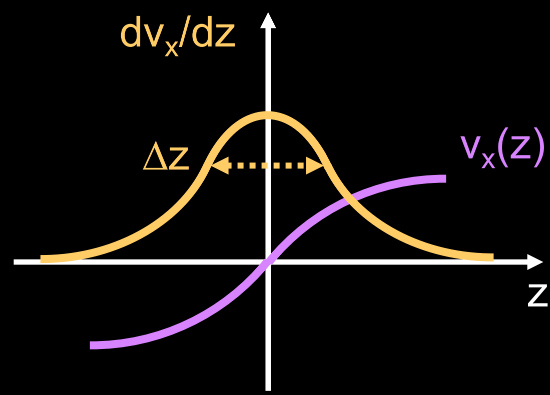

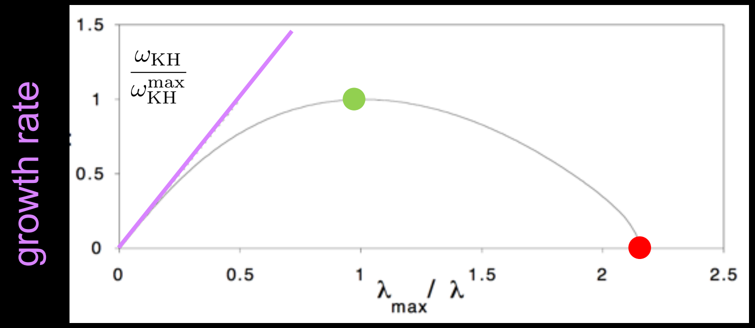

$$(\nabla \times v)_y \equiv \frac{\partial v_z}{\partial x} - \frac{\partial v_x}{\partial z}$$

$$\boxed{\omega_{\mathrm{KH}}^{\max} \sim 0.2\, |\nabla \times v|_{\max}}$$

$$\boxed{\lambda_{\max} \sim 7\, \Delta z}$$

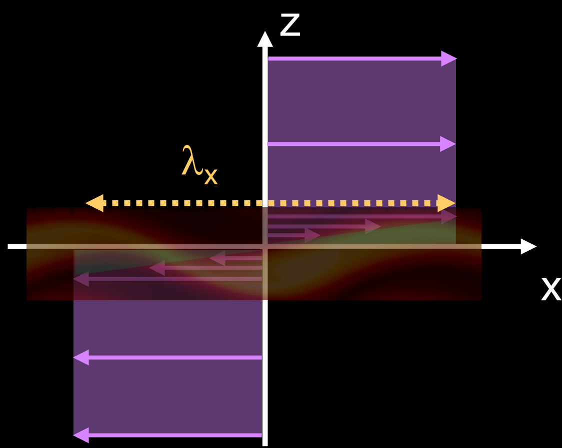

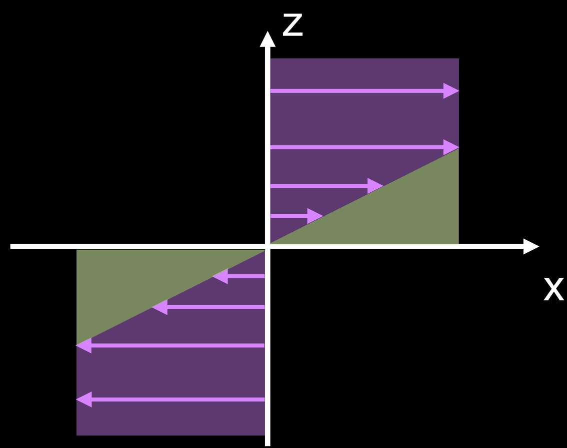

The instability feeds on the kinetic energy gained by smoothing of the velocity profile.

Perturbations with a wavelength shorter than ~3Δz are stable

Loss of large scale power from the growth of parasitic instabilities

Guilet+10

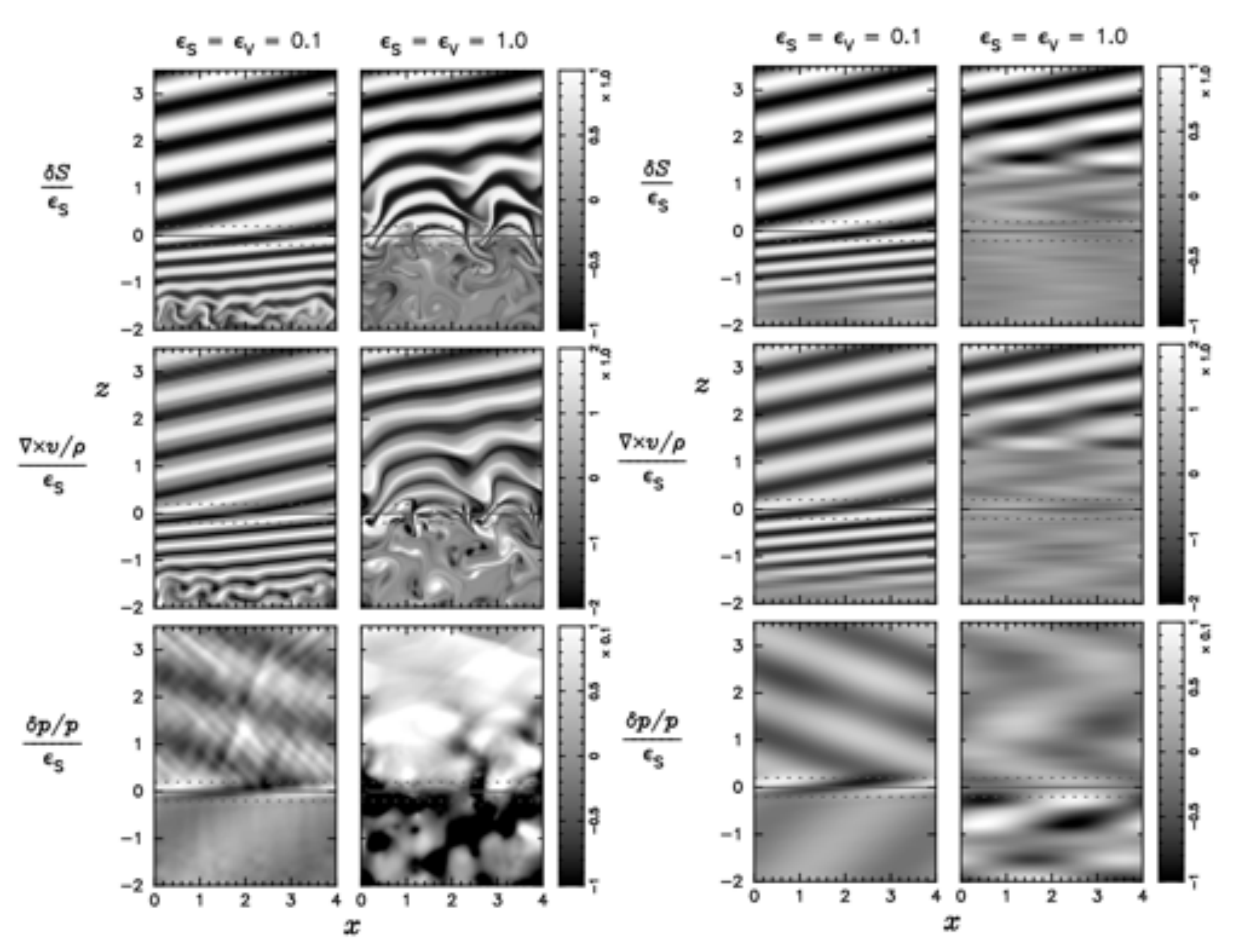

full waves

filtered waves (m_x=1)

From the linear instability mechanism, a short dvection timescale both favours SASI and stabilizes neutrinbo-driven convection (χ<3).

From the non linear saturation mechanism, large SASI amplitudes are expected if the advection velocity is high and if the cooling processes in strong.

The faster the advection, the more difficult the propagation of parasitic instabilities against the flow

The stronger the cooling, the more difficult the destabilisation of the entropy profile by SASI entropy waves

Comparison with numerical simulations

Guilet+10

Fernandez & Thompson 09 (no heating)

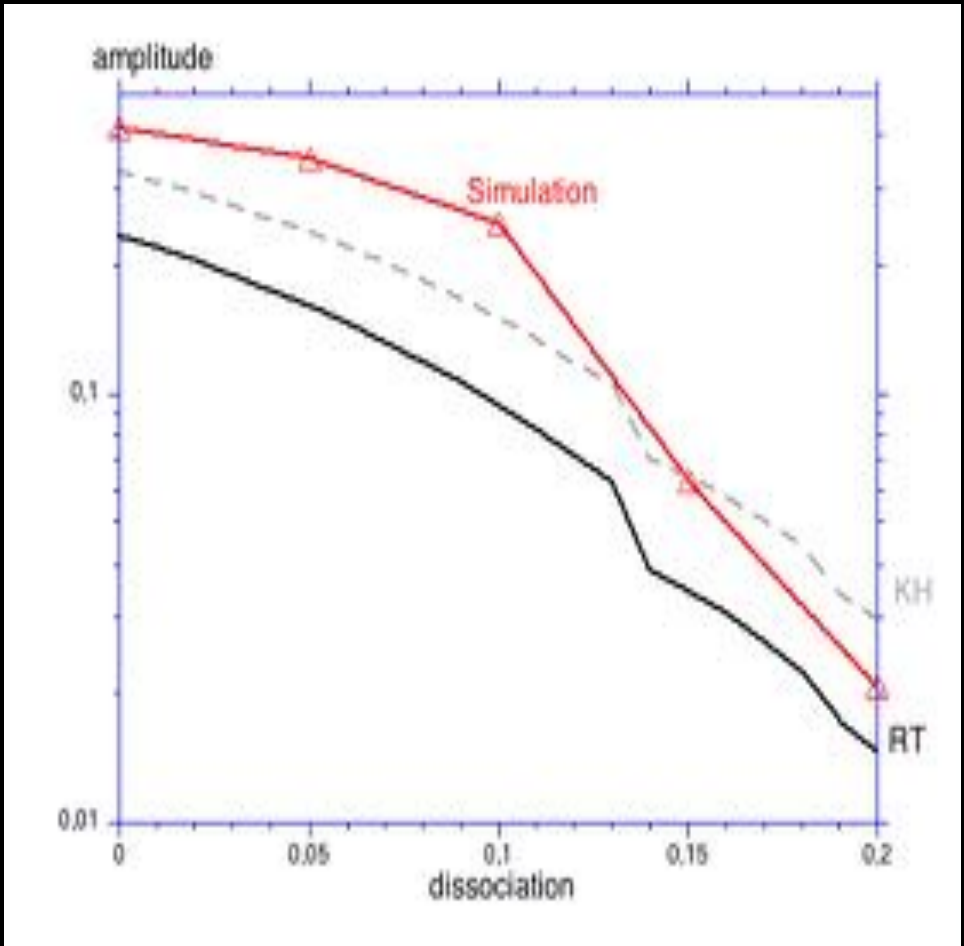

No other saturation mechanism has been proposed since Guilet+10

If neutrino heating increases sufficiently, ν-driven convection is expected to dominate the SASI:

Linearly, the increased thermal pressure makes the flow slower, which is both favourable to convection (increases χ) and makes SASI slower (longer τ_{adv})

Non linearly,
-neutrino heating weakens the stable entropy gradient and allows a faster RT growth of parasites on SASI entropy waves,
-the slower advection velocity also favours the propagation of parasites againt the stream,
-the turbulence driven by small scale convective motions acts as a viscous diffusive process for lage scale SASI waves.

Formal similarity between SASI and SWASI

accretion of gas on a cylinder

density ρ, velocity v, sound speed $c \propto \rho^{\frac{\gamma-1}{2}}$

$$\frac{\partial \rho}{\partial t} + \nabla \cdot (\rho v) = 0$$

$$\frac{\partial v}{\partial t} + w \times v + \nabla \left(\frac{v^2}{2} + c^2 \log \frac{\rho}{\rho_0} + \Phi \right) = 0$$ isothermal

$$\frac{\partial v}{\partial t} + w \times v + \nabla \left(\frac{v^2}{2} + \frac{c^2}{\gamma - 1} + \Phi \right) = \frac{c^2}{\gamma} \nabla S$$ adiabatic

inviscid shallow water accretion

depth H, velocity v, wave speed $c = (gH)^{\frac{1}{2}}$

$$\Phi = gz$$

$$c^2 = gH$$

$$\frac{\partial H}{\partial t} + \nabla \cdot (Hv) = 0$$

$$\frac{\partial v}{\partial t} + w \times v + \nabla \left(\frac{v^2}{2} + c^2 + \Phi \right) = 0$$

- Inviscid shallow water: intermediate between "isothermal" and "isentropic γ=2"

isothermal shock $\mathcal{M}_2 = \dfrac{1}{\mathcal{M}_1}$

hydraulic jump $\mathcal{M}_2 = \dfrac{2^{\frac{3}{2}} \mathcal{M}_1}{\left[(1 + 8\mathcal{M}_1^2)^{\frac{1}{2}} - 1 \right]^{\frac{3}{2}}}$

jump conditions: conservation of mass flux and momentum flux: energy is dissipated

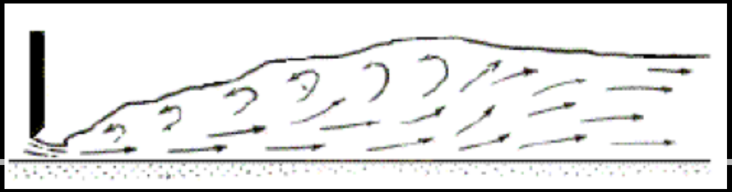

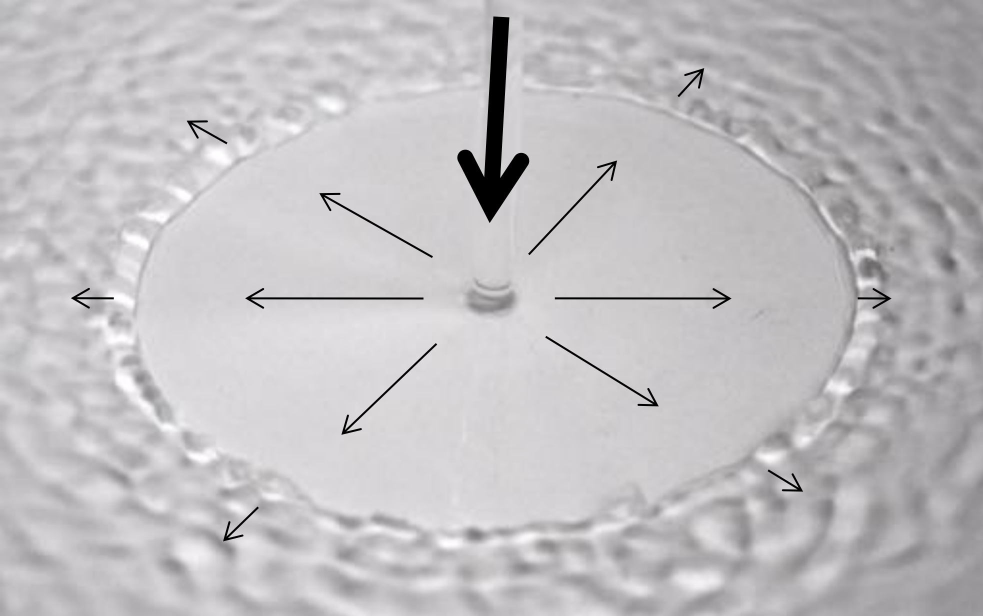

Analogy between hydraulic jumps and shock

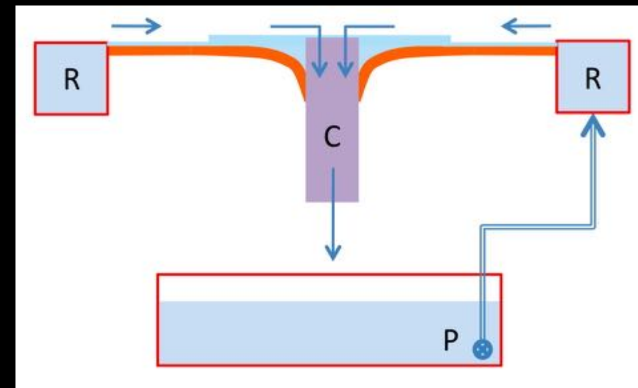

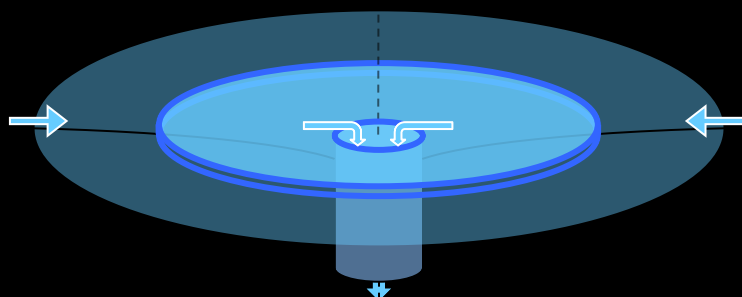

acoustic waves ⟷ surface waves
shock wave ⟷ hydraulic jump
pressure ⟷ depth

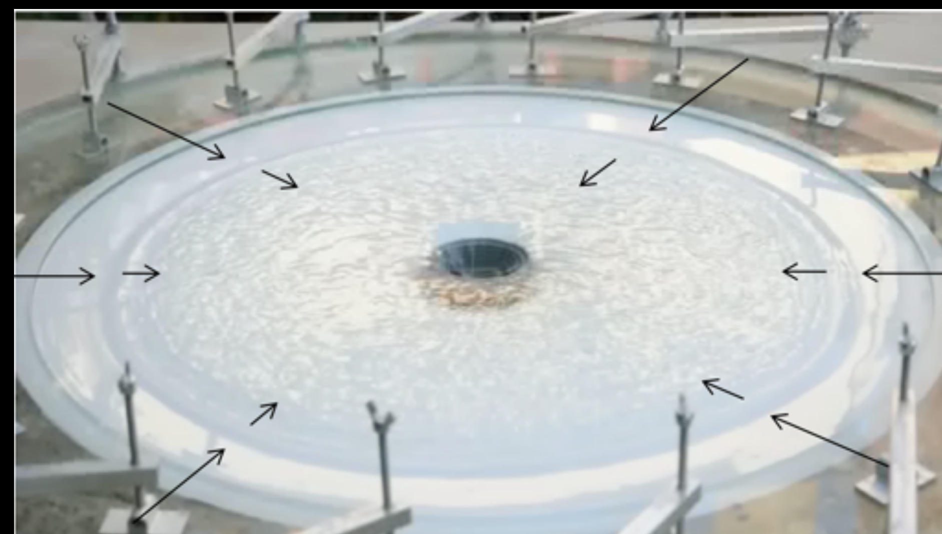

Hydraulic jump conditions

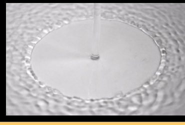

The shallow water flow is also described by 2 physical quantities: velocity and depth (no entropy analogue).
Depth plays the same role as the compressibility of a gas (i.e. surface density).
The jump conditions for a hydraulic jump are deduced from the conservation of mass flux and momentum flux.
Energy is dissipated in a viscous roller within the width of the hydraulic jump.

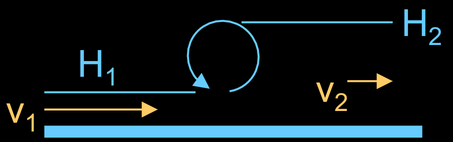

$$H_1 v_1 = H_2 v_2,$$
$$\frac{gH_1^2}{2} + H_1 v_1^2 = \frac{gH_2^2}{2} + H_2 v_2^2.$$

The Froude number is analogous to the Mach number $\mathrm{Fr} \equiv \frac{v}{(gH)^{\frac{1}{2}}}$

$$\mathrm{Fr}_1 H_1^{\frac{3}{2}} = \mathrm{Fr}_2 H_2^{\frac{3}{2}},$$
$$H_1^2(1 + 2\mathrm{Fr}_1^2) = H_2^2(1 + 2\mathrm{Fr}_2^2).$$

$$\left(1 + 2\mathrm{Fr}_1^2\right)\mathrm{Fr}_2^{\frac{4}{3}} = \left(1 + 2\mathrm{Fr}_2^2\right)\mathrm{Fr}_1^{\frac{4}{3}}$$

This polynomial of order 3 in $\mathrm{Fr}^{3/2}$ can be factorized by $(\mathrm{Fr}_1^{3/2}-\mathrm{Fr}_2^{3/2})$

$$(\mathrm{Fr}_2^{\frac{2}{3}} - \mathrm{Fr}_1^{\frac{2}{3}})(-2\mathrm{Fr}_2^{\frac{4}{3}}\mathrm{Fr}_1^{\frac{4}{3}} + \mathrm{Fr}_2^{\frac{2}{3}} + \mathrm{Fr}_1^{\frac{2}{3}}) = 0$$

$\mathrm{Fr}_2^{3/2}$ is thus a root of a second order polynomial $2\mathrm{Fr}_2^{\frac{4}{3}}\mathrm{Fr}_1^{\frac{4}{3}} - \mathrm{Fr}_2^{\frac{2}{3}} - \mathrm{Fr}_1^{\frac{2}{3}} = 0$

$$\mathrm{Fr}_2 = \frac{1}{8\mathrm{Fr}_1^2}\left[1 + (1 + 8\mathrm{Fr}_1^2)^{\frac{1}{2}}\right]^{\frac{3}{2}}$$

$$\frac{v_2}{v_1} = \frac{H_1}{H_2} = \left(\frac{\mathrm{Fr}_2}{\mathrm{Fr}_1}\right)^{\frac{2}{3}} = \frac{1}{4\mathrm{Fr}_1^2}\left[1 + (1 + 8\mathrm{Fr}_1^2)^{\frac{1}{2}}\right]$$

The jump conditions for hydraulic jumps differ slightly from the gas

For a strong jump:
$$\frac{v_2}{v_1} \propto 2^{-\frac{1}{2}}\mathrm{Fr}_1^{-1},$$
$$\mathrm{Fr}_2 \propto 2^{-\frac{3}{4}}\mathrm{Fr}_1^{-\frac{1}{2}}.$$

Isothermal shock:
$$\frac{v_2}{v_1} = M_1^{-2},$$
$$M_2 = M_1^{-1}.$$

SWASI: simple as a garden experiment

November 2010

October 2010

June 2010

May 2010

February 2012

February 2017

PRIX 2014
LE GOÛT
DES SCIENCES

Nov-Dec. 2013 & since 2015:
Palais de la Découverte, Paris

June 2014

December 2018

Dynamics of water
in the fountain

Dynamics of the gas
in the supernova core

diameter 40cm
3s/oscillation

1 000 000 x bigger
100 x faster

diameter 400km
0.03s/oscillation

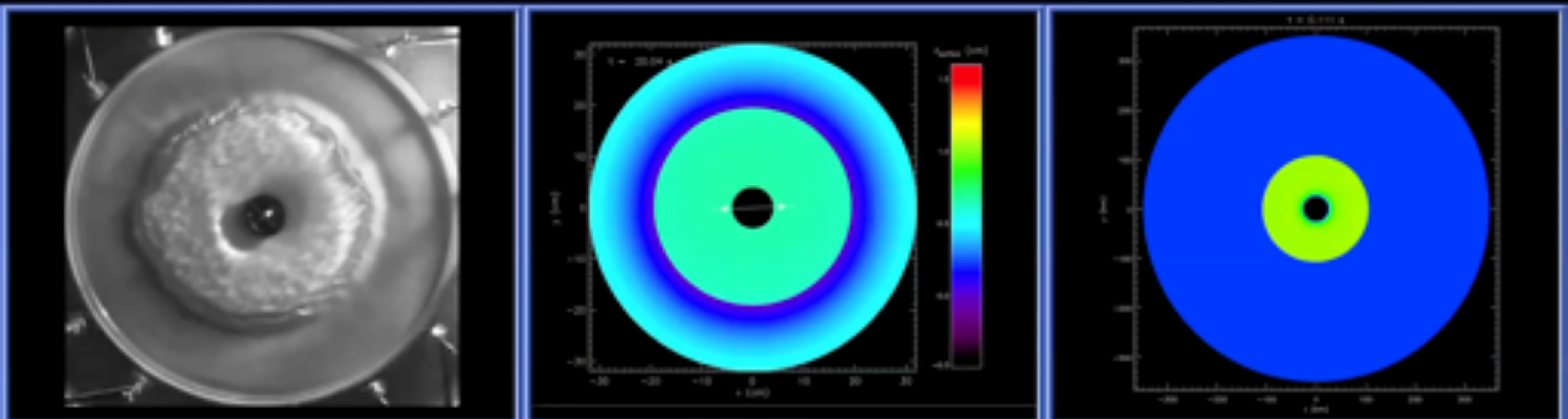

Expérience hydraulique

Simulation numérique de l'expérience hydraulique

Simulation numérique de l'onde de choc dans le coeur de la supernova

Comparaison to a 2D shallow water model

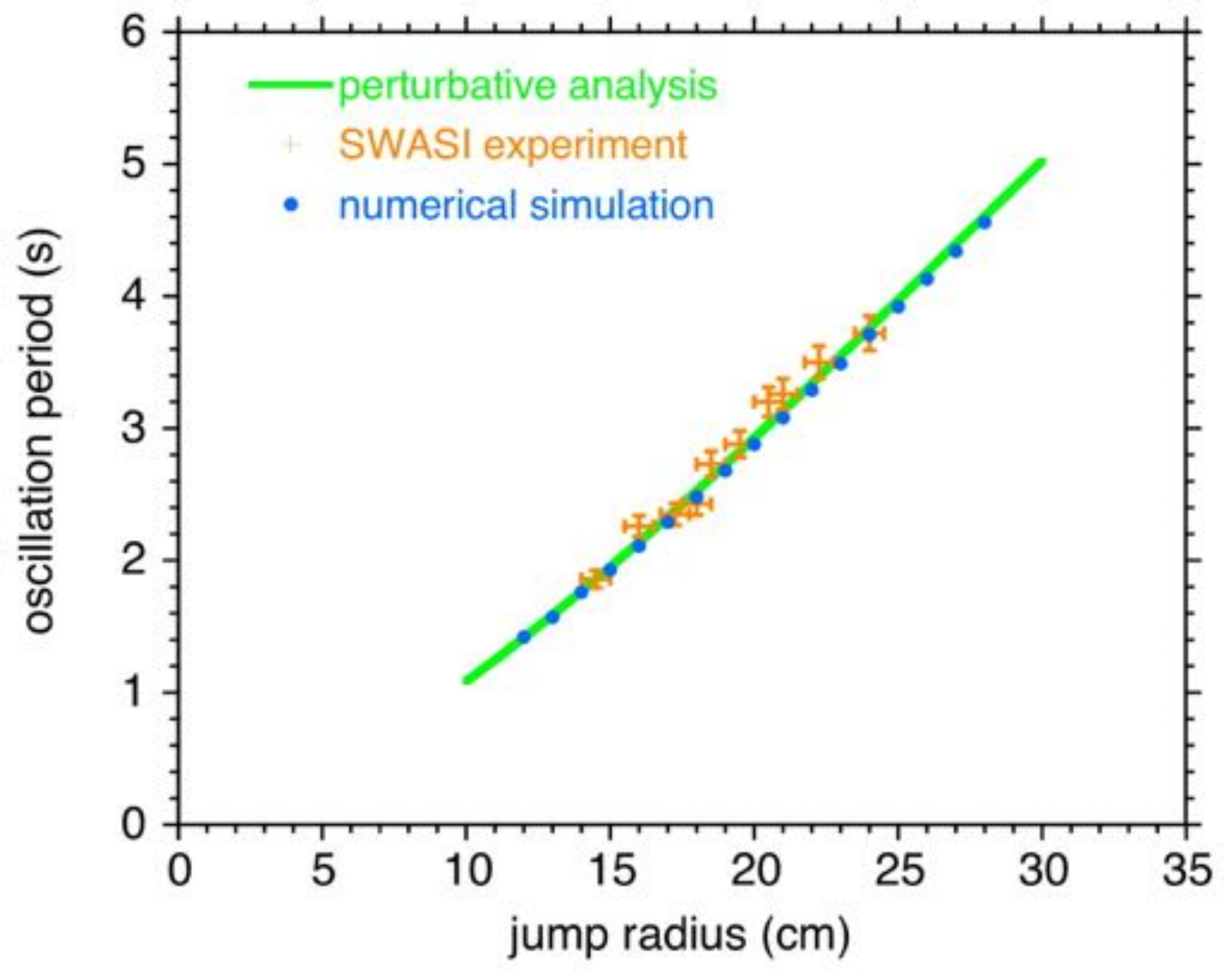

Foglizzo+12

Parameters of the experiment

Foglizzo+12

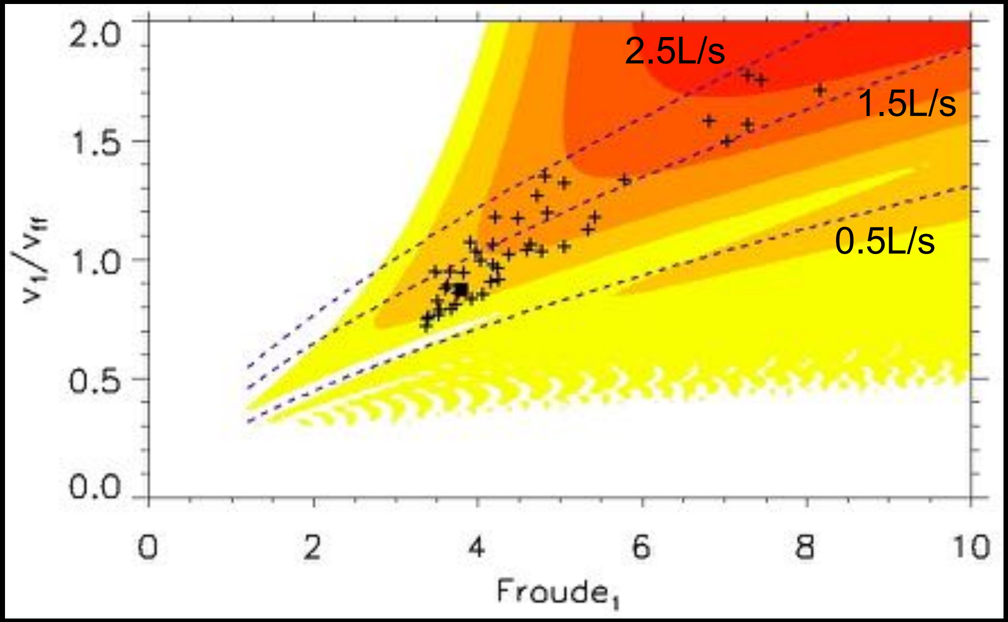

$$v = \frac{Q}{2\pi r H}$$
$$c = (gH)^{\frac{1}{2}}$$
$$v_{\rm ff} \equiv \left(\frac{2gR_\Phi^2}{r}\right)^{\frac{1}{2}}$$

$$\Phi \equiv gH_\Phi(r)$$
$$H_\Phi(r) \equiv -\frac{R_\Phi^2}{r}$$

$$\mathrm{Fr} \equiv \frac{v}{c} = \frac{Q}{2\pi r g^{\frac{1}{2}} H^{\frac{3}{2}}}$$
$$\frac{v}{v_{\rm ff}} = \frac{Q}{2^{\frac{3}{2}}\pi g^{\frac{1}{2}} r^{\frac{1}{2}} H R_\Phi}$$

$H\phi$=5.6cm
R_{inj}=33cm

$$\mathrm{Re} \equiv \frac{Hv}{\nu} = 650\left(\frac{H}{1\mathrm{mm}}\right)^{\frac{3}{2}}\left(\frac{\mathrm{Fr}}{4}\right)\left(\frac{20\mathrm{cm}}{r}\right)$$

at the outer boundary:

- -slit size H_{inj} ~ 0.3-1mm
- -flow rate Q ~ 0.7-2 L/s

→ (flow velocity & wave speed) → (Froude number & v/v_{ff})

- -rotation rate ~0-0.5Hz → angular momentum

at the inner boundary:

- -radius of the accretor R_{ns}=4-6cm
- -height of the inner cylinder → radius of the stationary jump R_{jp}=15-25cm → R_{jp}/R_{ns}

Advantages and limitations of the shallow water analogy

- simple & intuitive
- explore with an experimental tool
- inexpensive

$$\Phi = gz$$

$$c^2 = gH$$

$$\frac{\partial H}{\partial t} + \nabla \cdot (Hv) = 0$$

$$= -3\nu \frac{v}{H^2}$$

viscous drag

$$\frac{\partial v}{\partial t} + w \times v + \nabla \left(\frac{v^2}{2} + c^2 + \Phi \right) = \cancel{0}$$

product of verticaly averaged velocity or vorticity

γ=2

missing entropy gradient $\frac{c^2}{\gamma} \nabla S$

Theoretical framework:

- 2D slice of a 3D flow
- no buoyancy effects
- γ=2
- accreting inner boundary

Experimental constraints:

- viscous drag
- turbulent viscosity
- approximately shallow water
- vertical velocity profile
- hydraulic jump dissipation 3<Fr<8

Counter spinning inner regions

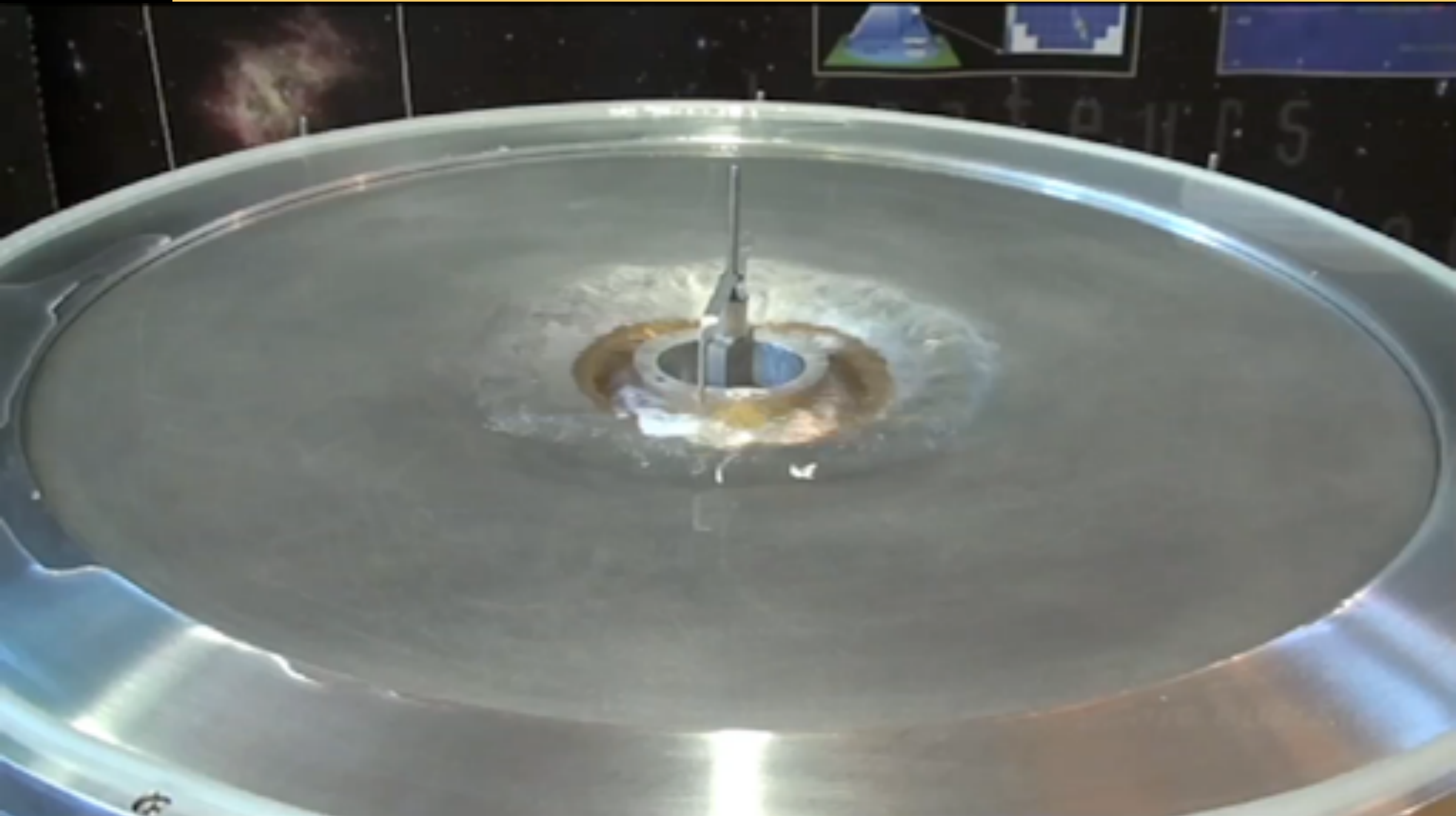

Spin up of the neutron star induced by the spiral mode of SASI

Kazeroni+17

Cylindrical stationary accretion, neutrino cooling mimicked by a cooling function

-the strength of SASI increases with the radius ratio $R = r_{sh}/r_{ns}$

-unexpected stochasticity and possible change in the direction of rotation

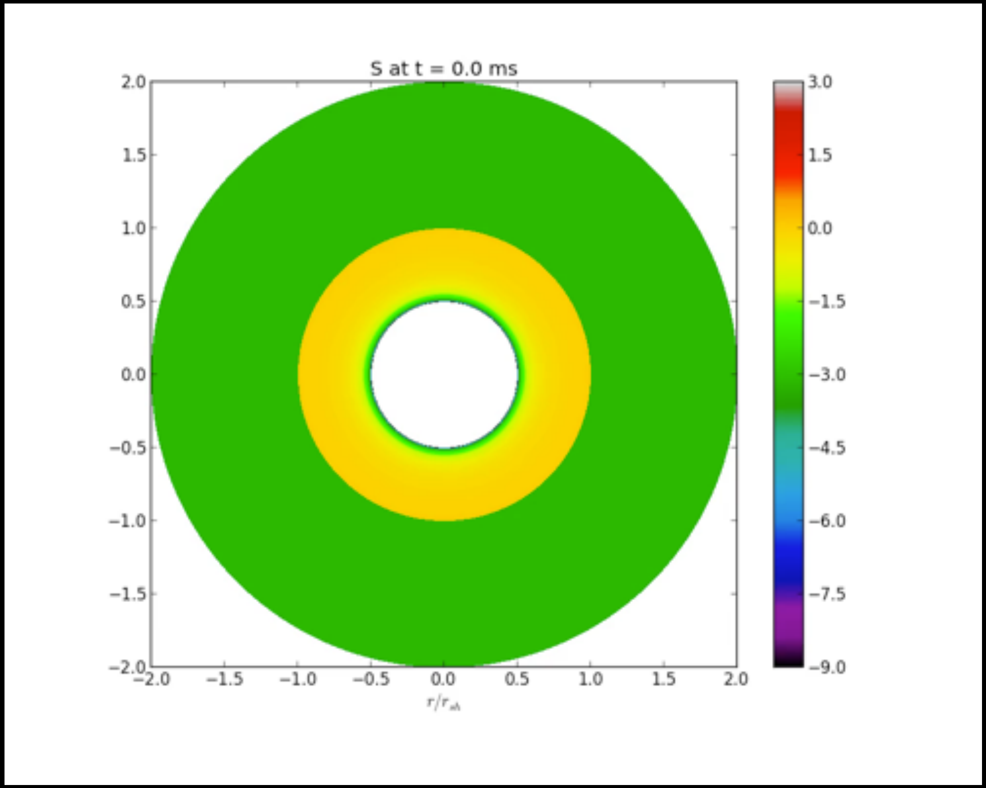

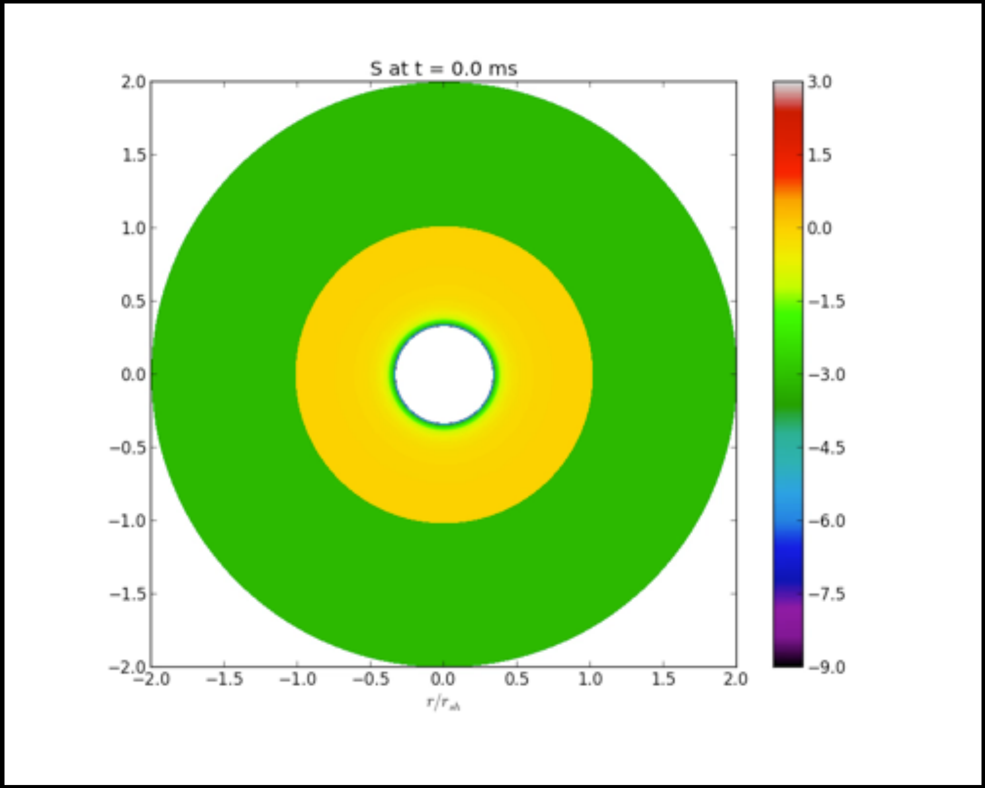

$r_{sh}/r_{ns} = 2$

$r_{sh}/r_{ns} = 3$

Outline

Impact of hydrodynamics the explosion physics

2D vs 3D

The basics of hydrodynamical instabilities

Neutrino driven convection

The Standing Accretion shock instability

Rotational effects: spiral SASI, low T/W, MRI

Redistribution of angular momentum by the spiral mode of SASI in 3D

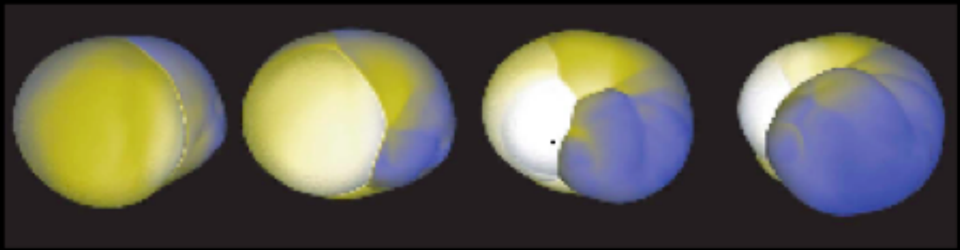

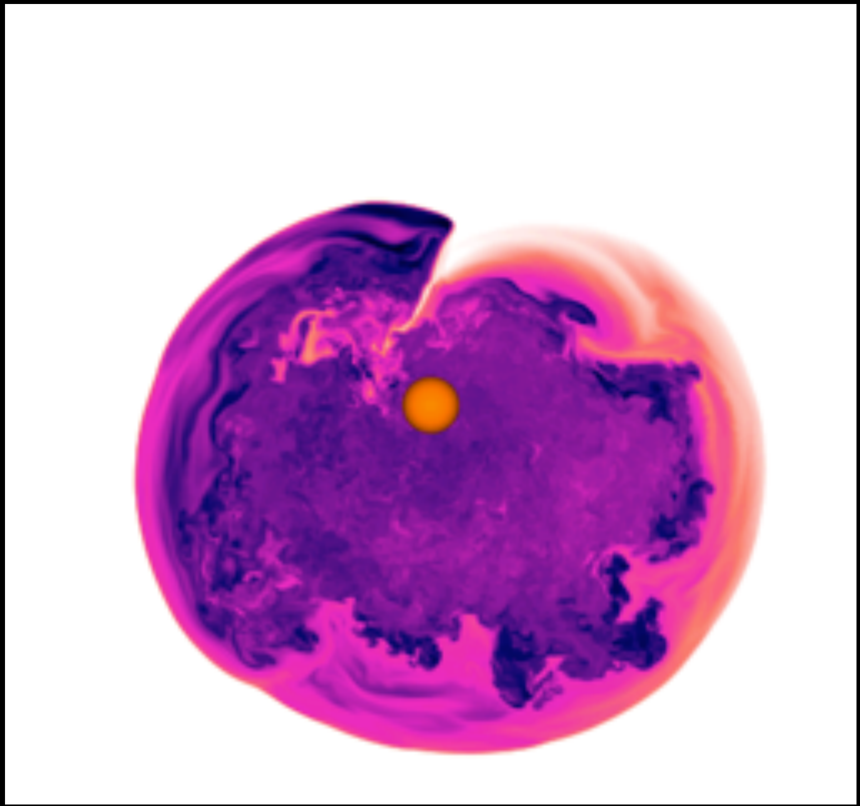

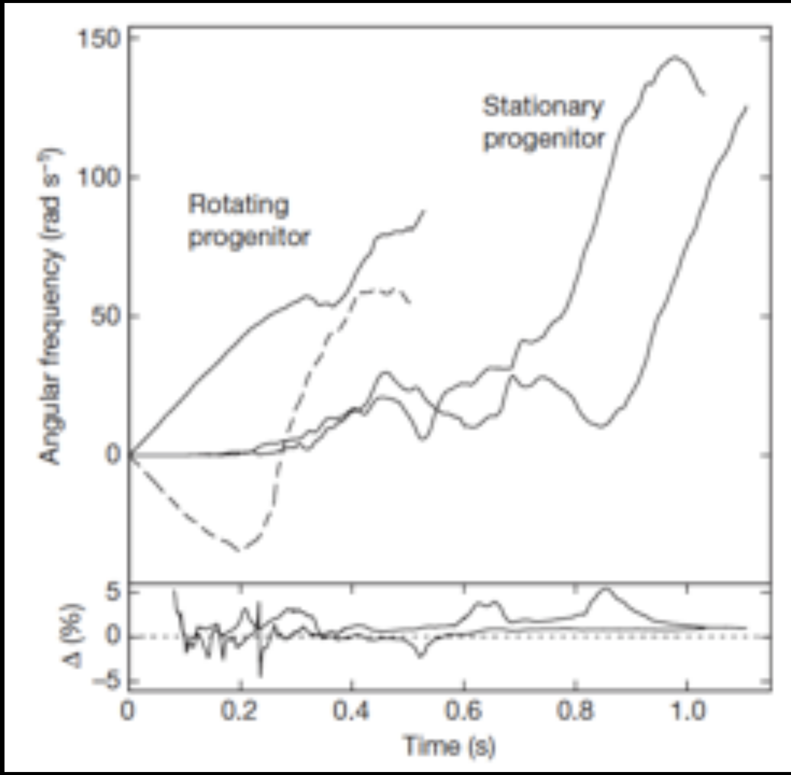

Blondin & Mezzacappa 07

Even if the progenitor is not rotating, SASI is able to spin up the neutron star and the ejecta in opposite directions.

Very few simulations include rotation

SASI

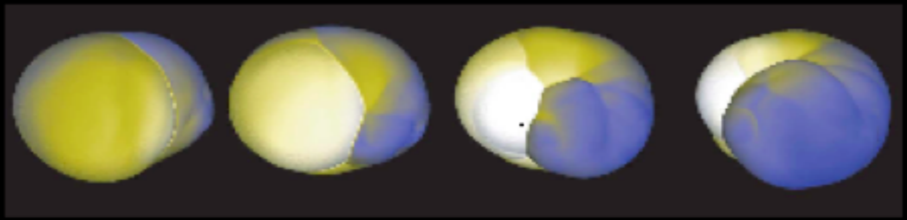

(Blondin & Mezzacappa 07)

$j = 10^{15}$ cm^2/s or $P_0 = 6$ ms

"Slow" rotating progenitor

Low-T/|W|

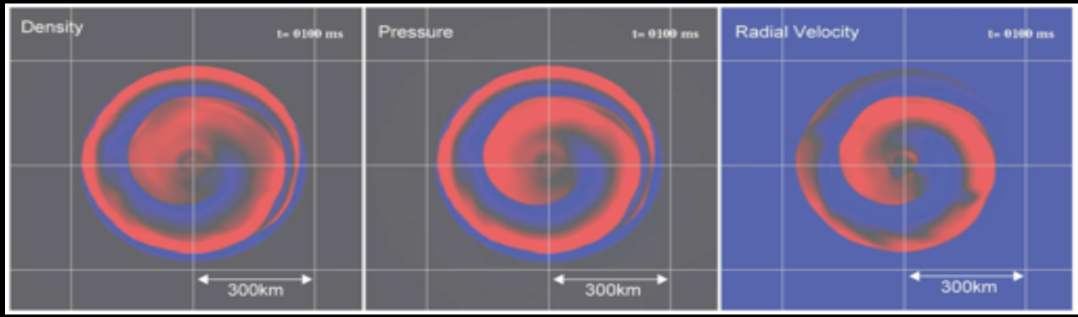

(Takiwaki+16)

$j = 4.10^{16}$ cm^2/s or $P_0 \approx 0.15$ ms

"Fast" rotating progenitor

stellar evolution favours: $j \sim 10^{15}$ cm^2/s (e.g. Heger+05)

What about intermediate rotation rates ?

Rotating progenitor: redistribution of angular momentum by SASI

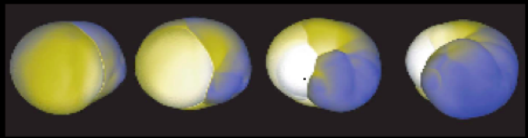

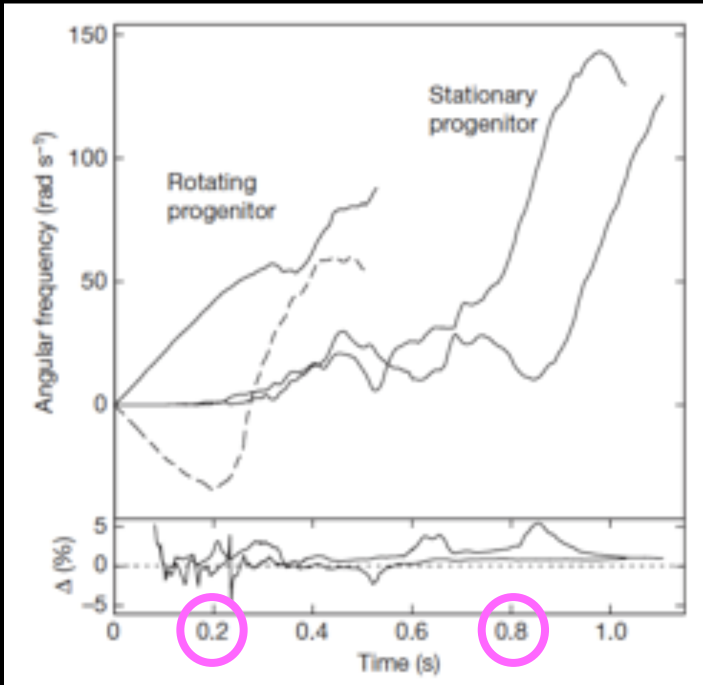

Blondin & Mezzacappa 07

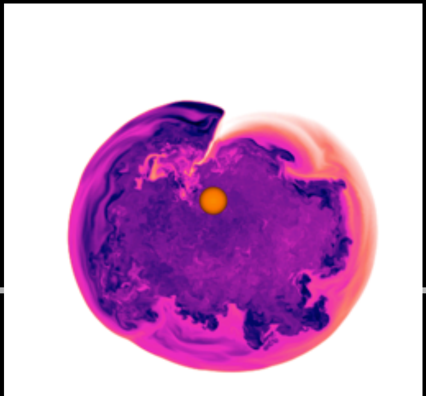

rotation period: 246s
injection slit: 0.55mm
flow rate: 1.17L/s

Effect of core rotation on SASI in a cylindrical flow

(Yamasaki & Foglizzo 08)

- Growth rate of the spiral mode

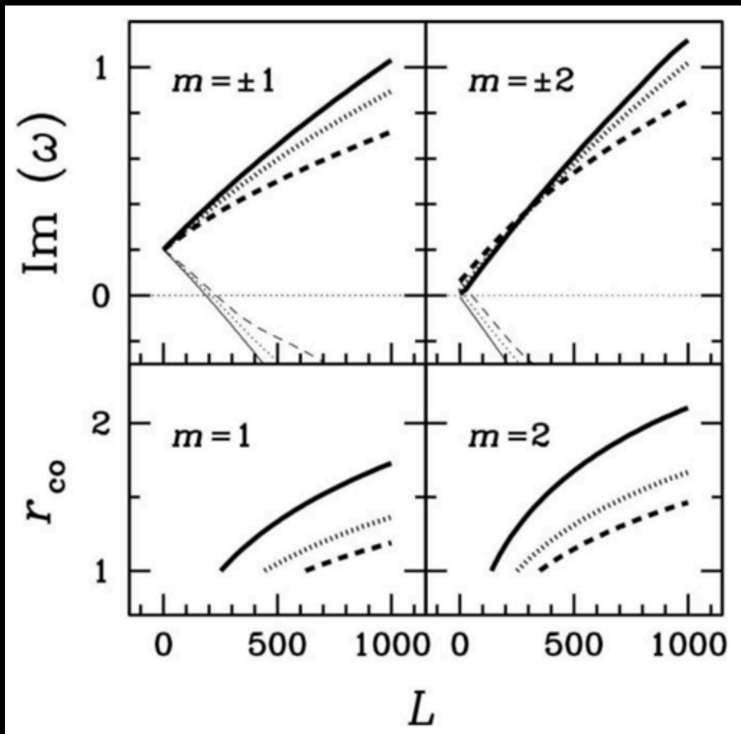

Even if the centrifugal force is dynamically negligible, differential rotation influences directly the prograde spiral mode of SASI through the Doppler shifted frequency $\omega - m\Omega$

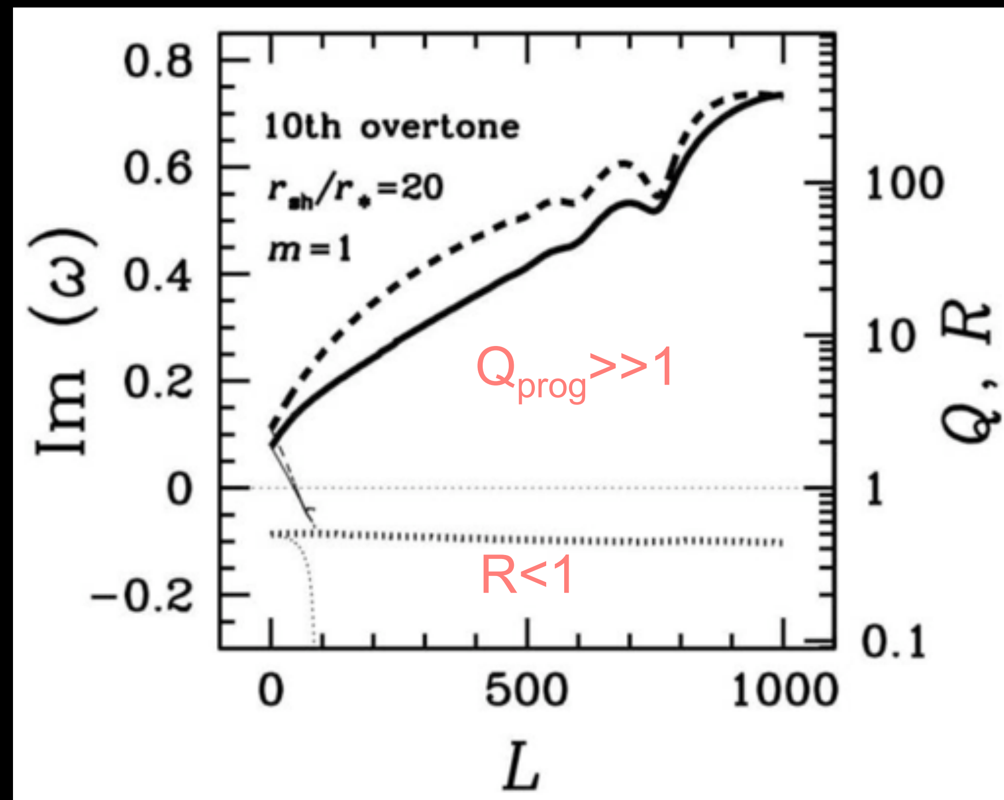

WKB analysis: the acoustic mode is stable.

Why is the prograde advective-acoustic mode so much favoured?

Comparison of rotation effects on shallow water equations and gas dynamics

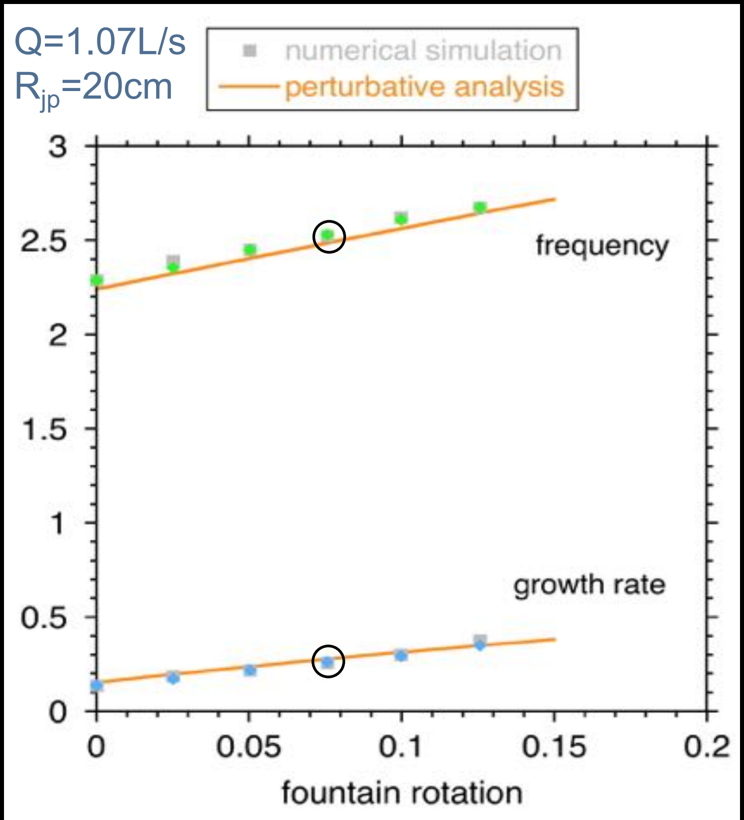

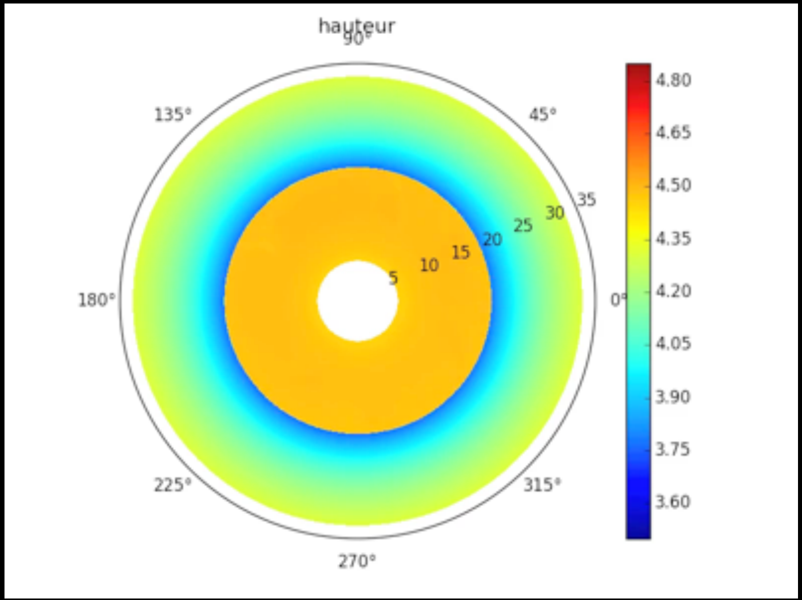

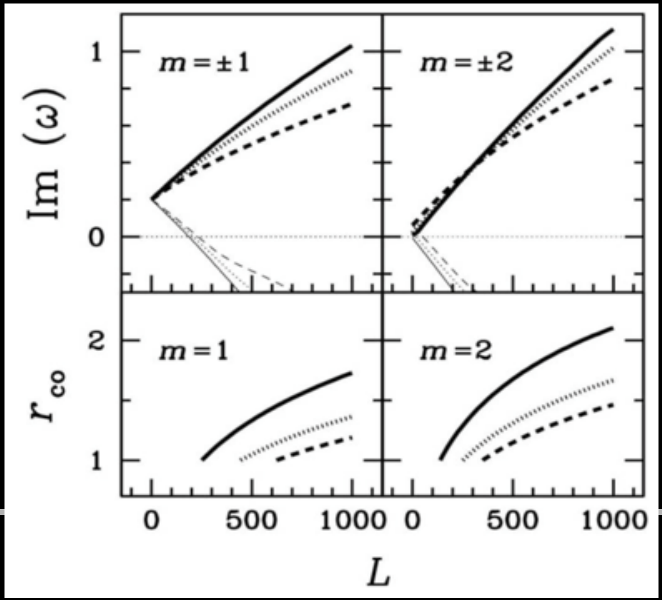

Yamazaki & Foglizzo 08

same linear increase of the growth rate as in YF08, despite

- the absence of buoyancy effects
- γ=2 instead of γ=4/3
- accreting inner boundary

What is the physical mechanism of this rotational destabilization?

Increasing the rotation rate (20% Kepler) : a robust spiral shock driven at the corotation radius

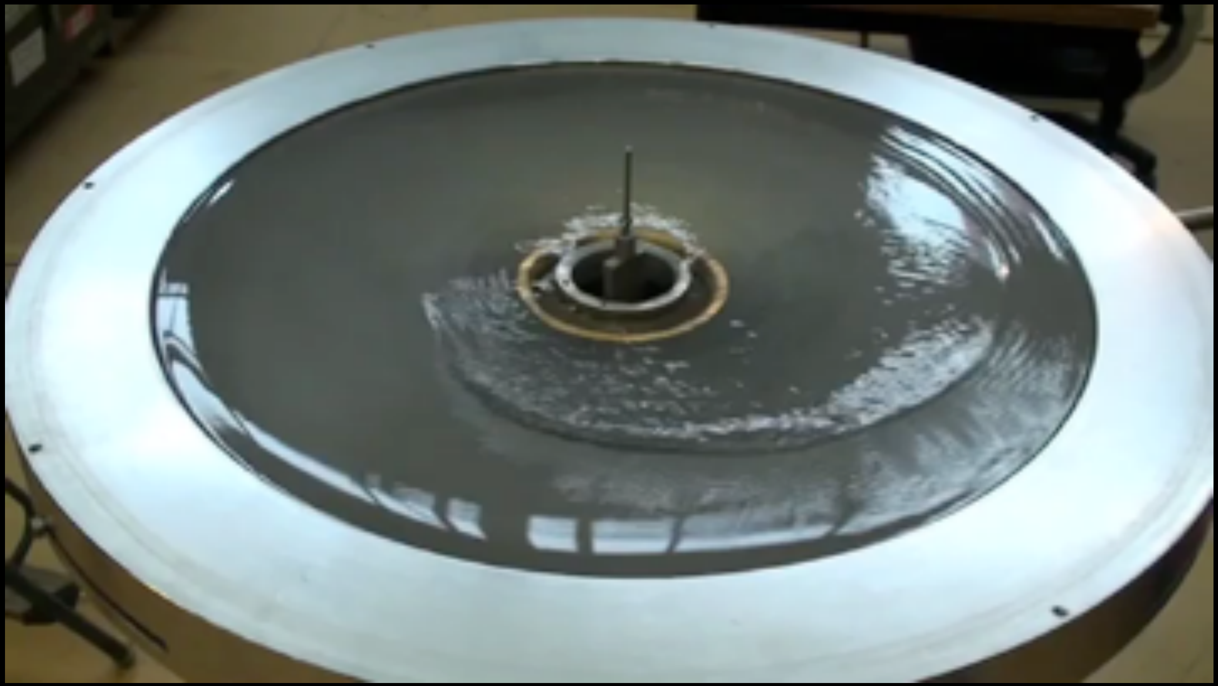

flow rate: 0.3L/s, slit size: 1.6mm

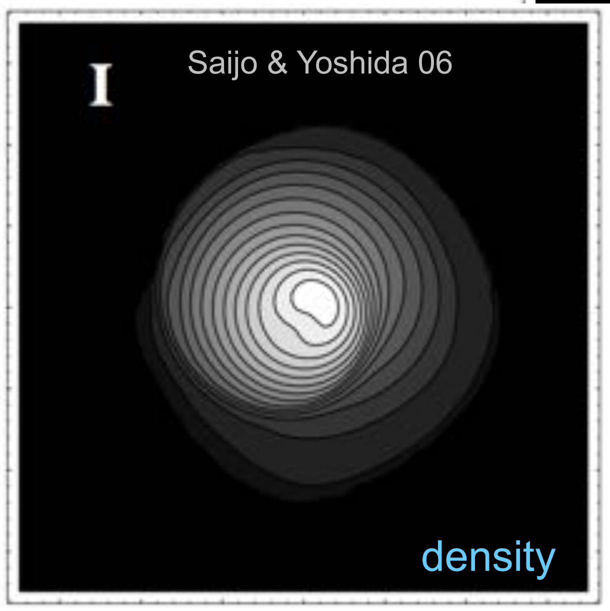

analogue to the “low T/W” instability of a neutron star rotating differentially
(Shibata+02,03, Saijo+03,06, Watts+05, Passamonti & Andersson 15)

boundary conditions are different in stellar core-collapse:
- inner advection
- outer accretion shock

recent 3D simulations by Takiwaki+16

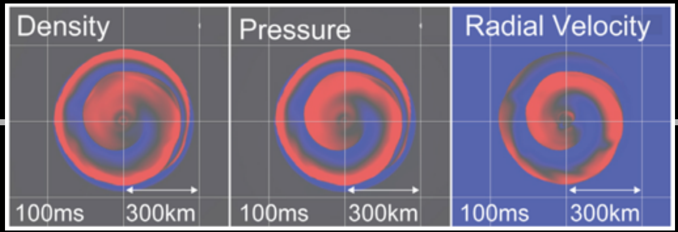

The corotation instability

Goldreich & Narayan 85

The dispersion relation of acoustic waves in a uniform gas with a uniform velocity v_0 along x

$(\omega - k_x v_0)^2 = k^2 c_0^2$ is rewritten in a rotating fluid with differential rotation Ω(r) using a local reference frame in cylindrical coordinates (r,θ)

A model equation is the parabolic cylinder equation (Goldreich & Narayan 85)

$$\frac{d^2 v}{dX^2} + \left(\frac{1}{4}X^2 - C\right) v = 0$$

The wavenumber of the acoustic perturbation is approximated as (k_r, m/r)

$$(\omega - m\Omega)^2 \sim \left(k_r^2 + \frac{m^2}{r^2}\right) c^2 \rightarrow k_r^2 \sim \frac{1}{c^2}(\omega - m\Omega)^2 - \frac{m^2}{r^2}$$

The fluid at the corotation radius r_{corot} rotates with the same phase velocity as the wave pattern $\Omega(r_{corot})=\omega/m$

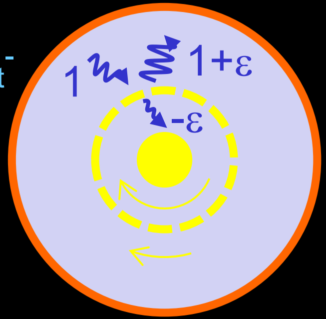

Acoustic waves are evanescent in the corotation region, delimited by two turning points r_t^+, r_t^- defined by k_r=0

$$\Omega(r_t) \sim \Omega_c \pm \frac{c}{r_t}$$

The azimuthal velocity of the fluid is
- -faster than the wave pattern at $r<r_{corot}$
- -slower than the wave pattern at $r>r_{corot}$

An acoustic wave carrying some azimuthal momentum in the direction of rotation increases the kinetic energy of the fluid for $r>r_{corot}$ and decreases it for $r<r_{corot}$

Evanescent propagation across the corotation region decreases the negative energy of the outer wave while increasing the positive energy of the inner wave: the outer wave is over-reflected as it approaches the outer turning point.

The corotation instability requires a reflecting boundary to close the amplification loop.

The corotation instability in core-collapse accretion

The description of over-reflected acoustic waves is limited to high frequencies to satisfy the WKB approximation

In a differentially rotating neutron star, the low T/W instability has been identified as a corotation instability of the fundamental acoustic mode l=m=2 (Passamonti & Andersson 15)

The corotation instability is expected to exist in a flow with radial accretion and a shock but the theory is missing and its interplay with SASI is not understood yet (Kuroda+14): transition from an advective-acoustic cycle to a purely acoustic cycle ?

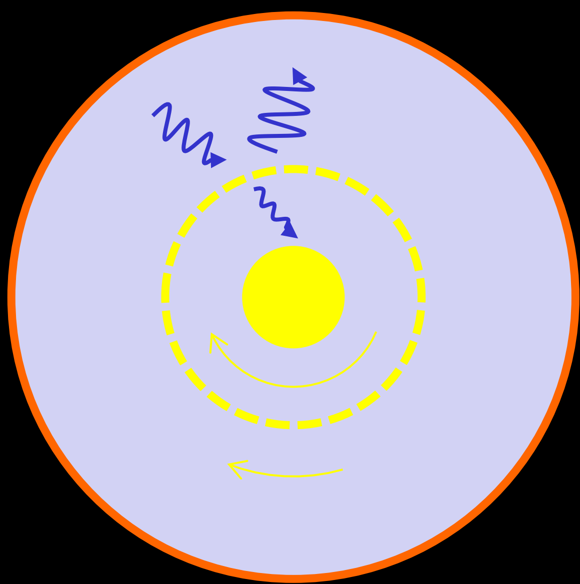

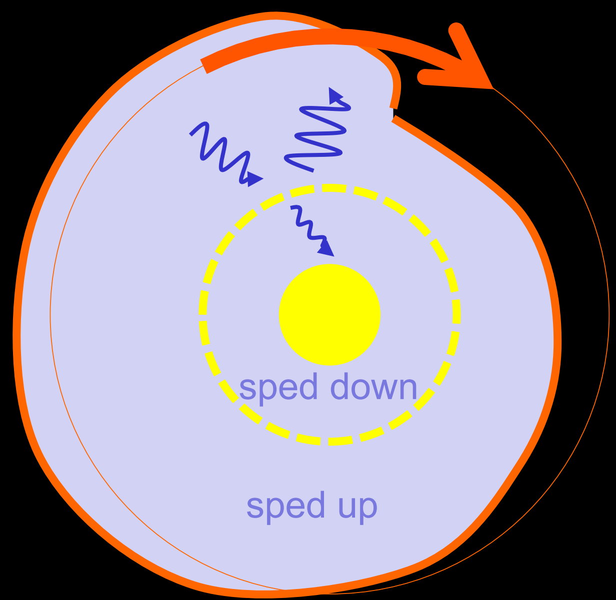

Gradual increase of the rotation rate:
continuous transition from SASI to the corotation instability

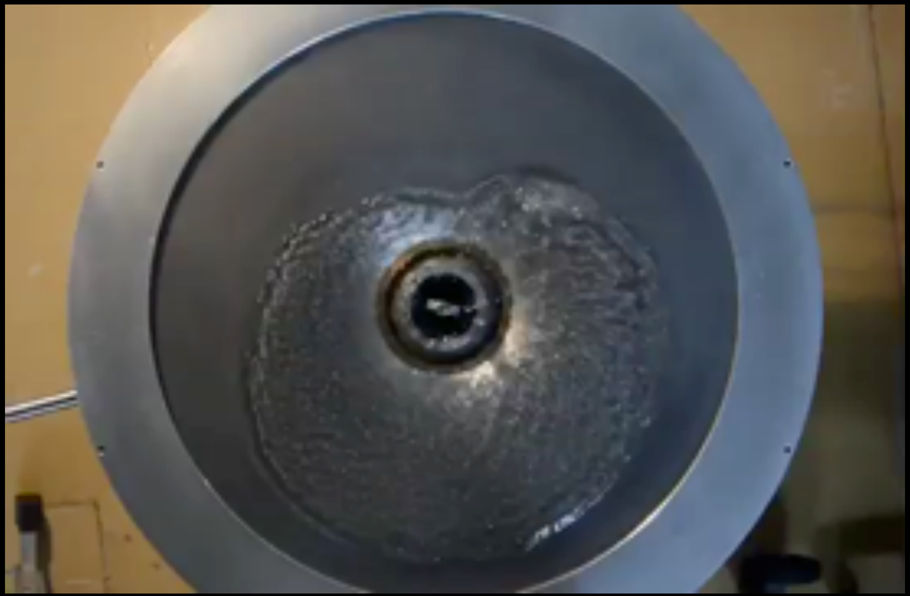

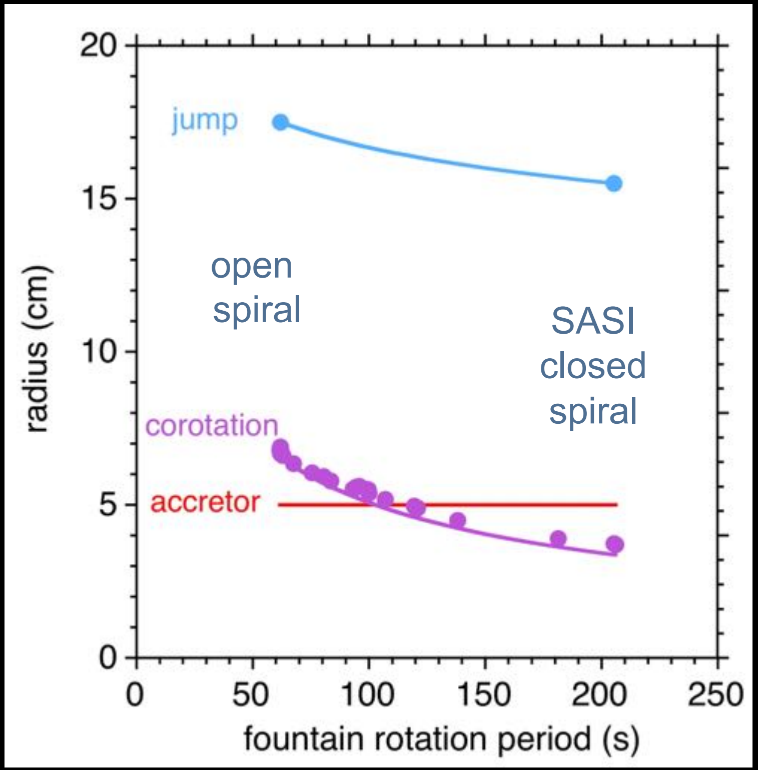

injection slit: 0.55mm
fountain rotation period: gradually decreased from 205s to 62s
flow rate: gradually decreased from 1.1 L/s to 0.59 L/s

Spin-up or spin-down of the neutron star?

(Kazeroni+17)

2D cylindrical simulations of shocked accretion with a cooling function

SASI alone

range of NS spin at birth

Neutron Star rotation frequency

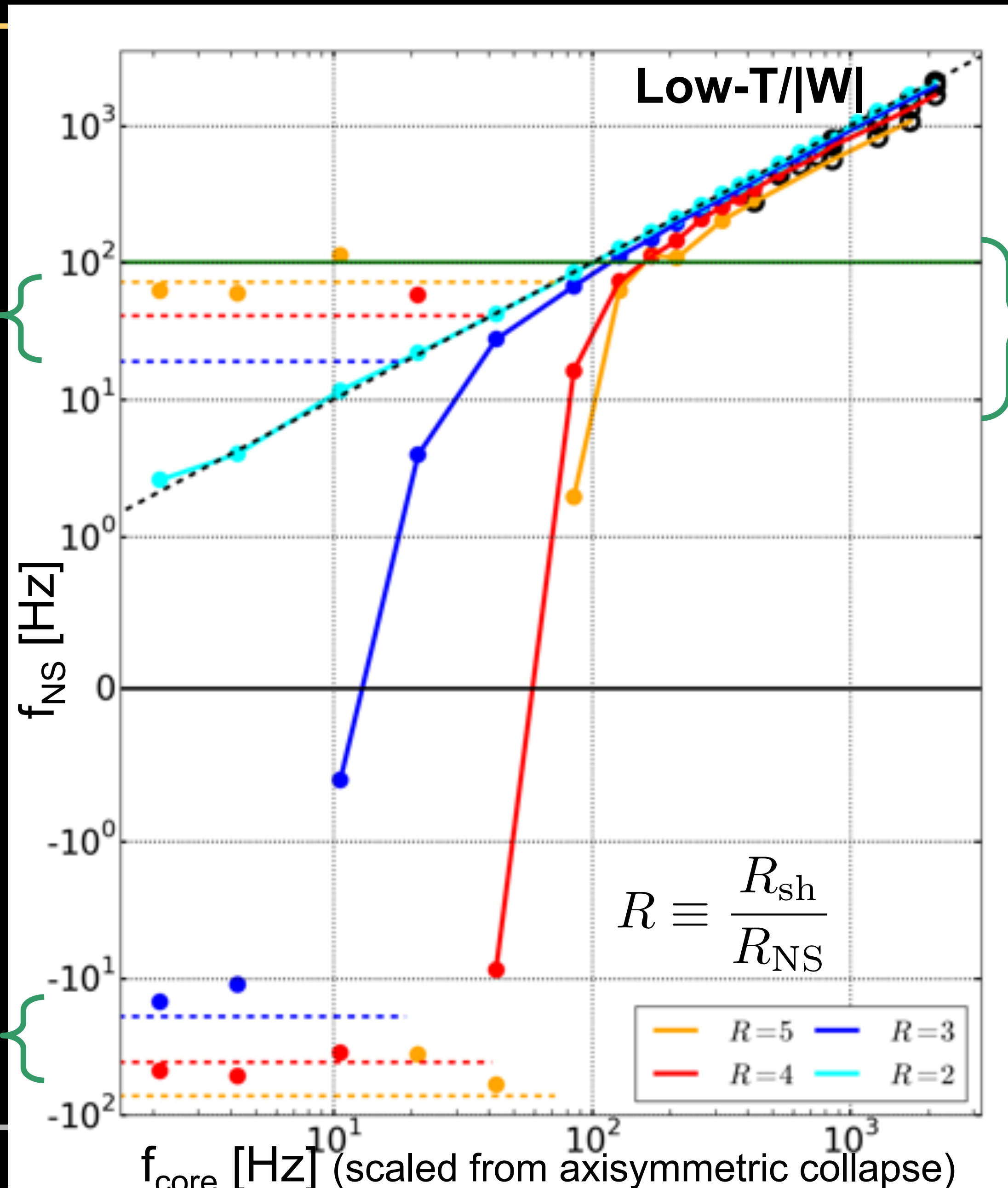

SASI alone

For a strong rotation rate, the corotation instability decelerates the neutron star by less than 40%.

Magnetic effects

Endeve+12

The turbulence induced by SASI is able to grow a significant magnetic field 10^{14}G at the surface of the protoneutron star, but with negligible consequences on the shock dynamics in 3D adiabatic simulations (Endeve+12), as well as in axisymmetric simulations of the full collapse unless the initial field strength is as large as 10^{12}G (Obergaulinger+14).

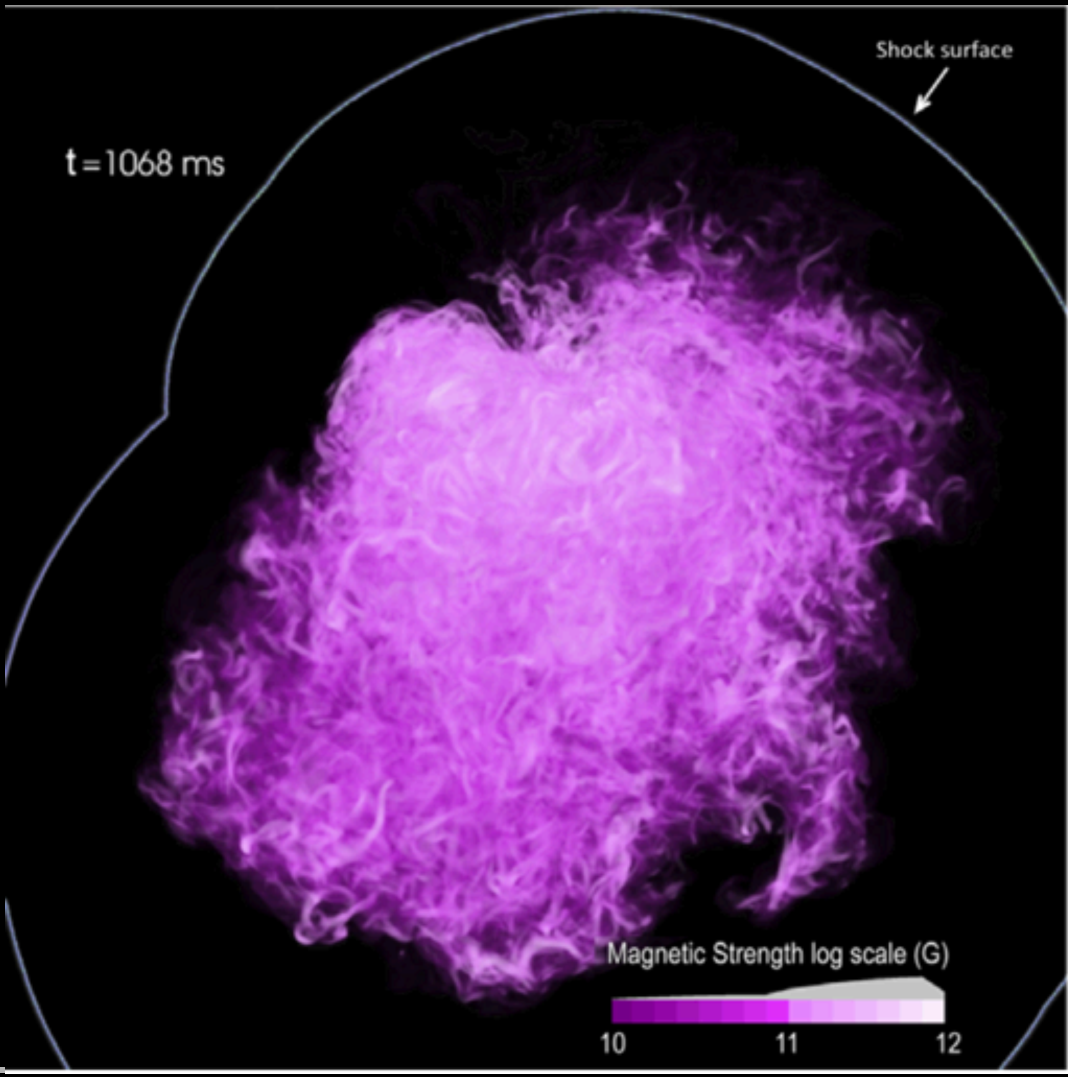

Magnetic effects with rotation: the magnetorotational instability

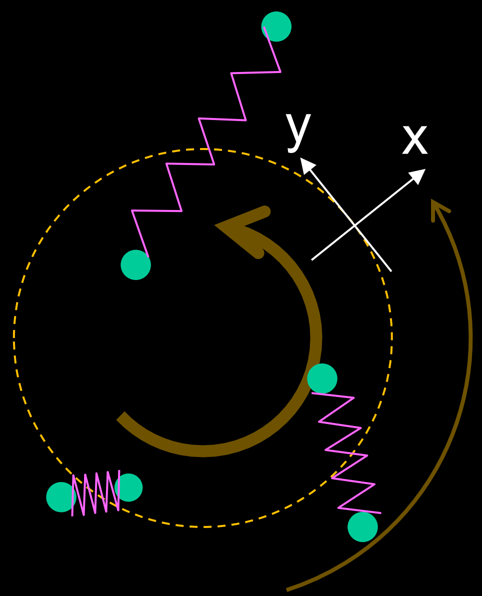

Differential rotation is able to amplify the magnetic field by connecting inner and outer orbits and acting as a restoring force (f_x, f_y)

The linearized system in the rotating frame is analogue to a particle attached with a spring to a guiding center

$$\frac{\partial^2 \xi_x}{\partial t^2} - 2\Omega \frac{\partial \xi_y}{\partial t} = -\frac{\partial \Omega^2}{\partial \ln R}\xi_x + f_x$$
$$\frac{\partial^2 \xi_y}{\partial t^2} + 2\Omega \frac{\partial \xi_x}{\partial t} = f_y$$

Hill equations

(Balbus & Hawley 92)

If B is along z, the restoring force is the magnetic tension in the direction perpendicular to the field, proportional to the Alfven speed V_A^2 associated to Alfven waves.

$$f_x = -(k_z V_{\mathrm{A}})^2 \xi_x$$
$$f_y = -(k_z V_{\mathrm{A}})^2 \xi_y$$

$$V_{\mathrm{A}} \equiv \frac{B}{(4\pi\rho)^{\frac{1}{2}}}$$
$$V_{\mathrm{c}} \equiv \frac{V_{\mathrm{A}} c_{\mathrm{s}}}{(V_{\mathrm{A}}^2 + c_{\mathrm{s}}^2)^{\frac{1}{2}}}$$

If B is along y, the spring is anisotropic: the restoring force f_y in the azimuthal direction is proportional to the cusp speed V_c^2 associated to slow magnetosonic waves (Foglizzo & Tagger 95)

$$f_x = -(k_y V_{\mathrm{A}})^2 \xi_x$$
$$f_y = -(k_y V_{\mathrm{c}})^2 \xi_y$$

Magnetic effects with rotation: the magnetorotational instability

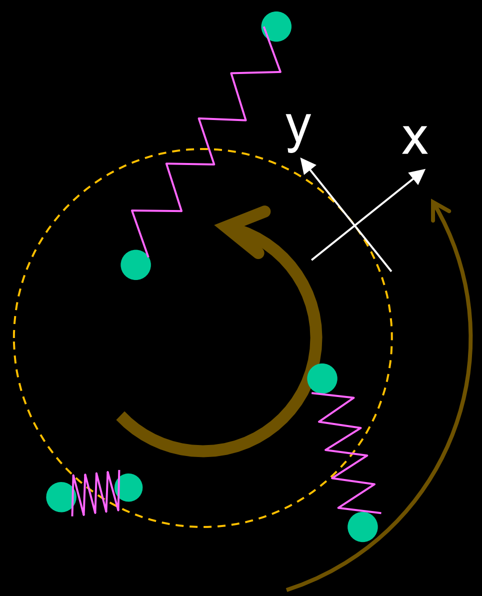

The dispersion of Alfven waves and slow magnetosonic waves modified by differential rotation is

$$\omega^4 - \omega^2 \left(\kappa^2 + k_z^2 V_{\rm A}^2\right) + k_z^2 V_{\rm A}^2 \left(k_z^2 V_{\rm A}^2 + \frac{\partial \Omega^2}{\partial \ln R}\right) = 0$$

where κ is the epicyclic frequency $\kappa^2 \equiv \frac{1}{R^3}\frac{\partial (R^2\Omega)^2}{\partial R}$

If the magnetic field is azimuthal, the dispersion relation involves both the Alfven speed and the sound speed.

$$\omega^4 - \omega^2 \left[\kappa^2 + \left(2 + \frac{V_{\rm A}^2}{c_{\rm s}^2}\right) k_y^2 V_{\rm c}^2\right] + k_y^2 V_{\rm c}^2 \left(k_y^2 V_{\rm A}^2 + \frac{\partial \Omega^2}{\partial \ln R}\right) = 0$$

The instability criterion is the decrease of the angular frequency, which destabilizes long wavelengths

$$(k \cdot V_{\rm A})^2 < -\frac{\partial \Omega^2}{\partial \ln R}$$

The maximum growth rate ω_{max} for a weak field is obtained for a wavelength λ_{max} proportional to the field strength B

$$\frac{2\pi V_{\rm A}}{\lambda_{\rm max}} \sim \Omega \left(-\frac{\partial \ln \Omega}{\partial \ln R}\right)^{\frac{1}{2}}$$

The growth of the magnetic field is possible until the magnetic tension stabilizes the longest available wavelength

$$\omega_{\rm max} = -\frac{1}{2}\frac{\partial \Omega}{\partial \ln R}$$

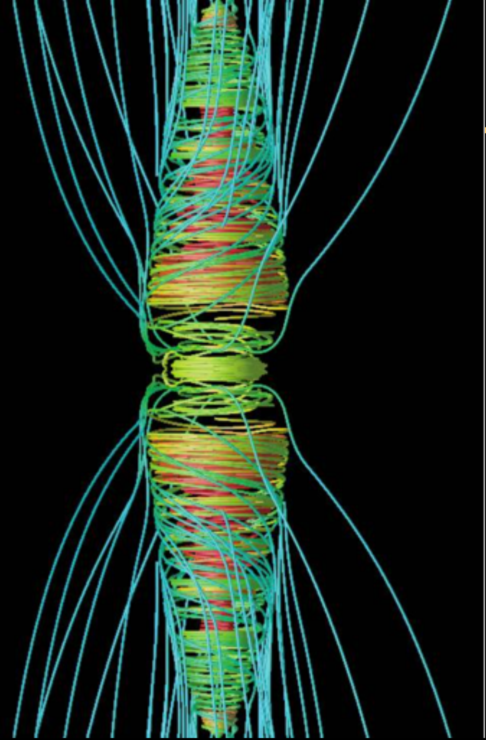

Burrows+07

Magnetic effects with rotation

$$\lambda_{\rm MRI}^{\rm max} \sim \frac{2\pi v_{\rm A}}{\Omega} \sim v_{\rm A} P \sim (10^4 \ {\rm cm}) P_{10} \frac{B_{12}}{\rho_{11}^{1/2}}$$

The small scale of this instability makes it very difficult to incorporate in numerical simulations of core collapse →assumption of a large scale poloidal field in early 2D simulations (Burrows+07)

This amplification is affected by the neutrinos which diffuse momentum and act as viscosity for long MRI wavelengths, or a drag for the shortest ones (Guilet+15).

Stable stratification of entropy in the direction of the shear can stabilize the MRI (Guilet & Müller 15). Conversely, the MRI and the unstable stratification can both contribute to build up the magnetic field of a magnetar (ERC MagBurst, Guilet 17-22)

A strong jet can be formed in 3D (Mösta+15): a possible scenario for gamma ray bursts and superluminous supernovae

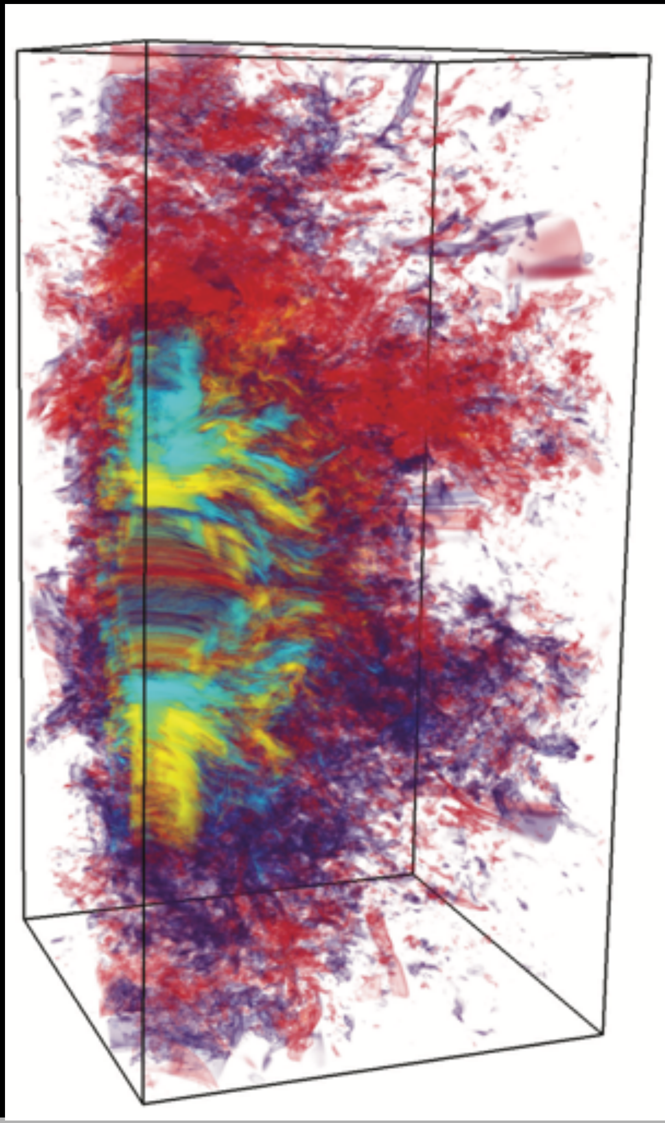

Mösta+15